REMARKS

The following remarks are submitted to address the issues raised in the Office Action mailed March 11, 2005. The applicant thanks examiner Marschel for assistance by phone in amswering technical questions that help make this response possible. The applicant makes particular note that in making a clear as possible response to answer the prior objections, it was found to be necessary to revise the wording in numerous of the previously-submitted specification, previously drafted by applicant's former counsel. It was felt by the applicant after careful consideration, that much of the original wording was unclear. There were also instances of typographical mistakes that had not been previously noticed. The applicant has therefore gone through the original specification very carefully, and provided corrections and alternate wording that should help to clarify many issues. The applicant also states that there is no new conceptual material presented in the newly-revised specification sent with this response; there is one instance of expanding the procedure of using a numerical constant to make easy and instant the use of the method under consideration. It is hoped that this description, which begins on page 20 and finishes on page 23 of the newly-submitted specification, will help to address the lack of enablement objection from the Office.

The MPEP instructions kindly provided by the examiner with his latest office response give rules regarding submission of an amended specification. Section 1.121(b)(2)(ii) indicates that strikethrough and underlining should be used. Also, section 1.121(b)(3)(i) indicates: "a substitute specification [may be made by submitting] in compliance with §§ 1.125(b) and (c)." A reading of that section, in particular subparagraph (d), indicated to the applicant that a complete substitute specification without strikethrough and underlining, is not permitted in a reexamination proceeding. Not exactly sure regarding the status of this application, the applicant has submitted the revised specification using strikethrough and underlining throughout. Acknowledging that the reading has been made difficult, the applicant will immediately submit the revised specification without strikethrough and underlining, if the Office so desires. The applicant requests an early contact regarding this particular matter if possible, to facilitate a quick submission of an easier to read document as necessary.

Declaration and Resubmission of case studies

The applicant submits with this response, a declaration of truthfulness as required by 37 USC §1.132 and §1.68, in regards to case studies originally submitted in her previous response dated January 7, 2005. The case studies are resubmitted with this response, and include some very minor wording changes for purposes of smoother reading and clarity. The wording changes in no way change the content of the reports. The declaration traverses the objection of the Office on this particular matter, as stated beginning at the last paragraph of page 3 and continuing onto page 4 of the most recent Office Action. The content of these case studies has also been included into the revised specification submitted with this response, beginning on page 30.

Amendments to claims

The applicant indicates that amendments to claims 5 and 19 are submitted, per the agreement to strike the word "therapeutic" from all claims, as previously submitted in the applicant's response and previously amended claims mailed on June 9, 2004. This specific wording change in amendments 5 and 19 should have been submitted to the Office on that date, but was inadvertently missed by counsel employed by the applicant at that point in time. This particular submission of amendments also corrects the objection raised on page 2 of the most recent Office Response (titled "Improper Amending Form").

The applicant proposes that the use of the phrase "genomic material" in the claims is unclear and indistinct, because some readers might interpret the adjective "genomic" as referring only to full genomes of biological organisms, which is unnecessarily limiting and inaccurate for the purposes of this invention. Therefore all newly submitted claims use the phrase "nucleic acid chain" instead of "genomic material".

The applicant also proposes that the use of the phrase "wavelength of the genomic material" is unclear and unscientific, because such material does not innately possess a wavelength (wavelength being a phenomenon associated with actively moving energies or emissions which can, however, couple with solid mass under proper length-matching

circumstances). Therefore, all newly submitted claims use the phrase "length parameter of the nucleic acid chain" instead of "wavelength of the genomic material", which establishes its length and coupling dependence thereof to the wavelength of the energy in the surrounding medium.

The applicant also proposes in most cases the use of the phrase "nucleotide bases" as opposed to the term "base pairs", because "base pairs" technically would apply only to double-stranded nucleic acid chains, and the method is intended to be useful for both double and single-stranded nucleic acid chains. Therefore, all newly submitted claims likewise reflect this change in terminology.

The applicant has also proposed minor wording changes in some of the claims which have the purpose of making the phrasing in the all claims consistent, and in some cases provides clearer or smoother reading, as will be evident from a reading of the newly-submitted claims.

After carefully studying previously submitted claims number 15 and 16, the applicant feels they are totally redundant material presented in the earlier numbered claims, and therefore has decided to cancel those two claims.

After carefully studying the previously submitted specification material regarding resonance associated with atoms and molecules, and the claim numbers 17 through 29 associated therewith, the applicant feels the subject matter of those claims and related materials are too divergent from the main body of this application, which addresses determination of resonant frequencies beneficial for debilitation or stimulation of biological nucleic acid chains. Therefore, the applicant has decided to cancel claims 17-29, and to delete the material associated with the subject matter of "atoms and molecules" in the specification.

Other remarks in response to Office objections

Further amendments to the claims are also submitted in an effort to clarify the exact intent of the claims and to address the questions raised by the Office regarding certain issues. On page 5 of the most recent Office Action dated 3-11-05, vagueness and indefiniteness in the claims pertaining to the subject matter of the invention was cited as problematic, and cause for rejection of the existing claims under 35 USC 112, paragraph 2.

Specifically, clarification was requested regarding whether "the practice is directed to influencing target genomic material or actually influencing the surrounding medium." Because the specification states and demonstrates that the mathematical parameters for the method specifically use characteristics of the medium that surrounds the nucleic acid chain, it can be stated that a first order effect is directed toward influence of the surrounding medium; however, because nucleic acids are highly influenced by electromagnetically-induced changes in the surrounding medium, there is also additional direct effect on the nucleic acid chain. Further description of effects is included below. For that reason, it cannot be accurately stated that the method is directed to affect only the surrounding medium, or only the nucleic acid chain material, because electromagnetic and/or mechanical effects on the surrounding medium are inextricably linked to reactionary electromagnetic and/or mechanical effects on the nucleic acid chain, and the two phenomena cannot be placed into separate categories of action because they are essentially co-dependent. Thus the applicant has changed the claim language to reflect these biophysical phenomena, by use of the phrase "medium-sensitive nucleic acid material".

Further clarification was requested regarding language originating at the end of claim 1 regarding the frequency emission as it relates to the device and/or electromagnetic radiation or energy coming from such a device. The applicant has attempted to clarify the language at the end of claim number 1, and has also attempted to clarify the role(s) of the device beginning at line 5 of claim number 1.

Page 2 of the most recent Office Action also cited lack of enablement as problematic, and cause for rejection of the application under 35 USC 112, paragraph 1. In response, the applicant submits an amendment to the current specification, such additional description (pages 20-23) being intended to more easily enable a person skilled in the art to make and/or use the invention. The additional description will make it easier for the user to quickly perform the necessary mathematical calculation to generate the desired resonant frequency. It includes use of a constant to instantly and accurately compute resonant frequencies for use in association with in-vivo tissue; and also includes suggestions for setting up a very basic spreadsheet, the use of

which would only involve entry of the number of nucleotides; subsequent computation of the applicable resonant frequency is performed by the spreadsheet.

On page 2, first full paragraph of the most recent Office Action, the examiner reiterates an objection regarding DNA conductivity by citing two U.S. patents (No. 6060327 and No. 6310179) which indicate use of DNA as molecular wires. Close examination of the methodology disclosed in these patents reveals however that certain specialized procedures, structures and circumstances must be used in order to achieve conductivity in the DNA molecules, none of which are inherent to native in-vivo DNA, which is the form of DNA targeted in this applicant's invention. Specifically, the sensors Keen invented in patent No. 6060327 require: 1) "molecular recognition headgroups" to be attached to the first ends of the DNA strands, including a process necessary to affix the headgroups to the DNA strands which later makes possible transfer of mobile charge carriers to and through the DNA strand [see claims 1, 15, 23, & 30]; 2) an electrode substrate to be attached to the second ends of the DNA strands, consisting of a photovoltaic diode or a component of a semiconductor chip [claims 12 and 13], the electrode substrate being necessary to allow the flow and subsequent reporting of the mobile charge carriers; 3) capability to align the DNA strands in a common orientation orthogonal to the electrode substrate, so that the multiple strands resemble liquid crystals [see column 7, lines 55-57; and column 9, line 66 through column 10, line 7).

Further to the issue of conductivity in polymers, the inventor of the aforementioned patent reveals at column 25, lines 52-55: "In some cases, the native form of the polymer will be an insulator, but upon appropriate doping, addition of impurities, hydration, conformational change, ionization, oxidation, reduction, etc. they become conductive...For example, a sensor signal may only be triggered by a combination of two events: a ligand binding with a molecular recognition headgroup and a pH change which causes the polymer wiring to become conductive." These sentences speak to some of the very specialized, high-tech processes used to make DNA truly conductive for wire use purposes. It also sets forth that native DNA is at least sometimes an insulative as opposed to conductive material. This concept is looked at in more detail below.

Statements at column 29, lines 4-9 in the above specification further describe the very specific circumstances necessary to make possible the measurement of artificially induced DNA conductivity as described in this patent (and in other researchers' experiences). The first sentence defines "long-distance electron movement through DNA" as only consisting of 40 angstroms or about 12 base pairs, and then continues that it "has been confirmed only in experiments in water solution. DNA has to be fixed to a terminal base, substrate, etc., coupled with the controlling of the thickness and orientation of molecules in order to measure the accurate conductivity of the fixed DNA."

This applicant further notes the aforementioned patent claim number 30 and numerous other locations in the patent specification, wherein single-stranded nucleic acid strands are characterized as "non-conductive", even under the specialized circumstances and setup described in the invention. This is a noteworthy condition, because a number of the successful outcomes with this applicant's method specifically targeted single-stranded nucleic acids, one example being RNA viruses. This would point to as reasonable assumption that conductivity along the single strand (under native, in-vivo conditions) was not a mechanism involved in the successful outcome using the method.

This applicant also notes that conductive movement of electrons through a maximum distance of 40 angstroms along a nucleic acid chain (under the specialized, non-native circumstances described above and in other research material), would not constitute the electronic circumstances necessary to classify the chain as an antenna, which requires the ability to move current through the entire length of the antenna.

The second patent cited in the examiner's most recent reply (Batz et al, U.S. No. 6310179), also reveals use of DNA under obvious non-native conditions. The first sentence of the abstract as well as claim no. 4 both state that nucleic acid analogues, specifically certain types of peptide nucleic acids (PNAs) are the molecules used in this invention. Column 1, lines 58-61 reveal that "Peptide nucleic acids as described in this reference [WO 92/20702] are characterized by having a non-naturally occurring backbone having attached nucleobases at defined positions...". This is clearly not a native biological DNA form, as targeted by this applicant's method. Other special characteristics of PNAs, which do not occur in native

biological DNA, are used to advantage for the purposes of creating conductive nucleic acid wires. Column 6, lines 40-44 state: "PNA having bound moieties are disclosed in WO95/14708. These PNA oligomers further give the opportunity to bind metal ions (thus doping the geometrical structure with metal ions) for increasing electrical conductivity within such oligo/polymeric structures." Further description regarding doping materials and procedures occurs at column 8, lines 1-7; and column 9 lines 26-30. Obviously, doping the PNA structure with metal ions or other conductive materials lends a distinct advantage for conductivity in the molecular wire. However, this is clearly not a normal condition for native DNA.

The aforementioned patent also states at column 8 lines 14-20 that nucleic acid analogues (the molecules used in this invention), are more stable than nucleic acids "under the condition of coating surfaces with metals. This speaks to the problem of native DNA stability. DNA is known by anyone who works with it to be a fragile substance and easily prone to strand breaks. If this were to occur during theoretical use as a molecular wire, the current would obviously cease flowing. Current heating of atomic particles in the wire, if not controlled, could contribute to this problem and may approach melting temperature regions of the native DNA. Concern with native DNA stability is further addressed in this patent at column 8, lines 21-29.

In a different patent assigned to Buchardt et al (U.S. No. 5714331), structural characteristics of PNAs are reiterated in the specification at column 2, lines 1-4 and lines 12-15. It also states in column 2, lines 20-31 that PNA/DNA or PNA/RNA duplexes have higher melting temperatures than DNA/DNA or DNA/RNA duplexes. It additionally cites the "neutrality of the PNA backbone, which results elimination of charge repulsion that is present in DNA/DNA or DNA/RNA duplexes", and that the melting temperature is "practically independent of salt concentration. DNA/DNA duplexes, on the other hand, are highly dependent on the ionic strength". This supports the fact that DNA is highly influenced by its surrounding medium.

The text cited by the examiner in this patent also includes a reference to U.S. Patent No. 5591578 by Meade. Titled "Nucleic acid mediated electron transfer", it is clear upon examining the abstract that these materials are again similar to "doped" nucleic acids. The abstract states "The present invention provides for the selective covalent modification of nucleic acids with

redox active moieties such as transition metal complexes." Column 1 lines 4-13 further add, "Field of the Invention – The present invention is directed to electron transfer via nucleic acids. More particularly, the invention is directed to the site-sensitive modification of nucleic acids with electron transfer moieties such as redox active transition metal complexes to produce a new series of biomaterials and to methods of making and using them. The novel biomaterials of the present invention may be used as bioconductors and diagnostic probes." This invention thus reveals that DNA need to be altered into a conductive state to use effectively for such purposes.

Yet another patent revealing use of metal-doped nucleic acids for conductive purposes is at U.S. No. 6432641 (Lee, et al). Revealingly, at column 1 lines 32-37 it states that certain research analysis showed native DNA to be a poor conductor.

Other literature supports the need to alter DNA to make it conductive. The last-cited inventor Thomas Meade is profiled as far back as 1995. An article from that year describes his work using ruthenium atoms to dope a double-helix DNA strand in order to make it more conductive [Paterson D., "Electric Genes", Scientific American: 33-34 (May 1995)]. Additional examples of similar research are reported in Purugganan MD et al, "Accelerated Electron Transfer Between Metal Complexes Mediated by DNA", Science 241: 1645-1649 (23 Sept 1988) and in Murphy CJ et al, "Long-Range Photoinduced Electron Transfer Through a DNA Helix", Science 262: 1025-1029 (12 Nov 1993). Both sources cite doping or intercalation techniques of metallic and/or other electrically active molecules intended to increase electron conductivity through the DNA stack. Numerous other journal articles are available demonstrating use of these techniques.

A review of the most recent literature helps shed light on issues of native DNA conductivity. For convenience of reading, the applicant will number the following sources.

1. One group discovered resistivity measurements no lower than 10^6 ohm·cm [see de Pablo, PJ et al, "Absence of dc-Conductivity in λ-DNA", Phys. Rev. Lett. 85 (23): 4992-4995 (4 Dec 2000)].
2. Storm et al report absence of conductivity and a lowest resistance parameter at 10 T-ohms for molecules longer than 40 nm, and state "it is concluded that DNA is insulating"

(see abstract of article), and in the last paragraph that "our results clearly limit the use of bare DNA as a conducting molecular wire" [see Storm AJ et al, "Insulating behavior for DNA molecules between nanoelectrodes at the 100 nm length scale", Applied Physics Letters 79 (23): 3881-3883 (3 Dec 2001)].

3. Zhang et al published a very interesting paper citing technical difficulties in measurements of DNA conductivity, the potential role of salt residues from the medium in confounding past results, and a resistivity no lower than 10^6 ohm·cm (see abstract), characterizing the electrical behavior of λ-DNA as insulating [see Zhang Y et al, "Insulating behavior of λ-DNA on the micron scale", Phys. Rev. Lett. 89, 198102 (2002)]. Zhang's resistivity measurements duplicate that of de Pablo in reference #1 above.
4. Another study reports in its abstract that "adsorbed DNA molecules have a resistivity similar to mica, glass, and silicon oxide substrates. Therefore adsorbed DNA is not a conductor, and it should not be considered as a viable candidate for MW [molecular wire] applications." See Gomez-Navarro, C. et al, "Contactless experiments on individual DNA molecules show no evidence for molecular wire behavior", Proceedings of the National Academy of Sciences U.S.A. 99 (13): 8484-8487 (25 June 2002).
5. In a large paper from 2004 that reviews DNA charge transport, the writers concluded that "electrical transport is feasible in short DNA molecules, in bundles and networks, but blocked in long single molecules that are attached to surfaces" (see abstract, lines 6-8). It is further added however, that the conductivity in such molecular wire arrangements "is rather poor" (p. 202, last paragraph). Text on p. 203-4 continues, "Therefore, if one indeed wants to use DNA as an electrical molecular wire in nano devices...then there are are a few possible options. One option is to use doping by one of the methods that are described in the literature (e.g., addition of intercalators, metal ions, or O_2 etc)." This information aligns with with processes found necessary for conductivity in the aforementioned patent material. Finally, the authors state in "Conclusions and Perspectives" (p. 223), "recent results seem to indicate that native DNA does not possess the electronic features desirable for a good molecular electronic building block, although

it can still serve as a template for other conducting materials. Selected mentioned pages from this large article are provided in the reference material with this response. See Porath D et al, "Charge Transport in DNA-Based Devices", Top. Curr. Chem. 237: 183-227 (2004). Full article also available at: http://www-mcg.uni-r.de/pubs/reprints/2004_TCC_237_183.pdf

6. Finally, a fascinating 2004 article further revealed nearly total lack of intrinsic DNA conductivity when the testing setup was placed in an inert gas humidity-free atmosphere. Even more interesting however, was that once the testing setup was placed in that atmosphere and equilibrium conditions were realized, any conductivity readings that had been previously present, significantly dropped within a period of five minutes. The authors stated "we could always detect a significant drop in electric conductivity and therefore and almost complete absence of long-range dc electric charge transport...this negative result was verified several dozen times." They conclude "In summary, we found that the intrinsic electrical properties of dsDNA for long range charge transport...is far below of any technological use. A possible way to improve the electrical conductivity might be additional doping of dsDNA or molecular engineering of hybrid systems...which can be used in future devices for molecular electronics or biosensor applications." This information not only verifies lack of inherent conductivity within the DNA molecule itself, but also places the focus of any possible electronic response coupling response primarily within the surrounding medium. See Kleine H et al, "Absence of intrinsic electric conductivity in single dsDNA molecules", Journal of Biotechnology 112 (1-2): 91-95 (26 Aug 2004). [An abstract of this article is included with the other articles; a clean full text was not yet available at the time of this response].

In conclusion, the recent research clearly indicates that native DNA exhibits electron transport only through some tens of angstroms in length (20-40 angstroms); that use of doping materials is necessary for any reasonable electron flow through longer stretches of DNA; that native DNA is inherently insulative (non-conductive) in nature; and that DNA conductivity is dependent on characteristics of the surrounding medium.

Based on the various research results cited above and in numerous other patents and publications, it does not stand to reason that DNA would approach the behavior of, or obey the laws of metallic conducting antennas. As mentioned earlier, for an antenna to support a frequency response it must be capable of passing current through its entire length, which a biologically active DNA chain cannot do.

Without being bound to theory, in one possible scenario if native biological nucleic acid chain and its surrounding medium is in the presence of a sufficiently strong alternating or pulsed DC electric or electromagnetic field influenced by an repeated event in time (i.e., a frequency); and when that particular repeating electromagnetic event has been carefully configured to have its wavelength in the surrounding medium match the specific length parameter of the nucleic acid chain; it is possible that the counterions and highly-oriented "water spine" which surrounds the nucleic acid backbone would be disturbed in space in accordance with the wavelength of the electromagnetic event. In other words, positive ions would be driven to one end of the wave event, and negative ions would be driven to the other end of the wave event. Because the surrounding ions would primarily consist of positively charged ions due to the intense negative charge present along the nucleic acid backbone, the motion of the positive charges in response to the field would constitute current moving within the electrical constraints of the wave length. Surrounding polar water molecules would at the least be rapidly rotating in response to the changing polarity of the field. Because some water molecules are closely associated with the grooves in the nucleic acid chain molecule, potentially forming their own chain-like structure (see Takashima, p. 253-254), potential dislodging of those water molecules could also occur. Takashima further states that structured water molecules are "presumed to be ubiquitous among biopolymers...Clearly, they are part of the polymer and cannot be removed without disrupting the internal structure." Without being redundant, there are numerous other papers recently published which stress that stability of the DNA molecule is crucially dependent on solvent water molecules and counterions.

The events of electromagnetic wave motion could potentially lead to destabilization of the chain molecule, because these various events could also induce effects that are mechanical

(acoustic) in nature. Because of the grooved nature of the chain – akin to being "ribbed" - it is not unrealistic that abrupt and repeated nudging of the positive ions and water molecules along the backbone of the nucleic acid chain could induce mechanical motion into the chain, with the very specific wavelength matching the length parameter of the chain. The total sum of effects is very likely to be electro-acoustic in nature. For all these reasons, it can be seen why choice of a particular wavelength in the surrounding medium is so important, which then provides the user with a frequency that will resonate the surrounding medium *with a particular wavelength*; it is, if you will, "resonant" for the surrounding medium of the nucleic acid chain *but only relating to one particular wavelength* intended to influence the chain along its specific length. The "uncloaking" of the chain molecule from its normal environment in a *length-specific* manner is critical to the effectiveness of this method, which is why the frequency must be calculated according to the parameters of the surrounding medium.

In another application, low-level AC or pulsed DC current delivered into the surrounding medium, could also set up the above-mentioned chain of events, because the variable motion of the current using a specific frequency geared for the surrounding medium, will cause motion of current at the corresponding wavelength for that medium, and set up related electrical and then electro-acoustic response motions within the parameters of the wavelength.

Once the sequence of events is carefully considered, it becomes apparent that while the ultimate aim of the mathematical process presented in this application is to come up with an appropriate "resonant" frequency, the underlying foundational mechanism is that of requiring the incoming wavelength to match a length parameter of the target object under consideration, in this case the medium surrounding a specific nucleic acid chain. This is at root, a wavelength matching process. A related phenomenon occurs in radio science, in which certain wavelengths of the radio spectrum are not used because when they go through a human body, the wavelength changes according to the wave travel velocity characteristics of the body, the wave then couple with the body height parameter, and the body absorbs energy at higher than usual amounts. For this reason the FCC does not allow emission in the sensitive wavelength ranges that cause such action. This phenomenon underlies the very same process under consideration in the methods presented in this application.

The most recent response of the Office beginning on page 4 last paragraph, reiterates a previous objection that coiling (as opposed to straight) could theoretically change resonance of the molecule, the in the same manner that metallic antennas behave.

The applicant has made an effort to study electrical response of antennas. Another way of stating "bending a straight antenna will change the resonant frequency", is to say "bending a straight antenna will change which incoming wavelength the antenna will optimally respond to". Another way of expressing the concept, is that the bending action will change the electrical wavelength.

When charges moving through an antenna reach the end(s) too soon, or when they are so slow that they cannot reach the end(s) before the time comes for them to reverse direction, the antenna cannot optimally respond to the incoming wavelength and thus frequency. Creating a bend affects the velocity of the moving charges, as well as the velocity of the wavemotion in the antenna material. The overt effect is to create a change in the dielectric constant and the impedance of the antenna.

Nonetheless, the physical length of a bent antenna remains very important in relation to the wavelength of the incoming wave. See Henney page 20-67, and Carr page 288-289.

In the case of nucleic acid molecules, the issue of current flow reaching the ends of the molecules cannot even come into play, especially in view of the research cited above. Biological nucleic acids cannot effectively conduct current, and therefore the consideration that a bend might change the resonant frequency response becomes a moot point, because the effect of bending a metallic wire produces entirely different atomic or molecular-level electrical consequences, than in or around a nucleic acid chain. For nucleic acids, the electrical effects on the surrounding medium may be far more important for purposes of this invention, than the effects on the nucleic acid chain itself. This is supported by recent research as well. Furthermore, it is not realistic to assume that coiling of a nucleic acid molecule would negate coupling action to it, because waves can and do couple to objects of varied shape. In that vein, having a curved metallic antenna does not negate its ability to respond to incoming waves.

If native in-vivo nucleic acid chains were ordinarily conductive, many organisms including mammals would be continuously conducting current due to the presence of

electromagnetic wave activity in the environment. It is perhaps the blessing of the surrounding ions and water molecules that protects nucleic acids from these effects – to some degree. If wavelength resonance considerations are put to beneficial use along with power levels of frequency-capable emission devices, the ability to selectively effect relevant nucleic acid chains is possible, through the door of their immediate environment.

REFERENCES PROVIDED WITH THIS RESPONSE

Paterson, D., "Electric Genes", Scientific American: 33-34 (May 1995).

Purugganan MD et al, "Accelerated Electron Transfer Between Metal Complexes Mediated by DNA", Science 241: 1645-1649 (23 Sept 1988).

Murphy CJ et al, "Long-Range Photoinduced Electron Transfer Through a DNA Helix", Science 262: 1025-1029 (12 Nov 1993).

de Pablo, PJ et al, "Absence of dc-Conductivity in λ-DNA", Phys. Rev. Lett. 85 (23): 4992-4995 (4 Dec 2000).

Storm AJ et al, "Insulating behavior for DNA molecules between nanoelectrodes at the 100 nm length scale", Applied Physics Letters 79 (23): 3881-3883 (3 Dec 2001).

Zhang Y et al, "Insulating behavior of λ-DNA on the micron scale", Phys. Rev. Lett. 89, 198102 (2002).

Gomez-Navarro, C. et al, "Contactless experiments on individual DNA molecules show no evidence for molecular wire behavior", Proceedings of the National Academy of Sciences U.S.A. 99 (13): 8484-8487 (25 June 2002).

Porath D et al, "Charge Transport in DNA-Based Devices", Top. Curr. Chem. 237: 183-227 (2004). Full article also available at:
http://www-mcg.uni-r.de/pubs/reprints/2004_TCC_237_183.pdf

Kleine H et al, "Absence of intrinsic electric conductivity in single dsDNA molecules", Journal of Biotechnology 112 (1-2): 91-95 (26 Aug 2004) [abstract only]

Takashima, Shiro. "Bound Water in Biological Macromolecules", chapter 8 from Electrical Properties of Biopolymers and Membranes. Bristol: Adam Hilger, 1989, p. 252-254.

Henney, Keith. Radio Engineering Handbook. New York: McGraw-Hill, 5th edition, 1959, p. 20-67.

Carr, Joseph J. Practical Antenna Handbook. New York: TAB Books, 2nd edition, 1994, p. 288-289.

CONCLUSION

Applicant states that a full and complete response has been made herein to the past Office Actions dated March 11 2005, and as such, asks that all amended claims submitted in this application be placed in condition for allowance. The applicant respectfully requests early consideration of the present application, entry of the amendments to claims and specification, and withdrawal of all rejections.

Respectfully submitted,

Charlene A. Boehm

Charlene A. Boehm
June 11, 2005

Charlene Boehm
320 Gilbert Rd.
Columbus, NC 28722
(828) 863-4317

code that identifies the person and destination. A driver—who has indicated that he is going in the same direction—will retrieve that information by telephone or with a communications device.

As an incentive to participate, drivers would receive a portion of a $1 to $2 fare, which would be credited to their account by the computer system. Car poolers would also be registered in the database as a security check. To be able to guarantee a ride, Behnke envisions extending his suburban transit system beyond the private car. If the computer is unable to match a rider with a car, a "smart" jitney, or roving van, would be dispatched, and it could be tracked with inexpensive satellite-aided navigation systems.

These ideas lack the high-tech allure of remotely controlled vehicles detailed in other ITS projects. But they try to minimize capital expenditures for financially drained local governments.

Despite work on a number of planning studies, Behnke has yet to see his vision realized. He may get a chance to see at least some of his ideas put to the test in a $2-million project called Athena. This transit project—to take place in the city of Ontario, some 45 miles east of Los Angeles—will receive federal and state funds.

Even with such an experiment, transit may never work in the suburbs. There are liability concerns about strangers riding in the same car. And, in general, getting Americans onto buses or trains, or even into car pools, has been a losing proposition. The number of public-transit trips per person dropped from 114 in 1950 to 31 in 1990. Commuters have little inclination to make transit a communal experience: the percentage of U.S. trips to work by car pool fell from about 20 percent in 1980 to roughly 13 percent in 1990. More fundamental approaches to the problem, such as higher gas taxes, are politically unpopular.

Despite the antitransit collective unconscious, there are a few recent success stories. An informal ride-sharing system in suburban Virginia is working smoothly: Washington-area employees hitch rides with drivers who then use a high-occupancy vehicle lane. Van services nationwide take travelers from airports to their suburban doorsteps.

Changes in transportation patterns could have a dramatic impact. Removing just one of every 10 cars on the road during the morning rush hour could cut congestion delays by nearly half while easing suburbanites' dependence on the automobile. It would also have the effect of filling those empty seats with something other than the hot air of radio talk-show hosts. —*Gary Stix*

Electric Genes

Current flow in DNA could lead to faster genetic testing

As more and more of the human genetic blueprint is unraveled, the pressure to know what it means for people grows. Does the baby have any serious genetic problems? Does that teenager carry genes predisposing her to breast cancer? Does a particular adult have the DNA associated with diabetes or with Alzheimer's disease?

During the past few years, it has become possible to provide answers to more of these questions—to find, for example, the *Apo E4* gene that indicates a greater risk of Alzheimer's or the *BRCA1* gene associated with certain cases of breast cancer. But at present such testing is limited to patients in research projects or those who have a family history of the disease. Widespread speculative genetic screening of populations is too costly to consider—even were it ethically acceptable. This situation may be about to change, at least from a technical standpoint.

Imagine having a machine that could screen almost instantaneously for hundreds, maybe even thousands, of genes. A similar device could also detect the presence of viruses in a person's blood or toxic bacteria in food. These prospects have become realistic as a result of discoveries made in the past few months at the California Institute of Technology.

Chemist Thomas J. Meade and molecular biologist Jon F. Kayyem have been exploring how electrons move in large molecules. Such processes underlie many important biological phenomena; for instance, the conversion of sunlight into plant food by the magnesium chlorophyll molecule depends on stimulation of electron movement through the chlorophyll by the incoming photons. Meade and Kayyem's molecule of study was DNA. They devised a way of binding atoms of ruthenium, a heavy metal, to ribose, one of the backbone components of the helical chains of DNA. Ruthenium atoms act like electrical connectors into and out of the molecule; they have the added virtue of neither disrupting nor distorting its overall shape. Although there has been a long history of using such metals to understand DNA, the ruthenium-ribose combination revealed something extraordinary.

The researchers examined the electrical properties of short lengths of double-helix DNA in which there was a ruthenium atom at each end of one of the strands. Meade and Kayyem estimated from earlier studies that a short single strand of DNA ought to conduct up to 100 electrons a second. Imagine their astonishment when they measured the rate of flow along the ruthenium-doped double helix: the current was up by a factor of more than 10,000 times—over a million electrons a second. It was as if the double helix was behaving like a piece of molecular wire.

For some time, chemists have suspected that the double helix might create a highly conductive path along the axis of the molecule, a route that does

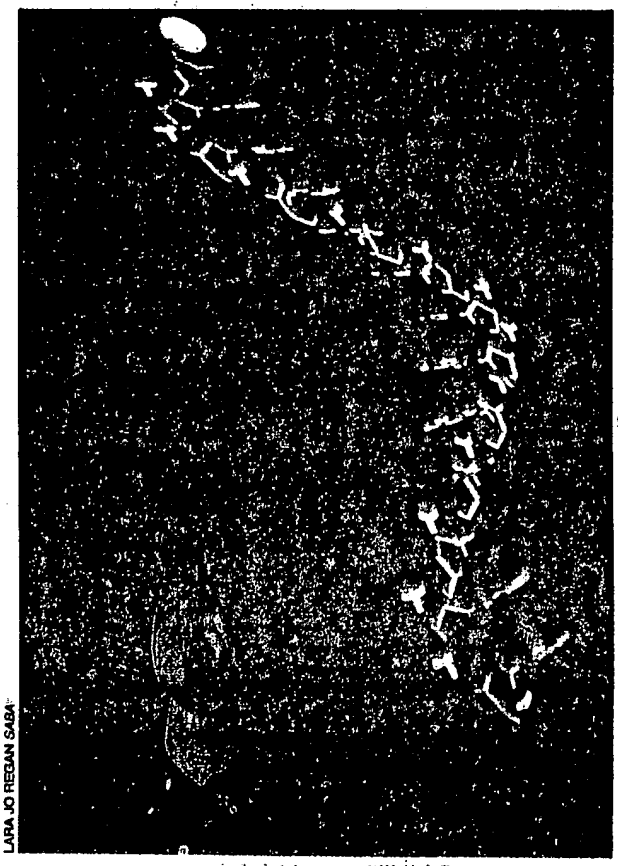

LARA JO REGAN SABA

CHEMIST THOMAS J. MEADE is one of a team that has electrified DNA. The technique could hasten cheaper, rapid genetic tests for certain diseases.

not exist in the single strand. Here was confirmation of this idea.

What Meade and Kayyem wanted to know next was whether this newly discovered property could be used to discriminate between DNA strands that were identical to the original and those that differed by one base pair out of the 15 (in other words, a match of 14 of the 15 base pairs). Practically, the test was to see if the perfect match carried significantly more current than the 14-out-of-15 match. To the scientists' delight, there was a large difference, although commercial implications inhibit candor when they are posed the question, "How big is the difference?" (Further, the work has not yet been peer-reviewed or published, so the team remains quite cautious about the details.)

Essentially what Meade and Kayyem have found is an electronic way to distinguish between different sequences of DNA. To convert this finding into a practical device will require concerted development, but even as is, it hints at useful technology. Workers can already build synthetic single DNA strands that can duplicate any known sequence. An amino acid sequence of the gp120 protein of HIV, for example, corresponds to a specific DNA sequence of bases.

Using Meade and Kayyem's invention, one could assemble this gp120 sequence base by base with a ruthenium-doped backbone on an electric current detector, such as a silicon chip. The ruthenium DNA strand could then be used to search for an HIV nucleic acid in a biological sample. If the matching complementary strand from the virus were present, it would bind tightly to the synthetic sequence, and a high flow of electrons would be possible along the molecule's axis. If there were no HIV sequence, there would be no perfect binding with the synthetic DNA, and no current would flow. The answer could be instantaneous—no waiting for gels, no electrophoresis—just a matter of waiting for an indicator to light up.

Meade suspects that the device would need between 15 and 20 bases of single-chain DNA deposited on a chip. Such a stretch of code would allow more than a billion different gene fragments to be specified. And a sophisticated indicator might allow the simultaneous detection of maybe even hundreds of genes. Kayyem is already installed in the Pasadena-based company Clinical Micro Sensors to exploit the discovery. Meade posits that the technique could be useful for any situation in which a rapid, accurate test for the presence or absence of a particular genetic sequence is important. No doctor's office, no farm, no kitchen may be without one. —*David Paterson*

4. F. R. Hallett and R. A. B. Keates, *ibid.*, p. 2403.
5. M. F. Carlier, T. L. Hill, Y. D. Chen, *Proc. Natl. Acad. Sci. U.S.A.* **81**, 771 (1984).
6. Y. D. Chen and T. L. Hill, *ibid.* **82**, 1131 (1985).
7. D. Kristofferson, T. J. Mitchison, M. W. Kirschner, *J. Cell Biol.* **102**, 1007 (1986).
8. T. Horio and H. Hotani, *Nature* **321**, 605 (1986).
9. Microtubule protein, prepared in a mixture of 0.1*M* MES K^+ (the potassium salt of 4-morpholineethanesulfonic acid), 2 m*M* magnesium acetate, and 1 m*M* EGTA buffer, *p*H 6.6 (MME) [R. A. B. Keates, *Can. J. Biochem. Cell Biol.* **62**, 803 (1984)], was estimated to contain 25% MAPs and 74% tubulin by scanning densitometry. We then added NaCl and glycerol to attain concentrations of 0.3*M* and 2*M*, respectively, and the solution was applied to a DEAE-Sepharose CL-6B column (1.5 cm by 8 cm). MAPs were eluted with 0.3*M* NaCl, 2*M* glycerol in MME. MAP-free tubulin was eluted with 0.5*M* NaCl, 2*M* glycerol in MME, and was dialyzed overnight against 5*M* glycerol in MME. We observed that the purified tubulin self-assembled into microtubules after increasing $[Mg^{2+}]$ to 5 m*M*, adding GTP to 1 m*M*, and raising the temperature to 37°C. One cycle of assembly and disassembly after the column step enriched for polymerization-active protein.
10. The sample (prepared and incubated as in Fig. 3A) was illuminated by a HeNe laser (15 mW, 632.8 nm) and was monitored at 90° to the incident beam. Intensity fluctuations detected by a quantum photometer (model 1140, Princeton Applied Research, Princeton, NJ) were correlated with a digital autocorrelator (model 1096, Langley-Ford Instruments, Amherst, MA). The resulting intensity autocorrelation functions were analyzed with a long-rod approximation developed specifically for systems such as microtubules (*3*). We determined microtubule lengths by using the exponential sampling method of Hallett and Keates (*4*), except that a nonnegative least squares routine [I. D. Morrison, E. F. Grabowsky, C. A. Herb, *Langmuir* **1**, 496 (1985)] was included in the fitting procedure. QELS-derived distributions have been verified with microtubule samples measured by electron microscopy (*4*). Typical length distributions were broad and highly skewed; a sample with a mean length of 16 μm contained components from 1 to over 60 μm.
11. R. A. Walker *et al.*, *J. Cell Biol.* **105**, 29a (1987).
12. S. W. Rothwell, W. A. Grasser, H. N. Baker, D. B. Murphy, *ibid.*, p. 863; M. Caplow, J. Shanks, B. P. Brylawski, *J. Biol. Chem.* **261**, 16233 (1986).
13. E. Schulze and M. W. Kirschner, *J. Cell Biol.* **104**, 277 (1987).
14. P. J. Sammak *et al.*, *ibid.*, p. 395.
15. We thank J. Marsh and C. Samuels for technical assistance. This work was supported by grants from the Natural Sciences and Engineering Research Council of Canada.

16 February 1988; accepted 13 July 1988

Accelerated Electron Transfer Between Metal Complexes Mediated by DNA

MICHAEL D. PURUGGANAN, CHALLA V. KUMAR, NICHOLAS J. TURRO,* JACQUELINE K. BARTON*

DNA-mediated long-range electron transfer from photoexcited 1,10-phenanthroline complexes of ruthenium, $Ru(phen)_3^{2+}$, to isostructural complexes of cobalt(III), rhodium(III), and chromium(III) bound along the helical strand. The efficiency of transfer depended upon binding mode and driving force. For a given donor-acceptor pair, surface-bound complexes showed greater rate enhancements than those that were intercalatively bound. Even in rigid glycerol at 253 K, the rates for donor-acceptor pairs bound to DNA remained enhanced. For the series of acceptors, the greatest enhancement in electron-transfer rate was found with chromium, the acceptor of intermediate driving force. The DNA polymer appears to provide an efficient intervening medium to couple donor and acceptor metal complexes for electron transfer.

AN UNDERSTANDING OF HOW ELECtrons are transferred over large distances is essential to the characterization of fundamental redox processes in biology such as oxidative phosphorylation and photosynthesis (*1*). The study of long-range electron transfer also contributes significantly to our ability to construct efficient molecular assemblies that can carry out electrochemical reactions. Studies of electron transfer between excited zinc porphyrins and heme centers in protein-protein complexes and between solvent accessible residues modified with pentammine ruthenium and the interior of structurally characterized metalloproteins have shown that electron transfer can occur over large distances through protein interiors (*2*, *3*). Theory indicates that such factors as donor-acceptor distance, thermodynamic driving force, and the nature of the intervening medium are critical in determining rates of electron transfer (*4*, *5*). Model compounds with variable exothermicity and distance between donor-acceptor pairs have been synthesized, and the rates of intramolecular electron transfer in these provide benchmarks for studies in more complex polymeric systems (*6*, *7*).

We report that the double-stranded DNA polymer may also mediate long-range electron transfer between bound donor-acceptor pairs. The apparent enhancement in photoinduced electron-transfer rates for donor-acceptor pairs bound to DNA versus being free in solution is several orders of magnitude (*8*, *9*). This apparent rate enhancement in the presence of DNA could be attributed to (i) the increase in local concentration of bound donor-acceptor pairs, (ii) facilitated diffusion of the bound pair along the DNA helix in a reduced dimensional space, and (iii) long-range electron transfer between donor and acceptor pairs with DNA as the intervening medium. By varying temperature, viscosity, and driving force, we show that DNA-mediated electron transfer from $Ru(phen)_3^{2+}$ to $M(phen)_3^{3+}$, where M = Rh, Cr, or Co, may occur, at least in part, through long-range electron transfer.

A current model for the interaction of tris(phenanthroline) metal complexes with DNA is shown in Fig. 1. The rigid metal complex, $Ru(phen)_3^{2+}$, appears to bind to double-stranded DNA primarily through two distinct modes: (i) intercalation, in which one of the phenanthroline ligands may insert and stack in between the base pairs, and (ii) surface or groove binding, in which the hydrophobicity of the phenanthroline ligands as well as the electrostatic charge of the ruthenium dication stabilize binding against the helical groove of the DNA polyanion (*10*, *11*). These binding modes have been characterized primarily through photophysical experiments, such as the differential quenching of two types of ruthenium excited states by anionic quenchers, the retention of polarized emission for the intercalative component when excited with polarized light, and the observation of two distinct lifetimes, 0.6 and 2.0 μs, for the surface-bound and intercalated ruthenium

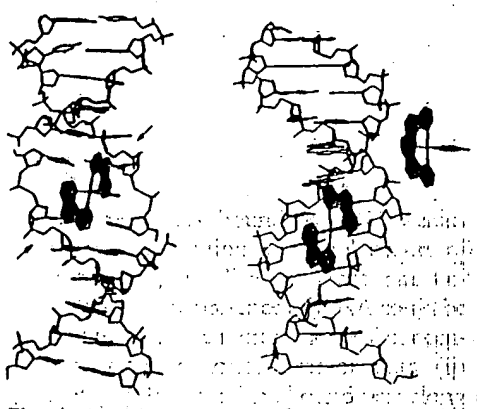

Fig. 1. Model for $Ru(phen)_3^{2+}$ bound to a B-DNA helix, showing (left) intercalation of the Δ-isomer and (right) the surface-binding of the Λ-isomer. For intercalated Δ-$Ru(phen)_3^{2+}$, the intercalated ligand is shown pointed into the page. The arrows indicate the alignment of the non-intercalated ligands along the right-handed helical groove. For the surface-bound Λ isomers, a side view (top) and front view (bottom, with the third ligand pointing out of the page) are shown.

Department of Chemistry, Columbia University, New York, NY 10027.

*To whom correspondence should be addressed.

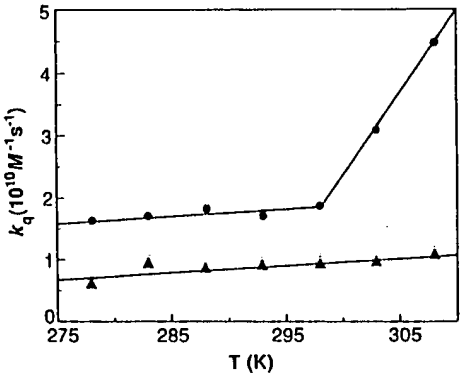

Fig. 2. Temperature dependence of the electron-transfer rate constants between (●) surface and (▲) intercalated DNA-bound donors and acceptors. The donor is Δ-Ru(phen)$_3^{2+*}$ and the acceptor is *rac*-Co(phen)$_3^{3+}$. Solution concentrations were as those described in Table 1. Lifetime measurements were made at least in triplicate.

excited states, respectively. Nuclear magnetic resonance and photophysical studies suggest that surface binding occurs from the minor groove of DNA, whereas intercalation of the complexes proceeds from the major groove. Although both enantiomers of the metal complexes bind to the helix through the two modes, opposite chiral selectivity is observed with these different binding modes. The right-handed propeller-like Δ-isomer intercalates preferentially into the right-handed B-DNA helix because of the reduced steric constraints between its nonintercalated ligands and the phosphate backbone, whereas for surface binding, where the complex lies against the right-handed helix, the Λ-isomer, which has a symmetry that complements that of the helix, is favored (*12*). The differing enantiomeric selectivities and the different excited state lifetimes for the two binding modes allow us to probe the effect of donor binding mode on electron transfer, since the photoinduced electron-transfer rate constants for the two modes may be separately determined in a time-resolved luminescence-quenching experiment by using DNA-bound cobalt, chromium, or rhodium complexes as electron acceptors.

Emission decays were determined for the ruthenium complexes by single-photon counting with a nanosecond flash lamp (full width at half maximum of 3 ns) as a function of titration with the electron acceptors M(phen)$_3^{3+}$ (M = Rh, Cr, and Co) and Co(bpy)$_3^{3+}$ (bpy = 2,2′-bipyridine). These electron acceptors, like the ruthenium complexes, bind to DNA noncovalently. For the phenanthroline series, intercalation and surface binding are possible, although Co(bpy)$_3^{3+}$ binds only electrostatically to the helix. The quenching mechanism with these donor-acceptor pairs is predominantly electron transfer. Evidence for electron transfer is supported by flash photolysis experiments. In addition, no Ru(phen)$_3^{2+}$-sensitized emission was observed from Cr(phen)$_3^{3+}$ or Rh(phen)$_3^{3+}$. Typical ruthenium concentrations used were 4 to 8 μ*M*, with ruthenium to nucleotide ratios ranging from 0.003 to 0.010, and acceptor concentrations varying from 0 to 80 μ*M*. Excited state lifetimes for both intercalative and surface-bound ruthenium were measured by deconvolution of the biexponential emission decay traces, and the rate constants were calculated for each component with the Stern-Volmer equation, $\tau_0/\tau = 1 + k_q\tau_0[Q]$, where τ is the lifetime of the luminescent species at quencher concentration [Q], τ_0 is the lifetime in the absence of quencher, and k_q is the bimolecular rate constant for quenching by photoinduced electron transfer (*13*). Since binding modes for the electron acceptors are not distinguished in this experiment, the analysis treats the acceptors as a single bound form.

Results of several quenching experiments with cobalt complexes as acceptors are summarized in Table 1. The electron-transfer rate constant from the surface-bound donor, k_q^s, is larger than k_q^i, the rate constant for electron transfer from the intercalatively bound species, for both Δ-Ru(phen)$_3^{2+}$ and Λ-Ru(phen)$_3^{2+}$. Small increases in the rate are apparent with Co(bpy)$_3^{3+}$, the nonintercalating and most weakly bound acceptor, in contrast to Co(phen)$_3^{3+}$. These results all point to a greater electron-transfer efficiency through surface rather than intercalative binding. In all cases, the rate constants for Λ-Ru(phen)$_3^{2+}$ are from 1.5 to 2 times greater than for Δ-Ru(phen)$_3^{2+}$, indicating enantiomeric selectivity. This observed stereoselectivity in electron-transfer rate constants is in contrast with the relative binding affinities of the complexes for DNA; phenanthroline complexes bind with greater affinity than bipyridyl complexes, and for Ru(phen)$_3^{2+}$, overall binding of the Δ-isomer is preferred. Enantiomeric selectivities for electron transfer that we observed differ from those reported previously, in which the donor-DNA ratio was much greater (1:30) (*8*). At the higher concentration ratios, the observed rate constants were governed largely by the local concentrations of donors and acceptors on DNA, and hence by relative binding strength. At low metal-DNA concentration ratios, nearly all of the donor molecules were bound, and the enhancements in electron-transfer rates, which are commensurately smaller, were not due to the effect of increased local concentrations. The observed stereoselectivity reflects fundamental differences in mechanisms for the electron transfer on DNA for the intercalated and surface-bound species, as well as their relative bound concentrations.

The fundamental differences between electron transfer from surface-bound and intercalated donors is even more dramatic upon examination of the temperature dependence of k_q^s and k_q^i with Δ-Ru(phen)$_3^{2+}$ as donor and Co(phen)$_3^{3+}$ as acceptor bound to DNA. The temperature dependence for these two cases is shown in Fig. 2. The surface-bound and intercalated Ru(phen)$_3^{2+*}$ behave quite differently with respect to electron transfer. The value of k_q^i increased little with temperature from 274 to 308 K. There was little variation in the value of k_q^s between 274 and 298 K, but above 298 K the quenching rate constant increased rapidly with increasing temperature. No change in DNA conformational state over this temperature range was detected by circular dichroism (CD). An Arrhenius plot of the data yields $\Delta H^{\ddagger}$ of ~2 kcal/mole for the intercalative electron transfer, and ~1 kcal/mole and ~16 kcal/mole for the two temperature regimes in the surface-bound case. Most simply, Fig. 2 provides verification of our model for intercalative and surface binding of tris(phenanthroline) metal complexes

Table 1. Electron-transfer rate constants (M^{-1} s^{-1}) from Δ- and Λ-Ru(phen)$_3^{2+}$ to *rac*-CoL$_3^{3+}$ (L = phen, bpy). The driving force for the excited-state electron-transfer quenching reaction is approximately +1.29 and +1.24 V with Co(phen)$_3^{3+}$ and Co(bpy)$_3^{3+}$ as quenchers, respectively (*20*). Samples were 4 μ*M* Ru(phen)$_3^{2+}$ and 1.2 m*M* calf thymus DNA in 50 m*M* NaCl and 5 m*M* tris buffer (pH 7.2). Lifetime measurements were made with a PRA single photon counting unit that used a Model 510 nitrogen-filled nanosecond flash lamp with a pulsewidth of 3 ns and interfaced with a Digital RX02 minicomputer. Excitation and emission wavelengths were at 447 and 600 nm, respectively. Data were deconvoluted with a PRA data analysis package. The rate constants k_q^s, k_q^i, and k_q^c are for the surface-bound and intercalated donor on DNA, and free donor in solution, respectively. The average errors in rate constants are approximately ±20%. The control data were obtained with *rac*-Ru(phen)$_3^{2+}$ donor in the absence of DNA.

Donor	Acceptor					
	rac-Co(phen)$_3^{3+}$			*rac*-Co(bpy)$_3^{3+}$		
	k_q^s	k_q^i	k_q^c	k_q^s	k_q^i	k_q^c
Δ-Ru(phen)$_3^{2+}$	1.7×10^{10}	9.0×10^{9}	1.4×10^{9}	2.4×10^{10}	1.2×10^{10}	2.0×10^{9}
Λ-Ru(phen)$_3^{2+}$	3.9×10^{10}	1.6×10^{10}	1.4×10^{9}	4.7×10^{10}	1.7×10^{10}	2.0×10^{9}

to DNA, and also indicates that at least two distinct mechanisms for DNA-mediated electron transfer between bound metal complexes must operate.

In order to minimize collisional pathways for electron transfer, and thus distinguish between diffusion and long-range electron-transfer mechanisms, we also used high-viscosity glycerol solutions in a series of quenching experiments. The CD spectra of DNA solutions at these glycerol concentrations indicated no gross change in conformation from the B-form (*14*). At low temperature ($T < 273$ K), these solutions are sufficiently rigid to significantly reduce molecular transport (*15*). The local viscosity around the metal complexes when bound to DNA might be different from the bulk viscosity. However, a significantly lowered viscosity relative to the bulk would be required over many solvent layers, because of the diameters of the metal complexes themselves, to permit diffusion. Moreover, binding to DNA appears in itself to diminish the mobility of the complex, rather than increasing its mobility, as would be required for a diffusion mechanism. For example, the steady-state luminescence polarization for $Ru(phen)_3^{2+}$ in 90% glycerol solution at 293 K is increased from 0.001 to 0.103 (both values ±0.002 SEM) in the presence of DNA; the limiting polarization for $Ru(phen)_3^{2+}$ in a solid matrix is 0.14 (*16*). With decreasing temperature, still greater decreases in the mobility of the bound complex would be expected. Quenching results for ruthenium-cobalt pairs in glycerol solutions are summarized in Table 2. The rate for intercalated donors decreases by a factor of 5 upon the addition of glycerol, and no further with increasing viscosity. The value of k_q^s remains constant at $\sim 2 \times 10^{10} M^{-1}$ s^{-1}, even in the highest viscosity regime at low temperature. With $Co(bpy)_3^{3+}$ as a surface-bound acceptor, no decrease in surface-bound rate was apparent even at high glycerol concentrations and low temperature. Thus, under conditions where diffusion is restricted, DNA-mediated electron transfer remained enhanced compared with rates in the absence of DNA. For the surface-bound donor, in particular, the rate constant was two orders of magnitude greater compared with solution rates, and this enhancement could be increased even further if higher donor-DNA ratios were used.

That DNA accelerates electron transfer between bound metal complexes under conditions of substantially restricted mobility is illustrated further in Fig. 3, in which the quenching of $Ru(phen)_3^{2+*}$ by $Co(phen)_3^{3+}$ is plotted for the surface-bound component, the intercalated component, and for DNA-free solutions, in 92% glycerol at 253 K. The linearity of the plots supports the notion that the complexes are randomly distributed along the strand with no sequestering or cooperative association of the complexes on the polymer (*17*). In this essentially rigid system with low concentrations of donors and acceptors on the DNA (at these concentrations, the average separation between metal centers is in the range of 15 to 35 Å), surface-bound and, to a lesser extent, intercalated $Ru(phen)_3^{2+*}$ continue to transfer electrons to bound $Co(phen)_3^{3+}$, indicating that DNA promotes long-distance electron transfer between bound donors and acceptors. In the absence of DNA, the rate drops to below $10^7 M^{-1}$ s^{-1}, too low to be measured satisfactorily with this technique.

The logarithm of the decay trace for emission from the ruthenium excited state in the absence of DNA, in the presence of DNA, and with DNA and 32 μ*M* $Cr(phen)_3^{3+}$ at 253 K in glycerol solution is shown in Fig. 4. As for higher temperature experiments, in the absence of DNA a single exponential decay was observed. Upon addition of DNA, a biexponential decay was apparent, consistent with the two binding modes, and with the addition of $Cr(phen)_3^{3+}$, quenching by electron transfer was observed for the two components. The shorter lived surface-bound component was quenched appreciably faster than the long-lived component. Since the metal complexes, although fixed on the strand, are separated by a range of

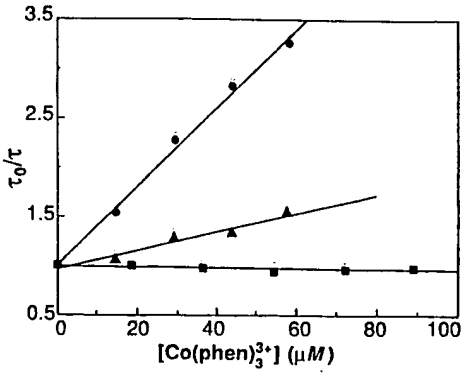

Fig. 3. Stern-Volmer plot of *rac*-$Ru(phen)_3^{2+}$ quenching by *rac*-$Co(phen)_3^{3+}$ in rigid glycerol solution (92% glycerol) at 253 K. Measurements were done with 4 μ*M* of $Ru(phen)_3^{2+}$ and 400 μ*M* of calf thymus DNA (●, surface, and ▲, intercalated), with the DNA excluded in the control experiments (■). Lifetime measurements were done in triplicate.

nearest-neighbor distances, the simple biexponential decays in emission were somewhat unexpected. The well-behaved binding isotherms, the absence of ruthenium self-quenching, and the high positive charges on both donors and acceptors all indicate that there was no clustering of metal complexes at the closest possible separation distance (4 base pairs), and thus a very shortlived component in emission corresponding to the particular contribution of donor acceptor reactions at the very closest distance was not observed. However, if the distribution of nearest-neighbor distances of donors and acceptors is broad (even for one type of donor), as occurs in a random distribution of donors and acceptors fixed in three-dimensional space, one might still expect a nonexponential decay in emission from the donor species (*18*). We determined the probability distribution for donors and acceptors fixed in one dimension along the DNA lattice (*19*) based upon equilibrium binding isotherms, previously obtained (*10*), which showed the metal complexes to be randomly distributed over 4-base-pair sites. Using this probability distribution of acceptor distances, we then calculated the expected sum of exponential decays in donor emission expected. We found that this sum of exponentials may be reasonably approximated by a single exponential in emission using the mean nearest-neighbor separation. Calculated decay traces based upon our probability distribution showed only a slight deviation from a single exponential, a deviation too small to be detected experimentally. Moreover, the best line fit through these calculated traces yielded donor lifetimes within 10% of experimental value. The good fit and close approximation of the sum of exponentials to a single exponential decay

Table 2. Electron-transfer rate constants in viscous media. Solutions were 4 μ*M* $Ru(phen)_3^{2+}$ and 400 μ*M* calf thymus DNA for measurement of k_q^s and k_q^i, and with no DNA for k_q^c. Average errors in the ratio constants are approximately 20%.

Acceptor	Conditions			Rate constants		
	Glycerol content (%)	Temperature (K)	η (cP)	$k_q^s \times 10^{10}$ (M^{-1} s^{-1})	$k_q^i \times 10^{10}$ (M^{-1} s^{-1})	$k_q^c \times 10^{10}$ (M^{-1} s^{-1})
$Co(phen)_3^{3+}$	0*	274	1.8	1.7	0.9	0.15
$Co(phen)_3^{3+}$	60	274	25	1.6	0.2	0.03
$Co(phen)_3^{3+}$	84	274	349	1.8	0.2	0.04
$Co(bpy)_3^{3+}$	84	274	349	2.4	0.2	0.02
$Co(phen)_3^{3+}$	92	253	12,163	2.4	0.2	(<0.001)†

*Data from Δ-$Ru(phen)_3^{2+}$ donor. †Too low to be measured by SPC lifetime quenching.

may be a function both of the fact that the distribution is over a one-dimensional lattice (with a reduced number of nearest neighbors compared with that in multidimensional space) and the fact that there may be a weak dependence of rate on distance.

The application of transition metal complexes to these electron-transfer studies makes varying the thermodynamic driving force and examining the effect of such variation on the electron-transfer rate convenient. If reactions between the metal complexes were diffusion limited, then little sensitivity in electron-transfer rate to free energy change between donor and acceptor would be expected. Table 3 shows electron-transfer rates for photoinduced electron transfer from $Ru(phen)_3^{2+*}$ to phenanthroline complexes of Rh, Cr, and Co in the presence of DNA in glycerol solutions at 293 and 253 K. In the absence of DNA at 298 K, with $Ru(phen)_3^{2+*}$ as donor and the acceptors $Rh(phen)_3^{3+}$, $Cr(phen)_3^{3+}$, and $Co(phen)_3^{3+}$, ΔE^0 is estimated to be 0.22, 0.64, and 1.29 V, respectively (*20*). In accord with Marcus theory, for this range of driving forces in the absence of DNA, the electron-transfer rate constants increase with increasing driving force (*21*). In the presence of DNA, however, the rate constants vary substantially with driving force and not as expected. The ratios of rate constants in the presence of DNA to the absence of DNA at 293 K with a surface-bound Ru donor and Cr or Rh acceptor are ~250 and ~50, respectively. At 253 K in rigid medium, for the series of acceptors $Co(phen)_3^{3+}$, $Cr(phen)_3^{3+}$, and $Rh(phen)_3^{3+}$, the electron-transfer rate constants with surface-bound $Ru(phen)_3^{2+*}$ are 2.4×10^{10}, 5.0×10^{10}, and $0.14 \times 10^{10} M^{-1}\ s^{-1}$, respectively. For intercalated $Ru(phen)_3^{2+*}$, enhancements vary similarly. This variation in enhancement for the series of metal complexes indicates that the accelerated rates on DNA cannot be a local concentration effect. The different $M(phen)_3^{3+}$ complexes bind equally well to DNA. Furthermore, DNA-facilitated diffusion cannot account for the enhancements, since the greatest change should be seen for the diffusion-limited Co acceptor, with relatively reduced enhancements for those reactions of lesser driving force. These variations in rate constant with free energy based upon a simple adiabatic reaction between the metal complexes are difficult to interpret with Marcus theory based on solvent reorganization energies for systems free in solution. Binding to DNA may alter these reorganization energies. In addition, the large rate enhancements seem to require that the DNA serves as an intervening medium, one which facilitates the electron transfer (*22*). The remarkable rate enhancement evident with $Cr(phen)_3^{3+}$ as acceptor may indicate a particularly close matching of the electronic states of DNA coupling the excited donor to the Cr complex.

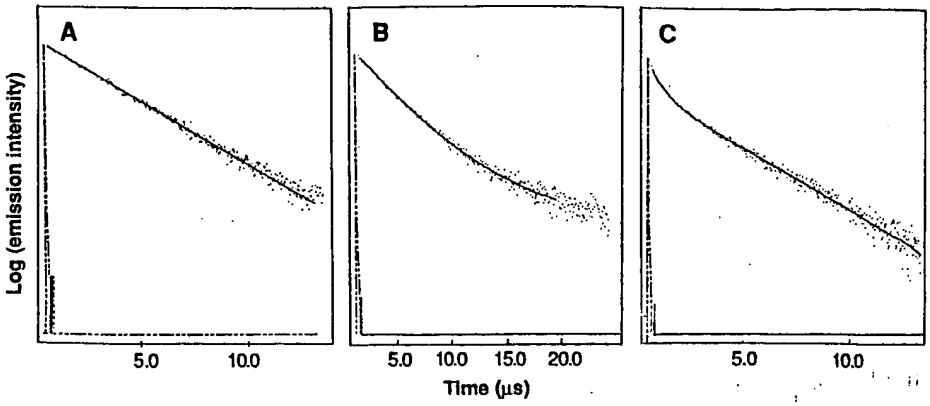

Fig. 4. Logarithmic decay traces obtained by single-photon counting for emission from $Ru(phen)_3^{2+*}$ at 253 K in 90% glycerol (**A**) in the absence of DNA, (**B**) in the presence of 600 μ*M* DNA and 4 μ*M* $Ru(phen)_3^{2+}$, and (**C**) with 480 μ*M* DNA and 32 μ*M* $Cr(phen)_3^{3+}$.

Table 3. Electron-transfer rate constants with $Ru(phen)_3^{2+*}$ as donor, illustrating variations with thermodynamic driving force. For an explanation of the determination of ΔE^0 in the absence of DNA, see (*20*). Average errors are approximately 20%. Solutions with DNA contained 4 μ*M* $Ru(phen)_3^{2+}$ and 600 μ*M* calf thymus DNA.

Acceptor	Temperature (K)	ΔE^0 (V)	Rate constants ($M^{-1}\ s^{-1}$)		
			$k_q^c \times 10^{10}$	$k_q^s \times 10^{10}$	$k_q^l \times 10^{10}$
		No DNA or glycerol			
$Co(phen)_3^{3+}$	293	1.29	0.14		
$Cr(phen)_3^{3+}$	293	0.64	0.05		
$Rh(phen)_3^{3+}$	293	0.22	0.02		
		DNA and 90% glycerol			
$Cr(phen)_3^{3+}$	293			11.7	0.96
$Rh(phen)_3^{3+}$	293			0.8	0.17
$Co(phen)_3^{3+}$	253		<0.001*	2.4	0.2
$Cr(phen)_3^{3+}$	253			5.0	0.64
$Rh(phen)_3^{3+}$	253			0.14	0.086

*Too low to be measured by SPC lifetime quenching.

Enhancements in diffusion-limited reaction rates for processes that occur on macromolecules have been reasonably attributed to enhanced diffusion of the reactants along the macromolecular surface (*23*). In several systems involving DNA-binding proteins, reductions in the dimensionality of space in which the reaction occurs can increase the rate by several orders of magnitude (*24, 25*). We initially thought that such one-dimensional diffusion along the DNA would also account primarily for the enhancements in DNA-mediated quenching rate between bound donor-acceptor pairs, as described here. Such a mechanism for slipping along the strand may serve, at least in part, to enhance the rates of DNA-bound electron transfer at higher temperatures.

Experiments in rigid solution and with variations in driving force, however, point to another mechanism for DNA-mediated electron transfers. The persistence of enhanced reaction rates upon binding to DNA under conditions sufficient to minimize the translational motion of the bound species indicates that long-range electron transfer may proceed through the DNA. Surprisingly, the more mobile surface-bound ruthenium complex appears to promote long-range transfer with greater efficiency than the intercalated species, despite the proximity of the latter to the extensive π framework of the stacked bases. This difference in electron transfer for the two bound forms may result in part from the differing orientations of the bound species on the DNA strand. Additionally, the results suggest that the sugar-phosphate backbone may play a significant role in electron transport (*26*). The solvent medium, oriented by the DNA polyanion, may provide a particularly low barrier for tunneling (*27*). The strong electronic coupling may also be a consequence of the accessibility of low-lying excited states on the DNA. The sensitivity of the rate to thermodynamic driving force supports this notion. Thus the efficiency of electron transfer depends upon binding mode, that is, orientation of donor and acceptor on the polymer, as well as upon the electronic states

of donor and acceptor, and how well these electronic states couple with the intervening DNA. It is not clear that nature has taken advantage of the DNA polymer as a mediator of electron transfer, but in fact oligonucleotides and polynucleotides should serve well as vehicles that may be readily manipulated to examine systematically the effects of medium, orientation, and separation distance on electron transfer in a polymeric system.

REFERENCES AND NOTES

1. D. Devault, *Q. Rev. Biophys.* **13**, 387 (1980).
2. S. L. Mayo, W. R. Ellis, R. J. Crutchley, H. B. Gray, *Science* **233**, 948 (1986); S. S. Isied, *Prog. Inorg. Chem.* **32**, 443 (1984).
3. J. L. McGourty, W. V. Blough, B. M. Hoffman, *J. Am. Chem. Soc.* **105**, 4472 (1983); N. Liang, C. H. Kang, P. S. Ho, E. Margoliash, B. M. Hoffman, *ibid.* **108**, 4665 (1986); K. P. Simolo, G. L. McLendon, M. R. Mauk, A. G. Mauk, *ibid.* **106**, 5012 (1984); G. L. McLendon and J. R. Miller, *ibid.* **107**, 7811 (1985).
4. J. J. Hopfield, *Proc. Natl. Acad. Sci. U.S.A.* **71**, 3640 (1974); M. Redi and J. J. Hopfield, *J. Chem. Phys.* **72**, 6651 (1980).
5. R. A. Marcus, *Annu. Rev. Phys. Chem.* **15**, 155 (1964); *J. Phys. Chem.* **72**, 891 (1968); R. A. Marcus and N. Sutin, *Biochim. Biophys. Acta* **811**, 265 (1985).
6. G. L. Closs, L. T. Calcaterra, N. J. Green, K. W. Penfield, J. R. Miller, *J. Phys. Chem.* **90**, 3673 (1986).
7. A. D. Joran, B. A. Leland, G. G. Geller, J. J. Hopfield, P. B. Dervan, *J. Am. Chem. Soc.* **106**, 6090 (1984); A. D. Joran *et al.*, *Nature* **327**, 508 (1986).
8. J. K. Barton, C. V. Kumar, N. J. Turro, *J. Am. Chem. Soc.* **108**, 6391 (1986).
9. P. Fromherz and B. Rieger, *ibid.*, p. 5361.
10. J. K. Barton, A. T. Danishefsky, J. M. Goldberg, *ibid.* **106**, 2172 (1984).
11. C. V. Kumar, J. K. Barton, N. J. Turro, *ibid.* **107**, 5518 (1985); J. K. Barton, J. M. Goldberg, C. V. Kumar, N. J. Turro, *ibid.* **108**, 2081 (1986); J. Rehmann, thesis, Columbia University, New York (1988).
12. J. K. Barton, *Science* **233**, 727 (1986).
13. N. J. Turro, *Modern Molecular Photochemistry* (Benjamin-Cummings, Menlo Park, CA, 1978), p. 246.
14. R. B. Macgregor, R. M. Clegg, T. M. Jovin, *Biochemistry* **26**, 4008 (1987); V. I. Ivanov, L. E. Minchenkova, A. Schyolkina, A. I. Poletayev, *Biopolymers* **12**, 89 (1973). The ratio of intercalation to surface binding of $Ru(phen)_3^{2+}$ does increase appreciably with glycerol present in solution. Thus it is likely that $Co(phen)_3^{3+}$ exists also predominantly in the intercalated form under these conditions.
15. T. Guarr, M. Mcguire, S. Strauch, G. McLendon, *J. Am. Chem. Soc.* **105**, 616 (1983). Under these conditions, the bulk viscosity is estimated to be 1.2×10^4 cP, and the calculated diffusion distance for the metal complexes not bound to DNA would be approximately 4 Å during the lifetime of the donor excited state.
16. I. Fujita and H. Kobayashi, *Inorg. Chem.* **12**, 2758 (1973).
17. The absence of self-quenching of the ruthenium excited state further supports this assumption.
18. M. Inokuti and F. Hirayama, *J. Chem. Phys.* **43**, 1978 (1965).
19. The distribution of separation distances was calculated with the nearest-neighbor distance distribution for a "hard rod gas" distributed randomly over a one-dimensional lattice

$$P(r)dr = \frac{N}{[L(1 - N\sigma/L)]} \times \left[1 - \frac{(r - \sigma)}{[L(1 - N\sigma/L)]}\right]^{N-1} dr, \quad r \geq \sigma$$

where N is the number of bound particles with an exclusion length σ bound to a lattice of length L. In our case, L is 200 base pairs, σ is 4 base pairs per bound molecule, and N is the sum of donor and acceptors. The mean distance, $\langle r \rangle$, is

$$\langle r \rangle = \Sigma r P(r)/\Sigma P(r)$$

See L. Tonks, *Phys. Rev.* **50**, 955 (1936).
20. Driving forces were calculated based upon data reported in the following references: B. Brunschwig and N. Sutin, *J. Am. Chem. Soc.* **100**, 7568 (1978); S.-F. Chen *et al.*, *ibid.* **103**, 369 (1981); E. Paglia and C. Sironi, *Gazz. Chim. Ital.* **87**, 1125 (1957).
21. In buffer at 293 K in the absence of DNA, the rates with either Cr or Co as acceptor appear to be diffusion controlled based upon measurements at different ionic strengths, whereas the reaction with Rh, having a substantially smaller free energy change, is activation limited.
22. Results that vary in this fashion with driving force may be interpreted in terms of donor-acceptor pairs in the Marcus inverted region. For these experiments, however, the DNA would still be involved in mediating such transfer. In a model system, the possible role of virtual states of an intervening π-electron system has been discussed. See H. Heitele and M. E. Michel-Beyerle, *J. Am. Chem. Soc.* **107**, 8286 (1985).
23. G. Adams and M. Delbruck, in *Structural Chemistry and Molecular Biology*, A. Rich and N. Davidson, Eds. (Freeman, San Francisco, 1968), p. 198; P. Richter and M. Eigen, *Biophys. Chem.* **2**, 255 (1974).
24. O. G. Berg, R. B. Winter, P. H. von Hippel, *Biochemistry* **20**, 6929 (1981).
25. B. J. Terry, W. E. Jack, P. Modrich, *J. Biol. Chem.* **260**, 13130 (1985).
26. Theoretical studies have actually noted that some charge transfer from the ribose units along the DNA backbone to the bases may occur, creating what is essentially a substantial hole framework on the DNA backbone. See P. Otto, E. Clementi, and J. Ladik [*J. Chem. Phys.* **78**, 454 (1983)] and E. Clementi and G. Corongiu [*Int. J. Quant. Chem. Quant. Biol. Symp.* **9**, 213 (1982)].
27. Replacing the NaCl in our buffer with 30 m*M* $MgCl_2$, which may perturb the solvent structure around the helix, causes a decrease for k_q^1 to $7 \times 10^9 M^{-1}\ s^{-1}$, with k_q^1 remaining constant.

28. We thank B. Berne for stimulating discussions regarding the near-neighbor distance distributions. Supported by National Science Foundation and the Army Office of Research.

14 April 1988; accepted 26 July 1988

Imaging of Phosphorescence: A Novel Method for Measuring Oxygen Distribution in Perfused Tissue

WILLIAM L. RUMSEY,* JANE M. VANDERKOOI, DAVID F. WILSON

The imaging of phosphorescence provides a method for monitoring oxygen distribution within the vascular system of intact tissues. Isolated rat livers were perfused through the portal vein with media containing palladium coproporphyrin, which phosphoresced and was used to image the liver at various perfusion rates. Because oxygen is a powerful quenching agent for phosphors, the transition from well-perfused liver to anoxia (no flow of oxygen) resulted in large increases of phosphorescence. During stepwise restoration of oxygen flow, the phosphorescence images showed marked heterogeneous patterns of tissue reoxygenation, which indicated that there were regional inequalities in oxygen delivery.

IN MAMMALIAN TISSUES, OXYGEN MUST be continuously supplied to maintain cellular homeostasis. Even moderate reductions of blood flow compromise physiological function. In order to investigate the nature of oxygen supply to tissue in detail, a method is needed for the accurate measurement of the concentration of oxygen at its site of transfer from the vascular bed to parenchymal cells. Methods that have been used to assess tissue oxygenation not only have individual technical problems but in general are weakened by their inflexibility. For example, oxygen microelectrodes are not always suitable because (i) they are restricted to specific locations within the tissue, thereby preventing evaluation of a large area, and (ii) they must be inserted into the tissue, which disturbs its local environment.

Recently we developed a method for measuring oxygen that is based on its ability to quench phosphorescence of selected lumiphores (*1*, *2*). This method is accurate and provides precise serial measurements of oxygen in the physiological range, from $10^{-3}M$ to less than $10^{-8}M$. To date, however, this methodology has been restricted to the in vitro study of biological samples that can be placed in a cuvette, such as suspensions of isolated mitochondria (*3*) and cells (*4*). We have shown that phosphorescence measurements can be used to obtain images of oxygen distribution in tissue without invasion of that tissue. Inhomogeneities of oxygen delivery to tissue of isolated perfused rat liver have been demonstrated with a video camera, which detects the phosphorescence of palladium (Pd)-coproporphyrin in the tissue perfusate.

When the tissue is illuminated, some light is absorbed by the Pd-coproporphyrin, which excites it to the triplet state. The

Department of Biochemistry and Biophysics, University of Pennsylvania School of Medicine, Philadelphia, PA 19104.

*To whom correspondence should be addressed.

Long-Range Photoinduced Electron Transfer Through a DNA Helix

C. J. Murphy, M. R. Arkin, Y. Jenkins, N. D. Ghatlia, S. H. Bossmann, N. J. Turro, J. K. Barton*

Rapid photoinduced electron transfer is demonstrated over a distance of greater than 40 angstroms between metallointercalators that are tethered to the 5′ termini of a 15–base pair DNA duplex. An oligomeric assembly was synthesized in which the donor is $Ru(phen)_2dppz^{2+}$ (phen, phenanthroline, and dppz, dipyridophenazine) and the acceptor is $Rh(phi)_2phen^{3+}$ (phi, phenanthrenequinone diimine). These metal complexes are intercalated either one or two base steps in from the helix termini. Although the ruthenium-modified oligonucleotide hybridized to an unmodified complement luminesces intensely, the ruthenium-modified oligomer hybridized to the rhodium-modified oligomer shows no detectable luminescence. Time-resolved studies point to a lower limit of 10^9 per second for the quenching rate. No quenching was observed upon metallation of two complementary octamers by $Ru(phen)_3^{2+}$ and $Rh(phen)_3^{3+}$ under conditions where the phen complexes do not intercalate. The stacked aromatic heterocycles of the DNA duplex therefore serve as an efficient medium for coupling electron donors and acceptors over very long distances.

Experiments in many laboratories have focused recently upon measurements of electron transfer rates between metal centers over long distances in proteins or protein pairs as a function of distance, driving force, and the intervening medium (*1*). Model complexes have also been prepared to explore systematically how different structural and electronic factors may mediate electron transfer reactions (*2*), and theories exploring optimal pathways for electron transfer have been devised to reconcile experimental studies (*3*). Among the many ideas put forth concerning how the medium may serve to modulate or direct electron transfer has been the notion that aromatic groups could serve as efficient "π-ways" over which electron transfer reactions might be promoted efficiently, yet few experimental measurements of electron transfer through π-stacks have been accomplished (*4*).

The DNA helix provides a novel medium through which to examine electron transfer processes (*5–8*) and, in particular, electron transfer through π-stacks. The DNA helix may be considered a polymer which contains a rigid, electronically coupled aromatic column of stacked base pairs within a water-soluble polyanion, the sugar-phosphate backbone. The DNA helix enhances rates of electron transfer between donors and acceptors which associate with DNA (*6–8*). Factors contributing to this enhancement include: (i) the effects of increased local concentration of the bound species; (ii) facilitated diffusion of the noncovalently bound species along the duplex; as well as (iii) the possibility of electron transfer at long range being mediated by the π-stack. In these systems, however, a multiplicity of binding sites of donors and acceptors on the helix makes it difficult to evaluate how each of these factors contribute to the overall rate.

In this report we demonstrate rapid photoinduced electron transfer over distances >40 Å between metallointercalators that are tethered to the 5′ termini of a 15–base pair (bp) DNA duplex. Intercalation of the donors and acceptors provides an interaction that can directly probe the nature of the purported π-way in DNA, and covalent attachment of one metal complex to each end of the helix permits measurements of quenching rates with discrete, well-defined species.

Both donor and acceptor bind to double-helical DNA by intercalation with affinities of $\geq 10^6\ M^{-1}$ (*9*, *10*). The donor, photoexcited bis(phenanthroline)(dipyridophenazine)ruthenium(II), $Ru(phen)_2dppz^{2+}$, shows no luminescence in aqueous solution, but luminesces intensely in the presence of DNA because intercalation of the dppz ligand protects the phenazine nitrogen atoms from quenching by water (*9*). The acceptor is bis(9,10-phenanthrenequinone diimine)(phenanthroline)rhodium(III), $Rh(phi)_2phen^{3+}$. Rh(III) complexes containing phi also bind tightly to nucleic acids via intercalation of this ligand (*10–12*). Two-dimensional nuclear magnetic resonance experiments provide direct evidence for specific intercalation by $Rh(phen)_2phi^{3+}$ in an oligonucleotide (*11*). Phi complexes of Rh(III), furthermore, promote DNA and RNA strand cleavage upon photoactivation (*12–14*). The electronic characteristics of these complexes are also well suited to this study. The lowest excited state (*) of $Ru(phen)_2dppz^{2+}$ is a metal-to-ligand charge transfer transition centered on the dppz ligand, and the luminescence observed in nonaqueous solvents can be quenched by electron acceptors (*15*). Likewise, the lowest excited state of $Rh(phi)_2phen^{3+}$ contains ligand-to-metal charge transfer character from the phi ligand (*16*), permitting an arrangement where

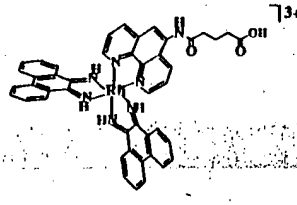

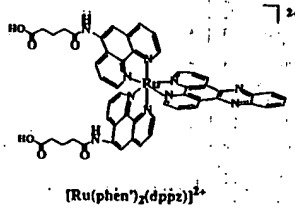

Fig. 1. Structures of the donor and acceptor complexes, $Ru(phen')_2dppz^{2+}$ and $Rh(phi)_2phen'^{3+}$, and schematic illustration of the doubly modified oligonucleotide showing the 34 Å interbase pair separation and the shortest donor-acceptor distance of 41 Å.

C. J. Murphy, M. R. Arkin, Y. Jenkins, J. K. Barton, Beckman Institute, California Institute of Technology, Pasadena, CA 91125.
N. D. Ghatlia, S. H. Bossmann, N. J. Turro, Department of Chemistry, Columbia University, New York, NY 10027.

*To whom correspondence should be addressed.

photoinduced electron transfer may be directed from the Ru(II) donor to the Rh(III) acceptor through the DNA helix (Fig. 1).

Luminescence quenching experiments with these metallointercalators in the presence of DNA indicate that $Rh(phi)_2phen^{3+}$ is an unusually efficient quencher of $Ru(phen)_2dppz^{2+*}$ emission (*17*). In experiments on the nanosecond time scale in the presence of DNA, static quenching of $Ru(phen)_2dppz^{2+*}$ emission by $Rh(phi)_2phen^{3+}$ contrasts the dynamic quenching of $Ru(phen)_2dppz^{2+*}$ by $Ru(NH_3)_6^{3+}$, which binds DNA through hydrogen bonding in the groove. These experiments with metallointercalators noncovalently associated with DNA have provided the impetus for synthesizing a well-defined electron transfer assembly with the donor and acceptor bound to the DNA at a discrete distance.

Oligonucleotides were metallated at their 5′ terminus by coupling of a 15-mer functionalized with a hexamethylene amine at its 5′ terminus to either $Ru(phen')_2dppz^{2+}$ (phen′ = 5-amido–glutaric acid–1,10-phenanthroline) (*18*) or $Rh(phi)_2(phen')^{3+}$ (*19–21*). Modeling studies suggested the ability of the tethered complexes to intercalate 2 bp in from the 5′ end of the metallated strand. The relative rigidity of a 15-bp double helix eliminates the possibility of collisions between metal complexes tethered to the same duplex even in the absence of intercalation.

Intercalation into the duplex by the covalently attached Ru complex may be monitored by observing the intense luminescence of the Ru-modified oligomer annealed to its complement. The Ru-modified oligonucleotide, without complement or in the presence of noncomplementary single-stranded DNA, displays little luminescence (*18*). Dilution studies have been consistent with intramolecular intercalation by the covalently attached Ru complex at concentrations ≤5 μM. Hybridization studies with mismatched complementary strands show that the covalently bound Ru complex preferentially stabilizes base mismatches near the site of covalent attachment, supplying additional evidence for intramolecular intercalation and underscoring the strong binding of the dppz ligand to DNA. All experiments reported here were accomplished at micromolar concentrations in the presence of 50 mM NaCl, conditions which strongly disfavor intermolecular aggregation.

Luminescence titrations of the ruthenated duplex with additional free $Ru(phen)_2dppz^{2+}$ demonstrate that the ruthenated duplex behaves as a 15-mer bearing one intercalator. As free $Ru(phen)_2dppz^{2+}$ is added to a solution of ruthenated 15-mer duplex (Fig. 2), the luminescence increases linearly until the emission reaches saturation at a ratio of 1.8 equivalents of free Ru(II) per duplex. Saturation of luminescence at this relative concentration is consistent with competitive binding of Ru complexes to the 15-mer duplex and an average binding site size of ~5 bp (*22*). When the analogous experiment is conducted with unmetallated duplex, saturation of luminescence occurs after 2.8 equivalents of $Ru(phen)_2dppz^{2+}$ are added. This comparison indicates that: (i) the metallated duplex is properly annealed, because an incompletely hybridized oligonucleotide would offer fewer binding sites for additional intercalators; and (ii) the covalently bound Ru complex is not ejected by the added intercalators. The DNA binding affinities of phi complexes of Rh(III) are somewhat lower than that of $Ru(phen)_2dppz^{2+}$ (*9*, *23*); consequently, $Rh(phi)_2phen^{3+}$ and its covalent analog are even less likely to displace the covalently bound Ru complex. Furthermore, photocleavage studies in which a 28-mer oligonucleotide duplex is cleaved by $Rh(phi)_2phen^{3+}$ in the presence and absence of $Ru(phen)_2dppz^{2+}$ indicate that the two complexes do not bind cooperatively (*17*); no change in the distribution of Rh(III) cleavage is observed in the presence of Ru complex.

Hybridization of the Rh-modified oligonucleotide to its unmodified complement permits the determination of the position of

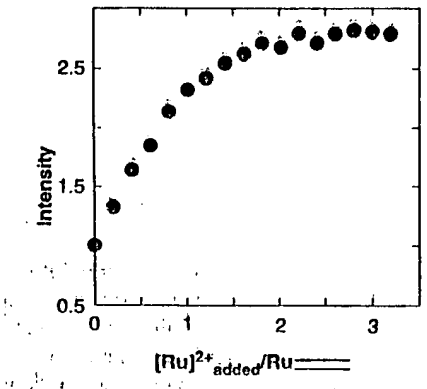

Fig. 2. Luminescence titration of 5 μM Ru-modified duplex with free $Ru(phen)_2dppz^{2+}$. $Ru(II)^*$ emission increases linearly, indicative of independent binding by the tethered and free metal complexes, until saturation. Luminescence intensity saturates at 1.8 eq of added $Ru(phen)_2dppz^{2+}$, showing that the covalently bound complex is not displaced by the added intercalators. The covalently ruthenated duplex behaves as an oligomer containing one bound intercalator.

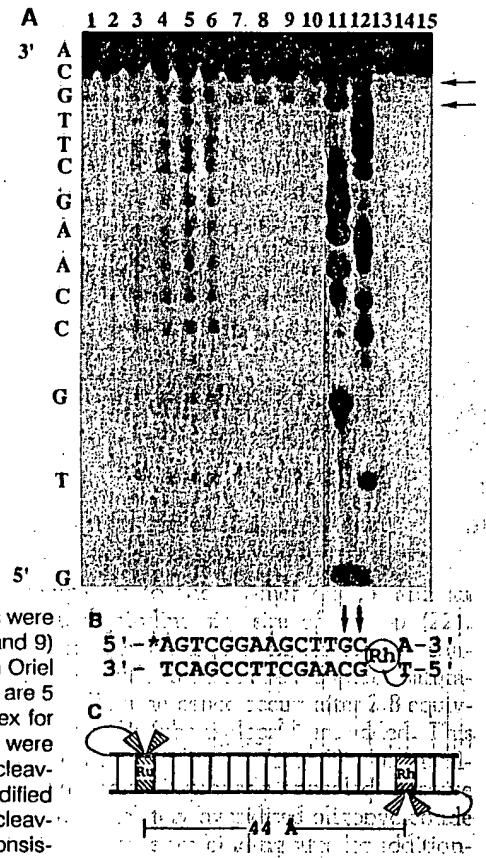

Fig. 3. Determination of the position of intercalators on the helix and separation distances between bound donors and acceptors. (**A**) Autoradiograph of a 20% polyacrylamide denaturing gel showing cleavage by covalently and noncovalently bound Rh. Lanes 1 and 2 and 7 to 10 show cleavage of *5′-AGTCGGAAGCTTGCA-3′ by $Rh(phi)_2phen'^{3+}$ covalently linked to the complementary strand. The intercalated Rh complex cleaves primarily 1 and 2 bp from the 5′ end to which it is covalently bound. Lanes 3 to 6 show the nonspecific cleavage by noncovalent $Rh(phi)_2phen^{3+}$ of the unmodified oligonucleotide. Lanes 13, 14, and 15 show labeled oligonucleotide irradiated without metal complex, the labeled oligonucleotide in the presence of $Rh(phi)_2phen^{3+}$ but without irradiation, and the labeled oligonucleotide after hybridization to the Rh-modified strand but without irradiation, respectively. Lanes 11 and 12 are Maxam-Gilbert sequencing reactions for G + A and C + T, respectively. Oligonucleotides were ^{32}P-labeled at the 5′ end with T4 polynucleotide kinase and annealed either to unmodified or Rh-modified complement. Samples were irradiated at 313 nm for 5 min (lanes 1, 3, 5, 7, and 9) and 7.5 min (lanes 2, 4, 6, 8, 10, and 13) with an Oriel model 6140, 1000W Hg-Xe lamp. Concentrations are 5 μM in duplex for lanes 1 to 4 and 1 μM in duplex for lanes 5 to 10. Varying amounts of radioactivity were loaded in order to emphasize the distribution of cleavage sites. (**B**) Schematic of duplex covalently modified at one end by $Rh(phi)_2phen'^{3+}$, showing sites of cleavage on the complementary strand. Cleavage is consistent with intramolecular intercalation of the Rh complex at interbase pair sites 1 or 2 bp in from the covalent linkage. (**C**) Schematic of the doubly modified duplex, showing a separation distance of the donor and acceptor. If we assume that both the Rh and the Ru complex can intercalate 1 to 2 bp from their linkage with equal probability, then 25% of the donor-acceptor pairs are separated by 41 Å, 50% by 44 Å, and 25% by 48 Å.

intercalation on the helix, because photoactivation of phi complexes of Rh(III) promotes strand cleavage directly at the intercalation site without a diffusing intermediate (*12*). Figure 3 shows the results of photoinduced strand cleavage of the Rh-modified duplex and, for comparison, photocleavage of the same oligomer by noncovalently bound $Rh(phi)_2phen^{3+}$. Covalent modification leads to cleavage on the unmodified ^{32}P end-labeled strand at positions 2 and 3 from the 3′ terminus with approximately equal efficiency. This result indicates the positioning of the intercalator with equal probability 1 or 2 bp in from the 5′ terminus of the metallated strand (*24, 25*). In contrast, a uniform distribution of cleavage across the strand is observed for the noncovalently bound Rh complex. Specific cleavage also confirms that the intercalation by the covalent species is primarily intramolecular at these concentrations and that the Rh-modified duplex is properly hybridized. Because the tether for the Ru intercalator is identical to that for the Rh complex, we deduce a comparable positioning of the bound Ru. Thus, as illustrated schematically in Fig. 3C, the photocleavage studies establish that the separation distance between bound intercalating ligands would be either 41, 44, or 48 Å in a duplex formed by annealing the Rh-modified strand to the Ru-modified oligomer (*26*).

Figure 4 displays the steady-state luminescence spectra of the Ru-modified oligomer annealed to its complementary strand and also annealed to the Rh-modified strand. Annealing the Ru-modified oligomer to its unmetallated complement yields intense luminescence. Annealing the two metallated strands together, however, leads to complete quenching of the Ru emission. Time-resolved luminescence decay experiments at 10-ns resolution were insufficient to determine the rate of electron transfer quenching in the fully metallated duplex (*27*). These measurements are consistent with the steady-state experiments that set an upper limit on the excited-state lifetime for the metallated duplex of 2.5 ns (*28*). Picosecond single-photon counting experiments were conducted and were also limited by the time resolution of the detector (300 ps), establishing a lower limit of $\sim 10^9\ s^{-1}$ for the quenching rate (*29*).

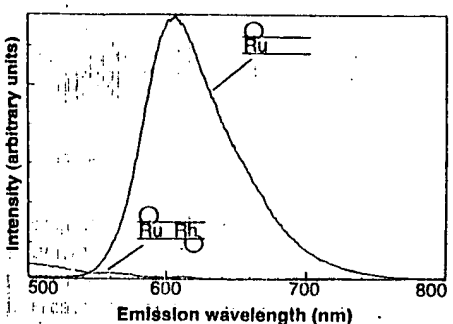

Fig. 4. Emission spectrum of 5 μM 5′-Ru(dppz)-$(phen')_2$-$(CH_2)_6$-5′-AGTGCCAAGCTTGCA-3′ annealed to its complement. The upper trace is for Ru-DNA + unmetallated complement, and the lower trace is for 5 μM Ru-DNA annealed to complementary Rh-DNA. Although intense emission is observed with the Ru-modified duplex hybridized to unmodified complement, complete quenching of the emission is apparent with complement modified to contain the Rh intercalator.

Table 1 compares the remarkable quenching seen when the Ru(III) donor and Rh(III) quencher are intercalated in the *same* helix to several companion experiments where intermolecular quenching may occur. A 5 μM solution of Ru covalently attached to the oligonucleotide and hybridized to an unmodified complement (B) shows comparable luminescent intensity to 5 μM $Ru(phen)_2dppz^{2+}$ noncovalently bound to the helix (A). Addition of the quenched, doubly modified duplex to the Ru-modified duplex (D) does not quench the luminescence from the Ru-modified duplex, demonstrating the absence of any adventitious quenchers in the Rh sample. The addition of 2.5 μM Rh-modified duplex to 2.5 μM Ru-modified duplex gives the intermolecular analog of the doubly metallated oligomer; in (E), 86% of the luminescence is retained. This experiment establishes that intermolecular quenching of a ruthenated duplex by one containing Rh(III) is not substantial and, therefore, quenching at these concentrations in the doubly metallated oligomer must be primarily intramolecular. From these studies as well as from the photocleavage experiments (Fig. 3), we estimate that at least 85% of this interaction is intramolecular at these concentrations. Because the Ru-bearing 15-mer can accommodate two additional intercalators (Fig. 2), it is not surprising that the addition of stoichiometric free $Rh(phi)_2phen^{3+}$ to the Ru-modified duplex (G) leads to substantial but not complete quenching of the Ru emission. As seen with the doubly metallated oligomer, free $Rh(phi)_2phen^{3+}$ efficiently quenches Ru luminescence. With noncovalent Rh complex, there is still residual emission because of the random distribution of Rh species on the Ru duplexes; a few duplexes accommodate two Rh complexes, and therefore some Ru duplexes remain unoccupied and unquenched. That the emission is not completely quenched further indicates that quenching in the doubly metallated duplex is intramolecular because the same concentration of $Rh(phi)_2phen^{3+}$ is present in both experiments.

Table 1. Luminescent properties of intramolecular metal-DNA intercalation complexes.

	Sample *	Relative intensity †
A	$Ru(phen)_2dppz^{2+}$ + ═	0.88
B	Ru═	1.00
C	Ru═Rh	0.00
D	Ru═Rh + Ru═	1.15
E	1/2 Ru═ + 1/2 ═Rh	0.43
F	Ru═ + 2 $Ru(phen)_2dppz^{2+}$	2.78
G	Ru═ + $Rh(phi)_2phen^{3+}$	0.08

*Ru═ refers to 5′-Ru(phen′)$_2$dppz-AGTGCCAAGCTTGCA-3′ annealed to its complement; Ru═Rh refers to 5′-Ru(phen′)$_2$dppz-AGTGCCAAGCTTGCA-3′ annealed to 5′-Rh(phi)$_2$phen′-TGCAAGCTTGGCACT-3′; and ═ refers to the duplex DNA. Samples were dissolved in buffer (5 mM tris, 50 mM NaCl, pH 7.2) to ≤5 μM. †All spectra were taken on an SLM Aminco 8000 spectrofluorimeter. Intensities were integrated from 500 to 800 nm and are relative to that of Ru═. The integrated intensities have an uncertainty of ±10%.

Thus, complete quenching is observed only when the acceptor is covalently bound to the same duplex as the donor. The intervening DNA helix facilitates the donor-acceptor interaction despite the large distance of separation between metallointercalators on the helix.

In principle, either electron or energy transfer quenching mechanisms may be operative over 40 Å distances (*30*). There are several reasons why the quenching in this system may most reasonably be attributed to a long-range electron transfer reaction rather than energy transfer. The large thermodynamic driving force for electron transfer of 0.75 eV (*31*) favors this mechanism. Precedence for an electron transfer quenching mechanism has been documented with other covalently linked Ru(II)-Rh(III) polypyridyl systems (*32*). Förster energy transfer is clearly ruled out because the donor excited state is not singlet in character and because there is no spectral overlap between the photoexcited Ru(II) donor and Rh(III) acceptor. Because transient intermediates have thus far not been detected on the nanosecond time scale, our experiments cannot rule out the possibility of triplet energy transfer as a component of the observed quenching. However, this interaction is itself a form of electron transfer. Moreover, that either mechanism should occur with such facility over this distance is unprecedented and appears to require a special participation of the DNA helix in the quenching step.

Electron transfer through the π-stack can be compared with the absence of quenching seen in a shorter metallated duplex under

conditions where no intercalation occurs. The complexes $Ru(phen)_2phen'^{2+}$ and $Rh(phen)_2phen'^{3+}$ have been linked to the smaller oligonucleotide 5′-CGATTAGC-3′ and its complement, respectively. $Ru(phen)_3^{2+}$ differs from $Ru(phen)_2\ dppz^{2+}$ with regard to the depth of its intercalation, with binding constants for intercalation three orders of magnitude lower than for $Ru(phen)_2dppz^{2+}$ (9, 33). Unlike $Ru(phen)_2dppz^{2+}$, $Ru(phen)_3^{2+}$ does luminesce in aqueous solution in the absence of DNA and shows an increase in luminescent lifetime when intercalated (33). As can be seen in Table 2, no long-lived luminescent lifetime is observed upon hybridization of the $Ru(phen)_3^{2+}$-tethered oligomer to unmetallated complement, indicating the absence of intercalation by this tethered complex. The inability of tethered $Ru(phen)_2(phen')^{2+}$ to intercalate is consistent with the more shallow and weaker intercalation of phenanthroline versus the dppz ligand. Also, the rate of ferrocyanide quenching of $Ru(phen)_3^{2+*}$ is the same when the Ru complex is free in solution as when it is covalently bound to the oligonucleotide duplex. Quenching of Ru luminescence by $Fe(CN)_6^{4-}$ is known to be inhibited when the Ru complex is intimately associated with the DNA polyanion; the failure of the 8-mer duplex to protect the metal complex from quenching is another indication that the tethered tris(phenanthroline) metal complex does not intercalate. Therefore, the duplex derivatized with both $M(phen)_3^{n+}$ complexes provides a covalently bound analog in which the metal complexes are not coupled to the π-stack. In contrast to the fully intercalated doubly metallated assembly, here no luminescence quenching of the Ru center is observed upon hybridization of the $Ru(phen)_3^{2+}$-modified oligonucleotide to the Rh-modified oligomer (34).

These results demonstrate that intercalation is required for electron transfer to occur. The absence of luminescence quenching when the covalently tethered donor and acceptor are not intercalated is fully consistent with the comparison seen earlier between the emission quenching of $Ru(phen)_2dppz^{2+*}$ by $Rh(phi)_2phen^{3+}$ versus $Ru(NH_3)_6^{3+}$ (17); when $Rh(phi)_2phen^{3+}$ serves as the electron acceptor, the luminescence is quenched on a subnanosecond time scale, whereas $Ru(NH_3)_6^{3+}$ quenches $Ru(phen)_2dppz^{2+*}$ emission at diffusion-controlled rates. $Ru(NH_3)_6^{3+}$ binds to DNA by electrostatic attraction and hydrogen bonding and is therefore not bound within the DNA π-stack. Similarly, since the tethered phenanthroline complexes are not intercalated, the pathway joining the donor and acceptor involves only σ-bonds, with no direct π-stack interaction. Our results indicate that the rapid electron transfer requires the coupling of donor and acceptor to the π-stack. More generally, the different quenching efficiencies found with these different pathways suggest that electron transfer can proceed much more readily through stacked π-systems than either through a covalent σ-framework or by ionic interactions.

Based on these results, we conclude that photoinduced electron transfer between intercalators occurs very rapidly over >40 Å through the DNA helix over a pathway consisting of π-stacked base pairs. From Marcus theory (35), one may calculate the extent to which the DNA π-stack couples donor and acceptor, which is denoted by the quantity β (units of $Å^{-1}$):

$$k_{et} \propto \exp[-\beta(d - r_0)] \qquad (1)$$

where k_{et} is the rate of electron transfer (s^{-1}), d is the distance between donor and acceptor, and r_0 is the distance of closest approach of donor and acceptor. From our measurements of driving force and distance and assuming a lower limit in the rate of $3 \times 10^9\ s^{-1}$, we estimate β to be ≤0.2 $Å^{-1}$ (36). This value may reasonably be compared to a value of β of 0.14 $Å^{-1}$ found for Ru(II)/Ru(III) centers covalently linked by a dipyridyl polyene bridge (37).

The DNA double helix therefore serves as an efficient medium for coupling electron donors and acceptors over very long distances (>40 Å). We have constructed a duplex assembly bearing a donor and an acceptor intercalated at each end which promotes electron transfer over distances that are comparable to those found in biological systems (38). The efficiency of DNA in mediating long-range electron transfer gives credence to the notion that noncovalently stacked aromatic heterocycles can serve as rapid "π-ways." Finally, these results offer the possibility that nature takes advantage of the electron transport properties of nucleic acids in some context.

Table 2. Luminescent properties of tris(phenanthroline)metal-DNA complexes. Samples were dissolved in buffer (5 mM tris, 50 mM NaCl, pH 7.2) to ≤5 μM. Time-resolved emission experiments were performed as in (28) but at 10°C to ensure duplex stability.

Sample	Lifetime (ns)

REFERENCES AND NOTES

1. B. E. Bowler, A. L. Raphael, H. B. Gray, *Prog. Inorg. Chem.* 38, 259 (1990); B. M. Hoffman, M. J. Natan, J. M. Nocek, S. A. Wallin, *Struct. Bonding* 75, 85 (1991); G. McLendon, *Acc. Chem. Res.* 21, 160 (1988).
2. A. D. Joran, B. A. Leland, G. G. Geller, J. J. Hopfield, P. B. Dervan, *J. Am. Chem. Soc.* 106, 6090 (1984); G. L. Closs, L. T. Calcaterra, N. J. Green, K. W. Penfield, J. R. Miller, *J. Phys. Chem.* 90, 3673 (1986); A. D. Joran *et al.*, *Nature* 327, 508 (1987); G. L. Closs and J. R. Miller, *Science* 240, 440 (1988).
3. D. N. Beratan and J. N. Onuchic, *Adv. Chem. Ser.* 228, 71 (1991); M. A. Ratner, *J. Phys. Chem.* 94, 4877 (1990); C. A. Naleway, L. A. Curtiss, J. R. Miller, *ibid.* 95, 8434 (1991); S. Larsson, *Chem. Phys. Lett.* 90, 136 (1982).
4. T. J. Marks, *Science* 227, 881 (1985); M. Tanaka, H. Yoshida, M. Ogasawara, *J. Phys. Chem.* 95, 955 (1991); P. G. Schouten, J. M. Warman, M. P. de Haas, M. A. Fox, H.-L. Pan, *Nature* 353, 736 (1991); M. R. Wasielewski, *Chem. Rev.* 92, 435 (1992).
5. T. A. Hoffmann and J. Ladik, *Adv. Chem. Phys.* 7, 84 (1964); E. Clementi and G. Coronglu, *Int. J. Quant. Chem. Quant. Biol. Symp.* 9, 213 (1982).
6. P. Fromherz and B. Rieger, *J. Am. Chem. Soc.* 108, 5361 (1986).
7. J. K. Barton, C. V. Kumar, N. J. Turro, *ibid.*, p. 6391; M. D. Purugganan, C. V. Kumar, N. J. Turro, J. K. Barton, *Science* 241, 1645 (1988).
8. A. M. Brun and A. Harriman, *J. Am. Chem. Soc.* 114, 3656 (1992).
9. A. E. Friedman, J.-C. Chambron, J.-P. Sauvage, N. J. Turro, J. K. Barton, *ibid.* 112, 4960 (1990); R. Hartshorn and J. K. Barton, *ibid.* 114, 5919 (1992); Y. Jenkins, A. E. Friedman, N. J. Turro, J. K. Barton, *Biochemistry* 31, 10809 (1992).
10. A. M. Pyle, E. C. Long, J. K. Barton, *J. Am. Chem. Soc.* 111, 4520 (1989).
11. S. S. David and J. K. Barton, *ibid.* 115, 2984 (1993).
12. A. Sitlani, E. C. Long, A. M. Pyle, J. K. Barton, *ibid.* 114, 2303 (1992).
13. A. M. Pyle, T. Morii, J. K. Barton, *ibid.* 112, 9432 (1990); K. Uchida, A. M. Pyle, T. Morii, J. K.

Absence of dc-Conductivity in λ-DNA

P. J. de Pablo,[1] F. Moreno-Herrero,[1] J. Colchero,[1,2] J. Gómez Herrero,[1,2] P. Herrero,[3] A. M. Baró,[1,2] Pablo Ordejón,[4] José M. Soler,[1,2,5] and Emilio Artacho[1,2]

[1]*Departamento de Física de la Materia Condensada, Universidad Autónoma de Madrid, E-28049, Madrid, Spain*
[2]*Instituto Nicolás Cabrera, Universidad Autónoma de Madrid, E-28049, Madrid, Spain*
[3]*Departamento de Bioquímica y Biología Molecular, Instituto Universitario de Biotecnología de Asturias, Universidad de Oviedo, E-33006, Oviedo, Spain*
[4]*Instituto de Ciència de Materials de Barcelona (CSIC), Campus de la UAB, E-089193 Barcelona, Spain*
[5]*Department of Physics, Lyman Laboratory, Harvard University, Cambridge, Massachusetts 02138*

(Received 14 June 2000)

The electrical conductivity of biomaterials on a molecular scale is of fundamental interest in the life sciences. We perform first principles electronic structure calculations, which clearly indicate that λ-DNA chains should present large resistance values. We also present two direct procedures to measure electrical currents through DNA molecules adsorbed on mica. The lower limit for the resistivity is $10^6\ \Omega \cdot$ cm, in agreement with our calculations. We also show that low energy electron bombardment induces a rapid contamination and dramatically affects the measured conductivity, thus providing an explanation to recent reports of high DNA conductivity.

PACS numbers: 87.15.–v, 87.14.Gg

Molecular devices are the final horizon in the miniaturization of electronic technology. The electrical transport properties of molecules are expected to differ dramatically from those of macroscopic conductors [1], and finding ways to measure these properties at such a small scale is an important challenge of the emerging nanoscience. In particular, DNA is a well-known molecule that appears as a promising molecular-wire candidate, which has been actively studied in the last few years [2–4]. Many of the efforts have a biochemical motivation, since understanding electronic transport through DNA is essential to characterize and control important life processes, such as radiation damage and repair [5,6]. However, the physical character of the problem of electronic transport through nanowires, and its importance for nanotechnology, has also motivated the study of DNA conductivity from a physical point of view [4,7,8]. In spite of its importance, the simple question of whether DNA is an electric conductor or not remains unsettled because of the complexity of the system and the difficulty of making clean-cut experiments. Recently, two outstanding works have been published, reporting very different transport properties. Fink and Schönenberger (FS) [9] find a linear *I-V* characteristic, with resistivities $\rho \approx 10^{-4}\ \Omega \cdot$ cm for λ-DNA (random sequence) molecules 1 μm long. Porath and co-workers [10] report *I-V* characteristics with a clear gap of about 2 V and resistances of 3 GΩ at 4 V, for 10 nm long free standing poly(*G*)-poly(*C*) DNA chains ($\rho \approx 10\ \Omega \cdot$ cm).

This qualitative discrepancy is especially frustrating because it is not even theoretically clear whether DNA should conduct or not. This ignorance is justified by the complexity of the problem, and by the fact that the molecular environment is determinant and difficult to control. Many different aspects such as the sequence variability, and the effects of counterions and thermal vibrations, can influence the electron transport in different ways. Transport models have been put forward where charge is carried by polarons [11], solitons [12], electrons, or holes [5]. However, crucial quantitative information about the electronic structure is still missing. We have resorted to first principles calculations to obtain it.

Density-functional-theory (DFT) calculations for large systems are now feasible thanks to recent developments in linear scaling algorithms, with which the computational cost scales linearly with the number of atoms in the system N, instead of as N^3. We have used the numerical-atomic-orbital method [13–15] of linear scaling DFT, in the SIESTA implementation. We used the generalized gradients approximation for exchange and correlation [16], norm-conserving pseudopotentials [17,18], and a basis set of numerical-atomic orbitals. Their finite range [15,19] was chosen as in Ref. [14], with tests performed for ranges 30% longer. The atoms involved in hydrogen bridges have orbitals of long range. A double-ζ basis is used for all atoms except for phosphorous and for the atoms involved in hydrogen bridges, for which the basis contains extra polarization orbitals. The linear scaling computations were done using Wannier confinement radii of 4–5 Å. Further technical details are as in Ref. [20], where the approximations have been explained and tested at length. This method has already been used with success in a variety of inorganic systems [21] and biomolecules [14,22,23]. In particular, a thorough study has been performed on up to 30 nitrogenated base pairs [20], obtaining a very satisfactory accuracy in both geometries and interaction energies.

The calculations were done for a double helix of infinite length in acidic dry conditions. A unit cell with eleven base pairs (3.058 nm) and 715 atoms was repeated in the direction of the chain. The simplest sequence was first considered: polyguanine-polycytosine. The structure was

 0031-9007/00/85(23)/4992(4)$15.00

completely relaxed, starting from an approximately known geometry [24] and following the atomic forces. This process required around 800 conjugate gradient steps. In the relaxed geometry, we performed a standard (order N^3) diagonalization of the Hamiltonian, to check the accuracy of the forces found by the order N method, and to obtain the Kohn-Sham eigenstates. The electronic structure close to the Fermi level shows well-defined minibands with eleven states per unit cell, one per basis pair. The topmost valence band has a bandwidth of 40 meV and is made of the π-like highest occupied molecular orbitals (HOMO) of the guanines. Their spacial distribution is shown in Fig. 1(a). Separated by an important band gap [25], the lowest conduction band has a width of 270 meV. It is made of the lowest unoccupied molecular orbitals (LUMO) of the cytosines, and it is shown in Fig. 1(b). These results may be of relevance for the experiments of Porath *et al.* [10] on repeated-sequence DNA, and they will be discussed elsewhere [27]. Notice that the wide band gap does not itself necessarily rule out electrical conduction, if there are enough hole carriers as a result of defects in the hydrogen atoms or counterions saturating the phosphates.

In order to address the situation for λ-DNA, we have performed a complete relaxation of a DNA chain analogous to the previous one, except for the swap of the guanine and cytosine bases in one of every eleven base pairs. The effect of the swap on the electronic structure of the chain is dramatic. The HOMO of the swapped guanine sinks 0.6 eV (15 times the HOMO bandwith) into lower valence band levels. This stabilization is due to charging effects, since guanines have an excess of electrons taken from cytosines. A guanine among cytosines is thus stabilized electrostatically. Figure 1(c) shows the analogous to 1(a) for the swapped structure, showing the cut in the HOMO-state channel, produced by the swapped pair. The situation is similar for the unoccupied band, albeit less dramatic. These results mean that, in terms of the one-dimensional Anderson model, the disorder fluctuations in λ-DNA, due to sequence variations, are substantially larger than the bandwidth, leading to electronic localization over very few base pairs and to an exponential decay of the conductance with length. This does not rule out residual conduction by hopping mechanisms (polaronic or not), although it should have a marked dependence on temperature and frequency [7].

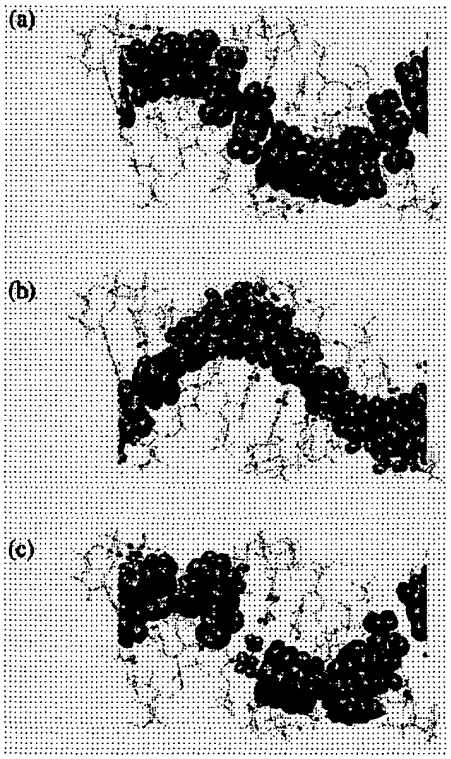

FIG. 1. Isosurfaces of constant density (5×10^{-4} e/a.u.^{3}) for (a) the eleven highest occupied states of poly(G)-poly(C); (b) the eleven lowest unoccupied states of the same; and (c) the eleven highest occupied states of the mutated DNA.

In order to verify our predictions, and to clarify the experimental situation, we have developed a simple and reliable technique [28] that allows measuring conductivity through long chain molecules. In the present work we apply this technique to study DNA conductivity. The λ-DNA sample was prepared as in Refs. [29,30]. The sample is then inspected by scanning force microscopy (SFM) to check the quality and surface density of DNA molecules. The SFM images show randomly distributed DNA chains 1.8 μm long, in good agreement with the selected DNA length. After deposition of the DNA, a region of mica 4 μm wide was left bare between two thermally evaporated Au electrodes, using a thin-wire shadow masking technique [31]. We have carefully checked that, during the whole evaporation process, the temperature never exceeds 310 K on the surface of the sample. Since molecular strand dissociation occurs only above 345 K, we do not expect any substantial thermal effects on the DNA structure. The gold patches, separated by the bare mica region, are then grounded with silver paint. In order to carry out the conductivity experiments, silicon nitride cantilevers, metallized with 20 nm titanium plus 60 nm gold films, were used as a second electrode. This sample preparation procedure results in a reliable method for making almost perfect electrical contacts in long molecules such as DNA.

Figure 2 shows a noncontact SFM image taken on the left border of the mica channel. Several DNA molecules appear clearly on the image, partially buried by the gold film, ensuring a good electrical contact. In order to measure DNA resistivity, we start by selecting one of the molecules and reducing the scan size until the molecule is on the center of a 10 nm wide image. The scan is then stopped and the tip is carefully driven to mechanical contact by elongating the piezoelectric scanner, while recording the normal force. At a previously selected normal force threshold, the tip motion is stopped and a

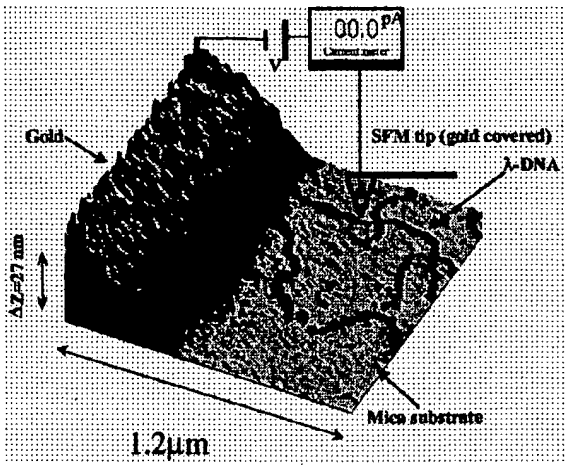

FIG. 2. Three-dimensional SFM image of the channel border, showing two DNA molecules in contact with the left gold electrode. The image size is 1.2 μm × 1.2 μm. We also present a scheme of the electrical circuit used to measure the DNA resistivity.

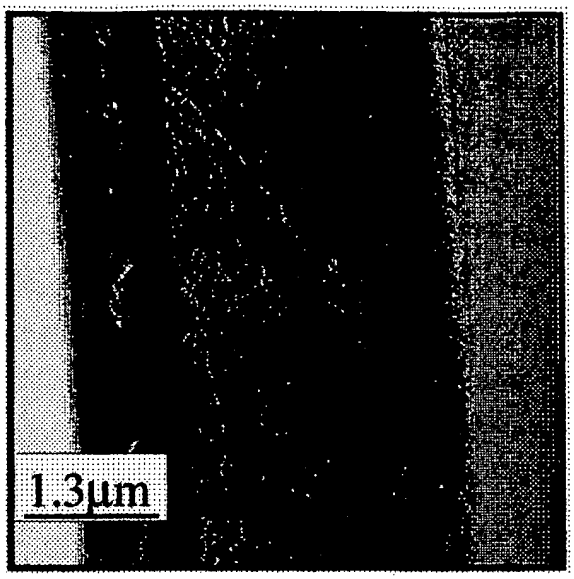

FIG. 3. λ-DNA strands connecting two gold electrodes spanned by a bare mica gap. By analyzing the image we conclude that at least 1000 DNA chains are connecting both electrodes. From the (absence of) current between both electrodes, a lower bound of $10^5\ \Omega \cdot$ cm per molecule is obtained for the resistivity of DNA at a bias voltage of 10 V.

current-voltage (I-V) measurement is performed [32]. Thermal drift effects can be ruled out by taking an image immediately before and after each I-V measurement. The experiment is repeated at different distances to the border of the gold electrode, as well as at different force thresholds. The current sensitivity was 1 pA, and a bias voltage of up to 10 V was applied, without detecting any current. Therefore, we conclude that the resistance of the molecule was at least $10^{12}\ \Omega$, and that the minimum value for the DNA resistivity is $\rho \approx 10^4\ \Omega \cdot$ cm. The same lower limit applied to every spot selected along the DNA molecule. In order to avoid any spurious current, we have limited the minimum horizontal distance between the conductive tip and the gold electrode to 70 nm. If the same I-V measurement is repeated on the gold electrodes, contact resistances of only about 30 Ω are obtained. A similar experiment performed with single wall nanotubes [31] gave resistances in the range $(0.5-10) \times 10^4\ \Omega$, depending on the selected nanotube. These low values prove the conductivity of our tips and the feasibility of making electrical contacts with a SFM tip to long molecules.

In order to improve the sensitivity of our measurement, we have carried out a second sample preparation by increasing the length of the DNA chains from 1 to 15 μm. Figure 3 shows a SFM image of the surface after preparation. From this image, we estimate that more than 1000 molecules connect both electrodes. With a bias voltage of up to 12 V between the gold electrodes, the measured current was below the noise level of 1 pA. Therefore, we calculate a minimum DNA resistance of $10^{16}\ \Omega$ per molecule, and a minimum resistivity of $10^6\ \Omega \cdot$ cm. This result is consistent with previous work of Braun *et al.* [4]. Our result may still be consistent with those of Porath *et al.* [10], if we take into account our electronic structure obtained for poly(C)-poly(G). However, our resistivity is 10 orders of magnitude higher than that of FS [9].

Since both, experiments and calculations, strongly suggest that λ-DNA is an insulator, we should try to discuss the extremely low resistivity reported in Ref. [9]. We suspect that this value may be strongly affected by the method used by FS to visualize the DNA molecules, a low energy electron projection microscope [33]. Since the electron energy involved in this microscope is small (50–200 eV), FS assume that the sample is not affected by the electron beam. However, this is in contrast with a well-established fact in molecular biology: when biological tissue is irradiated with high energy particles, the secondary low energy (10–40 eV) electrons emitted along the track are the most harmful in inducing DNA damage [34]. In addition, at the base pressure reported by FS (10^{-7} mb), electron-induced hydrocarbon cracking may also be present. In order to address these problems, we have irradiated samples such as those of Fig. 3 with a low energy electron beam (≈100 eV). After a dose of only 6500 C · m^{-2} (approximately 10 min at 10 A · m^{-2}), at a base pressure of 10^{-7} mb, the sample acquires metallic-like conductivity showing a clearly linear I-V characteristic, with a resistance of only $2 \times 10^8\ \Omega$. Further SFM inspection of the sample reveals that a contamination layer has been deposited on the surface and over the DNA, as a result of the electron bombardment. This shows that low energy electrons are not inert at all, and that special care must be taken to rule out their effects.

In summary, our first principles calculations indicate that the electrical conductivity of DNA should be strongly reduced by the sequence variability present in λ-DNA. In addition, two simple experimental techniques have been reported, which allow a clear visualization, and a direct measurement of the electrical transport through DNA and other long molecules adsorbed on a substrate. In agreement with the theoretical result, we have obtained an experimental lower bound of $10^6\ \Omega \cdot$ cm for the resistivity of λ-DNA, implying that it is a very good insulator. Finally, it has been shown that low energy electron bombardment can induce rapid contamination and affect dramatically the conductivity measurements.

We thank O. Custance, D. Sanchez-Portal, and J. A. Subirana, and especially Ron Reifenberger for extremely helpful discussions. We acknowledge support from Ministerio de Educación y Cultura through DGESIC Project No. PB95-0169 and a scholarship to P. J. D. and a contract to J. C. Support from CCCFC/UAM Fundación Areces, and the CAM through Project No. 07N/0024/1998 is also acknowledged. The CAM supports a scholarship to F. M.-H.

[1] Supriyo Datta, *Electronic Transport in Mesoscopic Systems,* Cambridge Studies in Semiconductor Physics and Microelectronic Engineering No. 3 (Cambridge University Press, Cambridge, 1997).
[2] C. A. Mirkin, R. L. Letsinger, R. C. Mucic, and J. J. Storhorff, Nature (London) **382**, 607 (1996).
[3] A. B. Alibisatos, K. P. Johnsson, X. Peng, T. E. Wilson, C. J. Loweth, M. P. Bruchez, and P. J. Schultz, Nature (London) **382**, 609 (1996).
[4] E. Braun, Y. Eichen, U. Sivan, and G. Ben-Yoseph, Nature (London) **391**, 775 (1998).
[5] D. N. Beratan, S. Priyadarshy, and S. M. Risser, Chem. Biol. **4**, 3 (1997), and references therein.
[6] S. O. Kelley and J. K. Barton, Science **283**, 375 (1999).
[7] P. Tran, B. Alavi, and G. Gruner, Phys. Rev. Lett. **85**, 1564 (2000).
[8] F. D. Lewis, X. Liu, S. E. Miller, R. T. Hayes, and M. R. Wasielewski, Nature (London) **406**, 51 (2000).
[9] H. W. Fink and C. Schönenberger, Nature (London) **398**, 407 (1999).
[10] D. Porath, A. Bezryadin, S. De Vries, and C. Dekker, Nature (London) **403**, 635 (2000).
[11] E. M. Conwell and S. V. Rakhmanova, Proc. Natl. Acad. Sci. U.S.A. **97**, 4556 (2000).
[12] Z. Hermon, S. Caspi, and E. Ben-Jacob, Europhys. Lett. **43**, 482 (1998).
[13] P. Ordejón, E. Artacho, and J. M. Soler, Phys. Rev. B **53**, R10441 (1996).
[14] D. Sánchez-Portal, P. Ordejón, E. Artacho, and J. M. Soler, Int. J. Quantum Chem. **65**, 453 (1997).
[15] E. Artacho, D. Sánchez-Portal, P. Ordejón, A. García, and J. M. Soler, Phys. Status Solidi (b) **215**, 809 (1999).
[16] J. P. Perdew, K. Burke, and M. Ernzerhof, Phys. Rev. Lett. **77**, 3865 (1996).
[17] N. Troullier and J. L. Martins, Phys. Rev. B **43**, 1993 (1991).
[18] L. Kleinman and D. M. Bylander, Phys. Rev. Lett. **48**, 1425 (1982).
[19] O. F. Sankey and D. J. Niklewski, Phys. Rev. B **40**, 3979 (1989); D. Sánchez-Portal, E. Artacho, and J. M. Soler, J. Phys. Condens. Matter **8**, 3859 (1996).
[20] M. Machado, P. Ordejón, D. Sánchez-Portal, E. Artacho, and J. M. Soler, physics/9908022.
[21] P. Ordejón, Phys. Status Solidi (b) **217**, 335 (2000), and references therein.
[22] P. Ordejón, E. Artacho, and J. M. Soler, Mater. Res. Soc. Symp. Proc. **408**, 85 (1996).
[23] M. V. Fernández-Serra, J. Junquera, C. Jelsch, C. Lecomte, and E. Artacho, Solid State Commun. (to be published).
[24] R. Chandrasekaran and S. Arnott, in *Biophysics, Nucleic Acids, Crystallographic and Structural Data II,* edited by W. Saenger, Landölt-Börnstein, New Series, Group VII, Vol. I, Pt. b (Springer-Verlag, New York, 1989).
[25] The calculated band gap is 2.0 eV, but this number is to be taken with caution since DFT tends to underestimate band gaps in insulators. The experimental band gaps for DNA in solution are close to 7 eV, but most of this gap is due to solvent effects [26]. The magnitudes considered in the discussion are not affected by these pathologies.
[26] D. M. York, T. S. Lee, and W. Yang, Phys. Rev. Lett. **80**, 5011 (1998).
[27] E. Artacho, P. Ordejón, D. Sánchez-Portal, and J. M. Soler (to be published).
[28] P. J. de Pablo, E. Graugnard, B. Walsh, R. P. Andres, S. Datta, and R. Reifenberger, Appl. Phys. Lett. **74**, 323 (1999).
[29] A. M. Myers, A. Tzagoloff, D. M. Kinney, and C. J. Lusty, Gene **45**, 299 (1986).
[30] M. J. Allen, E. M. Bradbury, and R. Balhorn, Nucl. Acids Res. **25**, 2221 (1997).
[31] P. J. de Pablo, M. T. Martínez, J. Colchero, J. Gomez-Herrero, W. K. Maser, A. M. Benito, E. Muñoz, and A. M. Baró, Adv. Mater. **12**, 573 (2000).
[32] We have collaborated with Nanotec Electrónica SL to develop the special algorithms for these experiments. A free copy of the software used herein can be found at www.nanotec.es.
[33] H. W. Fink, W. Stocker, and H. Schmid, Phys. Rev. Lett. **65**, 1204 (1990).
[34] B. D. Michael and P. O'Neill, Science **287**, 1603 (2000).

Insulating behavior for DNA molecules between nanoelectrodes at the 100 nm length scale

A. J. Storm, J. van Noort, S. de Vries, and C. Dekker[a)]
Faculty of Applied Sciences, Delft University of Technology, 2628 CJ Delft, The Netherlands

(Received 18 June 2001; accepted for publication 19 September 2001)

Electrical transport measurements are reported for double-stranded DNA molecules located between nanofabricated electrodes. We observe the absence of any electrical conduction through these DNA-based devices, both at the single-molecule level as well as for small bundles of DNA. We obtain a lower bound of 10 TΩ for the resistance of a DNA molecule at length scales larger than 40 nm. It is concluded that DNA is insulating. This conclusion is based on an extensive set of experiments in which we varied key parameters such as the base-pair sequence [mixed sequence and homogeneous poly(dG)·poly(dC)], length between contacts (40–500 nm), substrate (SiO_2 or mica), electrode material (gold or platinum), and electrostatic doping fields. Discrepancies with other reports in the literature are discussed. © *2001 American Institute of Physics.*
[DOI: 10.1063/1.1421086]

Recently, a number of contradicting findings were reported regarding the charge transport properties of DNA.[1] The experiments appeared to indicate metallic,[2–4] semiconducting,[5–7] and insulating[8,9] electronic properties. These transport experiments were inspired by electron-transfer experiments where one attaches donor and acceptor groups at both ends of DNA molecules and characterizes their electronic coupling through the DNA. Such experiments by Barton and co-worker[10] and others showed that electron transfer is possible in DNA over distances of several nanometers. The results of some direct transport experiments have suggested that transport is also possible over much larger length scales, of the order of microns.[2–4,7] In this letter, we report transport measurements on both individual DNA molecules as well as small DNA bundles (up to tens of molecules) that are connected on both sides to metallic electrodes. Our technique relies on well-defined electrodes with spacings in the range of 40–500 nm. Using state-of-the-art atomic force microscope (AFM) imaging we report images of individual DNA molecules positioned between electrodes. We find *no* evidence of any electronic conductivity for DNA molecules with various lengths and base pair sequences. Based on a set of experiments with a number of different sample layouts, we come to the conclusion that DNA at the single-molecule scale is insulating at length scales larger than 40 nm.

As an example of a typical result of our work, Fig. 1 shows a tapping-mode AFM height image of one of our devices with mixed-sequence double-strand DNA between gold electrodes spaced by 300 nm. On the SiO_2 in between the electrodes, individual DNA molecules are clearly discernable. Details of the assembly of this device are given below. The apparent height of the DNA is about 0.5 nm, and the width is about 10 nm, limited by the AFM tip radius. These values are typical of single DNA molecules.[11] From the height, width, and persistence length determined from the images, we conclude that indeed individual DNA molecules are connected between our electrodes. No conductance was found for this device. The bias voltage was slowly increased to 10 V and the currents observed remained below a noise level of about 1 pA. From this experiment we thus obtain a lower bound of 10 TΩ for the resistance of this device, in which a total of about 10 DNA molecules were connected in parallel between the electrodes.

The outcome of this experiment is in clear disagreement with a number of previously reported experiments. To investigate whether our result is due to the intrinsic electronic properties of DNA or due to external conditions, a series of experiments was conducted in which a number of key parameters was varied, e.g., the base-pair sequence of the DNA, the type of substrate, the distance between the electrodes, and the contact material. An attempt was also made to dope the DNA electrostatically with an external gate electrode.

The basic sample layout for all experiments discussed in this letter is similar: DNA molecules are deposited from an aqueous buffer solution onto a substrate patterned with pairs of closely spaced thin metallic lines that are connected to larger pads which facilitate contact to the electrical equipment. The electrodes are fabricated using electron-beam lithography and subsequent liftoff. Noble metal (platinum and

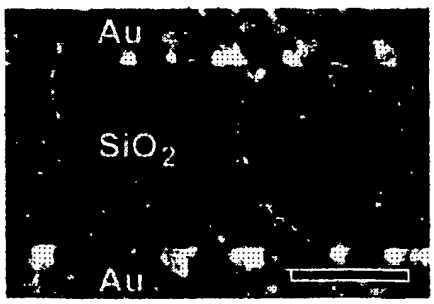

FIG. 1. Tapping-mode AFM height image of three DNA molecules connected between two gold electrodes that are separated by 300 nm. Scale bar: 200 nm. The measured resistance of this device was higher than 10 TΩ.

a)electronic mail: dekker@mb.tn.tudelft.nl

gold) films were used as electrode materials. The metal thickness was about 15 nm, and was evaporated on top of a 3 nm titanium sticking layer. After liftoff, residues of the organic poly(methyl methacrylate) double-layer resist were removed by immersion in fuming nitric acid. DNA molecules were deposited from a 20 mM HEPES buffer solution (*p*H 6.5). The DNA concentrations were in the range of 1–250 ng/μl, and 5 mM of $MgCl_2$ was added to promote DNA adhesion to the surface. A droplet of about 3 μl is deposited on the substrate for about 20 s, after which the sample is rinsed with de-ionized water and dried in a flow of nitrogen gas. The presence of DNA molecules was confirmed by AFM imaging. Electrical transport measurements were performed at room temperature under ambient conditions.

The first set of experiments discussed here was performed on DNA with a mixed sequence immobilized on a silicon oxide substrate. Because DNA binds only weakly to the SiO_2 and is easily rinsed off, we used DNA modified with thiol (–SH) groups at both ends of the molecule. The sulfur atom of the thiol group will bind strongly to the platinum or gold of the electrodes, which chemically anchors the molecule to the metal at its terminal ends. Double-strand DNA with a $(CH_2)_6SH$ group at each 5′ terminal phosphate was obtained by performing a polymerase chain reaction (PCR) with λ DNA as a template using thiolated primers, following the procedure of Hegner *et al.*[12] Dithiothreitol (DTT) was added to prevent oxidation of the thiols during the PCR. Using this technique, DNA fragments of 900 and 4500 base pairs were obtained and purified that were 300 nm and 1.5 μm long, respectively. These fragments contain a mixed sequence of bases, and are representative of natural DNA. Figure 1 shows an AFM image of the 1.5 μm fragments positioned on Au electrodes spaced by 300 nm. Because the DNA is much longer than the distance between the electrodes, a considerable length of DNA overlaps both electrodes and this facilitates good electrical contact. As mentioned above, no electron transport was observed for this sample. The same absence of conductance was observed for a number of similar samples with electrode spacings in the range of 200–500 nm.

Considerable effort was put into the fabrication of smaller spaced electrodes, without losing the possibility of imaging in between the electrodes using AFM.[13] Figure 2(a) shows DNA located across a gap of about 40 nm. In this experiment we deposited DNA from a 1 ng/μl solution of thiolated PCR fragments of 900 base pair lengths. AFM inspection showed a small amount of DNA material between the electrodes. From the width and height of the DNA it is estimated that at most five DNA molecules are present in parallel between the electrodes. No charge transport was observed for bias voltages up to 10 V. From this experiment we again find a lower bound for the device resistance of 10 TΩ.

Experimental[14] and theoretical[9] studies of DNA charge transport suggest higher transport rates poly(dG)·poly(dC) DNA compared to for mixed-sequence DNA. To investigate this experimentally, we assembled devices with poly(dG)·poly(dC) DNA molecules with an average length of several microns.[15] No thiol groups were present on this molecule. It was found that DNA is immobilized on the SiO_2 surface after rinsing and drying for relatively high DNA concentrations of about 100 ng/μl in buffer solutions of 20 mM HEPES and 5 mM $MgCl_2$. Reactive-ion etching before metal deposition was used to make the surface of the platinum electrodes the same height as the SiO_2 substrate in order to prevent kinks in the DNA and to minimize tip convolution effects. Figure 2(b) shows poly(dG)·poly(dC) molecules on electrodes spaced by 200 nm. Figure 2(c) shows a magnification of the image displayed in Fig. 2(b). Due to the high concentration, not only single molecules are observed, but also thicker bundles of molecules, which are estimated to have at least 10 parallel strands of DNA. No conduction was found for these samples either. We estimate that in this experiment there are roughly 50 DNA molecules connected in parallel. Similar results were obtained on devices with a spacing of 100 nm.

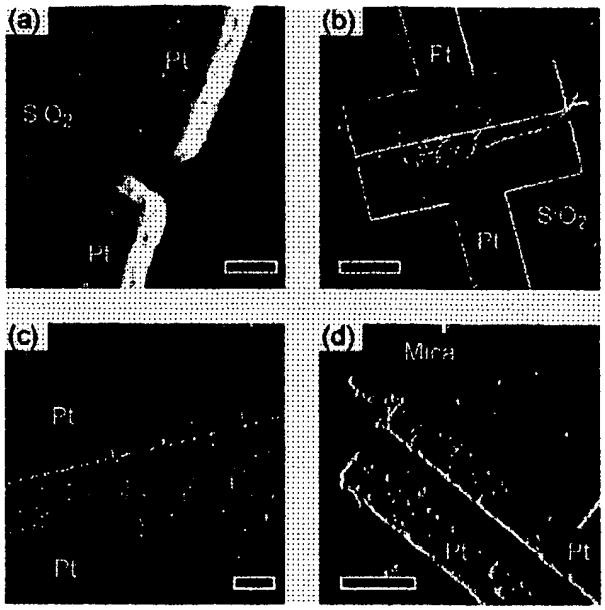

FIG. 2. AFM images of DNA assembled in various devices. (a) Mixed-sequence DNA between platinum electrodes spaced by 40 nm. Scale bar: 50 nm. (b) Height image of poly(dG)·poly(dC) DNA bundles on platinum electrodes. The distance between electrodes is 200 nm, and the scale bar is 1 μm. (c) High magnification image of the device shown in (b). Several DNA bundles clearly extend over the two electrodes. Scale bar: 200 nm. (d) Poly(dG)·poly(dC) DNA bundles on platinum electrodes fabricated on a mica substrate. Scale bar: 500 nm. For all these devices, we observe an absence of conduction.

Additionally we attempted to electrostatically dope the DNA with additional charge carriers in order to increase the conductance. This was done by applying a gate voltage to the silicon substrate with respect to one of the electrodes. No increase in conductance was found for gate voltages in the range of −50 V to +50 V. The thickness of the silicon oxide was 200 nm.

Finally, we discuss the possible influence of the substrate. Both Kasumov *et al.*[4] and Cai *et al.*[6] reported finite DNA conductance in devices in which the DNA was immobilized on mica substrates. Using a slightly modified fabrication recipe, we were able to fabricate patterned electrodes on mica substrates, with an electrode spacing of 200 nm. Figure 2(d) shows poly(dG)·poly(dC) molecules between platinum contacts on mica. DNA was deposited from a high-concentration buffer solution with approximately 250 ng/μl

DNA. Under these conditions, DNA self-assembles into networks similar to those observed in the work of Cai *et al.*[6] Subsequent electrical transport experiments showed a high resistance of about 1 TΩ, a typical value that we also found for mica devices before DNA deposition. In a flow of dry nitrogen gas, this value was found to increase. We therefore attribute this background conduction to the thin water layer present on the hydrophilic mica.[16]

We conclude that DNA is insulating at length scales longer than 40 nm, with a 10 TΩ lower bound for the resistance of a DNA molecule. Our experiments were performed using straightforward lithography, standard DNA buffer conditions, and high-resolution sample characterization using AFM imaging. The suggested formation of an electronic π band[17] appears not to occur over length scales of 40 nm or more, even for homogeneous poly(dG)·poly(dC) sequences. In most theoretical models it is assumed that the charge transport rate through DNA decays exponentially with distance.[18] Experimental evidence of exponential decay was reported by Cai *et al.*[6] Our findings are therefore not necessarily in disagreement with DNA charge transport experiments performed on the scale of a few nanometers, where relatively high transport rates have been reported.[5,10]

Our results are in agreement with the results of De Pablo *et al.*[9] and with Braun *et al.*,[8] who also found the absence of electronic transport through DNA. Clear disagreement is found with the work of Kasumov *et al.*[4] and of Fink and Schönenberger[3] who reported high conductivity of λ DNA on the scale of 0.5 μm. For a single DNA molecule about 500 nm in length, they observed typical resistances of about 300 kΩ and 3 MΩ, respectively, which is at least six orders of magnitude lower than that observed in our experiments. In the experiments by Fink and Schönenberger, a small DNA bundle was freely suspended in vacuum, but Kasumov *et al.* used a layout similar to ours. Kasumov *et al.* used electrodes consisting of thin rhenium film covered with sputtered carbon on a mica substrate. We use platinum and gold contacts instead, but we do not see how this difference can lead to the dramatically different experimental results. Cai *et al.*[6] found resistance of about 200 GΩ for bundles of poly(dG)·poly(dC) at a length scale of 200 nm. If we compare this value to our lower boundary of 1 TΩ for similar bundles of 200 nm length, there is only a slight discrepancy.

Our results clearly limit the use of bare DNA as a conducting molecular wire. The self-assembling properties of DNA, however, may be very useful for nanotechnology, for example, as a scaffold to construct self-assembled electronics based on the technique of DNA metallization discussed by Braun *et al.*[8]

The authors thank E. Yildirim, H. W. Ch. Postma, K. A. Williams, B. Rousseeuw, A. K. Langen-Suurling, and R. N. Schouten for experimental assistance and discussions. This research was financially supported by the Dutch Foundation for Fundamental Research on Matter (FOM) and the European Community IST-FET project "DNA-based Electronics."

[1] For a review, see, for example, C. Dekker and M. A. Ratner, Phys. World **14**, 29 (2001).
[2] Y. Okahata, T. Kobayashi, K. Tanaka, and M. Shimomura, J. Am. Chem. Soc. **120**, 6165 (1998).
[3] H. W. Fink and C. Schönenberger, Nature (London) **398**, 407 (1999).
[4] A. Y. Kasumov, M. Kociak, S. Gueron, B. Reulet, V. T. Volkov, D. V. Klinov, and H. Bouchiat, Science **291**, 280 (2001).
[5] D. Porath, A. Bezryadin, S. De Vries, and C. Dekker, Nature (London) **403**, 635 (2000).
[6] L. T. Cai, H. Tabata, and T. Kawai, Appl. Phys. Lett. **77**, 3105 (2000).
[7] A. Rakitin, P. Aich, C. Papadopoulos, Y. Kobzar, A. S. Vedeneev, J. S. Lee, and J. M. Xu, Phys. Rev. Lett. **86**, 3670 (2001).
[8] E. Braun, Y. Eichen, U. Sivan, and G. Ben-Yoseph, Nature (London) **391**, 775 (1998).
[9] P. J. De Pablo, F. Moreno-Herrero, J. Colchero, J. G. Herrero, P. Herrero, A. M. Baro, P. Ordejon, J. M. Soler, and E. Artacho, Phys. Rev. Lett. **85**, 4992 (2000).
[10] S. O. Kelley and J. K. Barton, Science **283**, 375 (1999).
[11] S. J. T. van Noort, K. O. van der Werf, B. G. de Grooth, N. F. van Hulst, and J. Greve, Ultramicroscopy **69**, 117 (1997).
[12] M. Hegner, P. Wagner, and G. Semenza, FEBS Lett. **336**, 452 (1993).
[13] The small nanoelectrodes made by the technique reported by D. Porath in Ref. 5 do not allow AFM imaging between the electrodes.
[14] M. Bixon, B. Giese, S. Wessely, T. Langenbacher, M. E. Michel-Beyerle, and J. Jortner, Proc. Natl. Acad. Sci. U.S.A. **96**, 11713 (1999).
[15] Material obtained from Amersham Pharmacia Biotech., Piscataway, NJ.
[16] R. Guckenberger, M. Heim, G. Cevc, H. F. Knapp, W. Wiegrabe, and A. Hillebrand, Science **266**, 1538 (1994).
[17] D. D. Eley and D. I. Spivey, Trans. Faraday Soc. **58**, 411 (1962).
[18] J. Jortner, M. Bixon, T. Langenbacher, and M. E. Michel-Beyerle, Proc. Natl. Acad. Sci. U.S.A. **95**, 12759 (1998).

Insulating behavior of λ-DNA on the micron scale

Y. Zhang[1], R. H. Austin[1], J. Kraeft[2], E. C. Cox[2], and N. P. Ong[1]
[1]*Department of Physics, and* [2]*Department of Molecular Biology,*
Princeton University, Princeton, New Jersey 08544
(Dated: July 11, 2004)

We have investigated the electrical conductivity of λ-DNA using DNA covalently bonded to Au electrodes. Thiol-modified dTTP was incorporated into the 'sticky' ends of bacteriophage λ-DNA using DNA polymerase. Two-probe measurements on such molecules provide a hard lower bound for the resistivity $\rho > 10^6\,\Omega$cm at bias potentials up to 20 volts, in conflict with recent claims of moderate to high conductivity. By direct imaging, we show that the molecules are present after the measurements. We stress the importance of eliminating salt residues in these measurements.

The question whether DNA is electrically conducting has generated broad interest. The initial spurt of interest arose in photoexcitation experiments which were interpreted in terms of long-range electron transfer [1]. In the past few years, there have been upwards of 20 papers reporting the results of more direct electrical measurements ranging from contactless meaurements at microwave frequencies to DC measurements. A distressingly wide range of conductivity values – from $\rho < 10^{-4}\,\Omega$cm to $\rho > 10^6\,\Omega$cm – has been reported [2, 3, 4, 5, 6]. Proximity-induced superconductivity in DNA has also been claimed [7]. Recently, local polarization measurements by 'electrostatic force microscopy' have been used to show that λ-DNA is insulating [8, 9]. We note, however, that the force-microscopy experiments probe conductivity at relatively weak bias potentials.

In many of the DC measurements, contact with the metal electrodes (usually Au) was achieved by laying down the molecules directly on the electrodes. Although expedient, this approach raises several concerns. It is very difficult to prove that the DNA molecule is in direct physical contact with the electrodes. Even if contact is attained, the weak physical adhesion between DNA and Au may produce an insulating contact and possibly account for the wide variation in reported resistivities [10]. A recent experiment on octanedithiol [11] has shown that deliberate chemical bonding between organic molecules and metal electrodes is a pre-requisite for achieving reproducible conductivity results. Thus a better approach would be to achieve direct chemical binding between the open ends of λ-DNA and Au. The bonds should be strong enough to withstand shear forces in a flow, and should survive the measurement process. A second concern is the shunting effect of buffer residue. Because of its finite conductance, the buffer salts which coat the electrodes and substrate produce a spurious conductance signal. Hence adequate salt removal is important. We report the results of experiments performed along these lines. Our results show that λ-DNA is a good insulator up to bias potentials of 20 volts.

Chemical binding between organic molecules and Au is usually achieved by the Au-thiol (SH) chemical bond [12]. Commercially available oligonucleotides modified to incorporate the thiol group usually have carbon-chain spacers (C3 or C6) between the thiol group and DNA [3, 6, 13], which may present barriers to electron transfer. To avoid the spacer problem, we adopted an approach in which the DNA base-pair is bound *directly* to gold electrodes by a Au-thiol bond. This approach should provide the most direct conductance channel between the gold electrode and the putative electronic "π-way" proposed for the DNA helix [14].

λ-DNA is a double-stranded DNA helix comprised of 48,502 base pairs (length $\sim 16\,\mu$m). At the extremities, there are single-stranded 12-base 5' overhangs ('sticky ends'), with the complementary sequences

5′−GGG CGG CGA CCT, 5′−AGG TCG CCG CCC,

where A,C,G,T are the nucleotides adenine, cytosine, guanine and thymine, respectively. Our technique relies on the incorporation of T's modified to include the desired thiol group [15, 16]. The 'sticky' ends are filled in by a standard reaction [17] using the Klenow fragment of DNA polymerase and the three deoxynucleoside triphosphates dATP, dGTP, and S^4-dTTP (see Fig. 1-A). Because of the preponderance of modified dTTPs (and absence of dCTP) in solution, we can incorporate a significant number of modified T's at both ends of each DNA molecule [18]. To prevent the Klenow fragment from excising T's that are not Watson-Crick matched to the template, we use a mutated form of the Klenow fragment which lacks the 3'→5' proof-reading activity [19].

We tested the incorporation of the nucleotides into the DNA ends by a ligation assay [20]. Unmodified λ-DNA is readily ligated by T4 DNA ligase to form multimers. In the modified λ-DNA, however, the sticky ends – now filled in by the incorporated bases – are blunt, and multimer formation is strongly suppressed. The reaction products were analyzed by pulsed-field gel electrophoresis. As shown in Fig. 1-B, unmodified λ-DNA ("natural-λ") was efficiently ligated (lane 3). To control for the possibility that unincorporated S^4-dTTP inhibited ligation, λ-DNA monomers were ligated in the presence of all 3 dNTP's minus the polymerase ("control-λ"), and the ligation was also efficient (lane 6). The majority of the thiol-modified λ-DNA ("HS-λ"), however, remained as monomers (lane

Phys. Rev. Lett. 89, 198102 (2002)

5). This provides strong evidence that the protocol is effective in incorporating bases into the ends of λ-DNA.

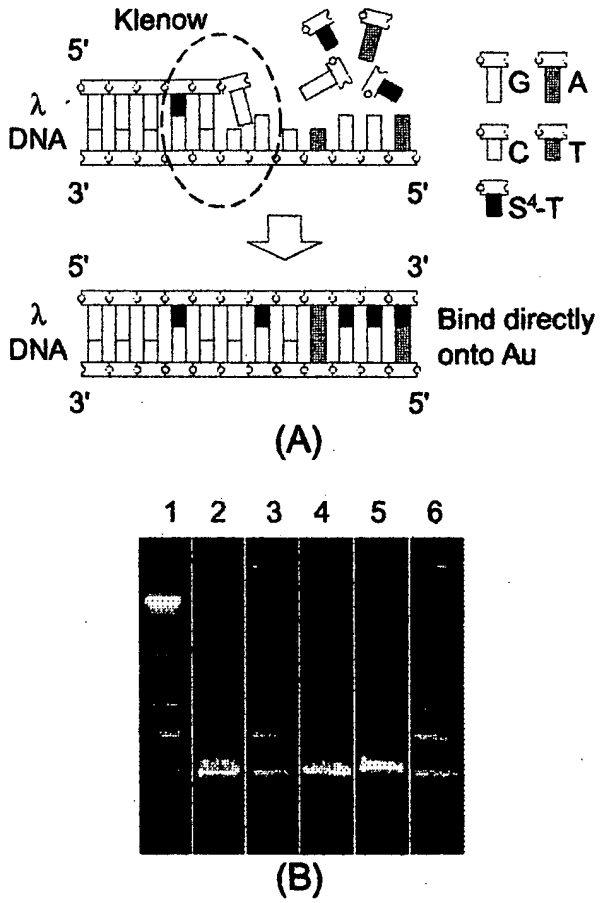

FIG. 1: (A) The schematic of the incorporation of deoxynucleoside triphosphates into λ-DNA 'sticky' ends using the Klenow fragment (3'→5' exo$^-$); (B) Pulsed-field gel (PFG) electrophoresis of thiol-modified and natural λ-DNA before and after ligation [21]. Lane 1: λ-DNA PFG marker (New England Biolabs); 2: unmodified "natural-λ" monomers; 3: ligated "natural-λ" multimers; 4: thiol-modified λ-DNA ("HS-λ") monomers; 5: "HS-λ" after ligation, with no significant multimer formation; 6: "control-λ" after ligation, proving that the presence of unincorporated S^4-dTTP and other dNTPs does not inhibit the ligation reaction.

Using standard photolithography, we constructed Au electrodes on a quartz substrate in parallel strips, 4 μm wide and 5 mm long, and separated by 4 or 8 μm. The Au surfaces were rigorously cleaned [22] before depositing the modified DNA. At several stages during these experiments, it was important to observe the molecules in an optical microscope. To image the thiol-modified DNA molecules, we stained them with the fluorescent intercalating dye TOTO1 (Molecular Probes), and then loaded them on the chip. After a 20-min. incubation period, many of the molecules were observed to be attached to the electrodes at one end. The unattached molecules were carefully rinsed in 1×TE [23]. The chip was then covered with a clean coverslip, and a flow of the buffer solution was applied perpendicular to the electrodes. We observed that DNA molecules anchored at one end were stretched by the buffer flow to bridge the space between the electrodes. Many of these molecules subsequently attached to the second electrode by their free end. After this occurs, the flow may be repeatedly reversed to demonstrate that the anchored DNA molecules bow out with the flow while their ends remain anchored (Panels A and B of Fig. 2. See video in Ref. [24]). This is direct evidence that chemical binding between the ends to Au is much stronger than physical adhesion of the rest of the molecule to either quartz or Au. (For the specific DNA samples used in the resistivity measurements, we carried out the dye-staining step *after* the measurements to avoid inadvertent damage from dye intercalation.)

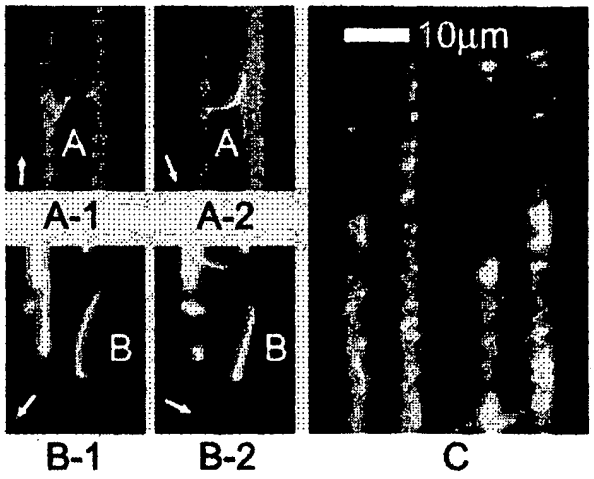

FIG. 2: Images of HS-λ DNA on quartz chips with Au electrodes. The DNA molecules were pre-stained with TOTO1. Observations were through a Nikon Eclipse TE300 inverted microscope equipped with a 60× oil-immersion lens (N.A.=1.4), and excited by a collimated Ar:Kr ion laser at 488 nm. Fluorescence images were collected at 533 nm by an intensified CCD camera (RoperScientific, Princeton Instruments) and digitally enhanced. Au electrodes appear as vertical stripes. Arrows represent the flow direction. Panel A-1 & 2: Molecule A, anchored at both ends, and flexing with the flow. Panel B-1 & 2: Both ends of molecule B were attached on the same electrode, with the mid-segment moving freely in the buffer, showing that the attachment was specific to the thiol-modified ends. Panel C: Many HS-λ DNA molecules spanning two electrodes. The image was taken after the Mg^{2+} and NH_4Ac rinsing. Scale bar applies to all panels [24].

As discussed above, a crucial step in the experiment was the removal of buffer. In preliminary experiments, we repeatedly observed a finite, semiconductor-like, history-dependent conductance after loading DNA solution and

removing the buffer solution. The inset of Fig. 3 is a representative I-V curve of the buffer salt residue, 1×TE. Such spurious signals are of particular concern when DNA is laid down on electrodes in a thick bundle, because the salts trapped between the DNA molecules can form conduction paths. The spurious background vanished after we adopted the following procedure. Chips containing bridging DNA molecules were carefully rinsed in 5 mM ammonium acetate (NH_4Ac, pH 6.6), a volatile buffer that can be completely removed in high vacuum. A drawback of this rinsing is that a large fraction of the anchored DNA molecules are cut after rinsing and drying. However, rinsing in 10 mM $MgSO_4$/40 mM Tris-HCl (pH 8) *before* the NH_4Ac rinsing introduces Mg^{2+} ions which coat the quartz surface with weak positive charges [6]. As the negatively charged DNA molecules stick to the substrate by electrostatic interaction, damage due to NH_4Ac rinsing is minimized. Panel C of Fig. 2 shows a typical image of anchored DNA after Mg^{2+} and NH_4Ac rinsing. [Rinsing with the $MgSO_4$ solution also led to binding of unmodified λ-DNA. However, the yield of anchored molecules was much smaller.]

To perform the electrical measurements, unstained thiol-modified λ-DNA was attached to the Au electrodes as described above. After the final NH_4Ac rinsing, the chip was dried in the dark to avoid possible photon-induced damage. Two-probe I-V measurements were performed in moderately high vacuum ($< 10^{-7}$Torr).

A typical room-temperature I-V curve, measured on λ-DNA spanning electrodes 4 μm apart, is shown in the main panel of Fig.3. The voltage was swept between ±20 V. A linear fit to the data in Fig. 3 yields $dI/dV = (-3 \pm 9) \times 10^{-14}$S. Using a cross-section of ~3 nm^2 per molecule, and the estimated number of bridging molecules (~1000), we obtain the bound on the resistivity of $\rho > 10^6$ Ωcm in electric fields E up to $\sim 10^4$V/cm. Measurements performed on several chips yielded consistent results. No current was detected within the noise level of our measurement(~ ±10 pA), despite sustained and deliberate efforts to improve electrical contacts between the base pair stack of λ-DNA and Au.

Immediately after the measurements, a buffer solution with an appropriate amount of TOTO1 dye dissolved in 1×TE was loaded on the chip. By direct optical microscopy inspection of the post-stained DNA, we confirmed that there were ~1000 DNA molecules bridging the electrodes, and thus the measurements did not destroy the DNA.

As a final check that the observed images are those of λ-DNA, we introduce DNase to digest the molecules [29]. Complete deletion of all fluorescent DNA molecules was observed. These tests leave very little room for doubt that a large number of *intact* DNA molecules were chemically bound to the electrodes during the electrical measurements [25].

The bound $\rho > 10^6$ Ωcm in our experiment and the large bias potential applied (20 V) is at odds with many recent reports of moderately high conductivity. In some DC experiments, the DNA molecules formed bundles or networks between the microfabricated electrodes [26, 27, 28]. As noted above, high conductance may arise from residual salts trapped between the DNA strands. Contamination from other sources (C or Re) may be a problem as well in the experiment on proximity-induced superconductivity in λ-DNA [7]. Microwave absorption experiments have been used to infer that $\rho \simeq 1$ Ωcm at 295 K in λ-DNA [30]. The high microwave conductivity, 10^6 times larger than our bound, is very difficult to reconcile with our data. If λ-DNA had such a high uniform conductivity, all the applied potential should fall across the contacts (~2-3 nm) to produce an E-field $\sim 10^8$ V/cm, high enough to produce a large tunneling current, if not breakdown of the contact barrier altogether. This is not observed. Possibly, the microwave

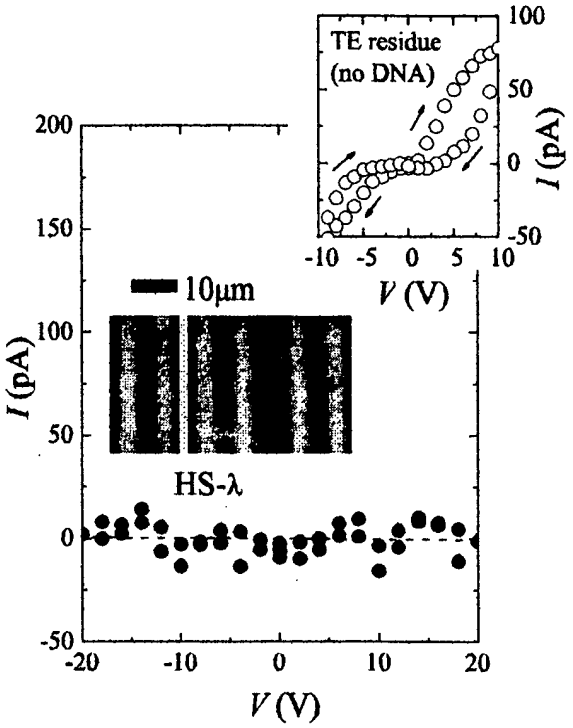

FIG. 3: The two-probe current vs. voltage (I-V) curve for a sample of λ-DNA bridging 2 parallel Au electrodes separated by 4 μm (the sample comprises ~1000 molecules). The DNA was rinsed with NH_4Ac before the measurement to remove the buffer salt residue. The dashed line is a linear fit to the data. The inset shows the two-probe I-V curve for a test chip containing 1×TE buffer solution (without DNA). The chip was dried in vacuum but not subject to NH_4Ac rinsing. The observed conductance is entirely from trace TE salt residue. Both measurements were done in vacuum ($< 10^{-7}$ Torr) at 295 K. Open-circuit impedance between any two electrodes was always ≫10 TΩ.

is detecting very short dissipative regions embedded in the insulating molecule.

Two groups recently used electrostatic force microscopy to probe the electrostatic polarization of DNA [8, 9]. Our results are consistent with their conclusion that DNA is insulating. However, the electrostatic force microscopy technique probes conductivity in the limit of weak bias potentials, so it does not rule out a transition to moderately large conductivity above a bias threshold of several volts (as reported in some experiments [4, 31]). The present experiments show that insulating behavior extends to bias potentials as high as 20 volts.

We are grateful to P. M. Chaikin for invaluable suggestions, and acknowledge fruitful discussions with Shirley S. Chan, J. Tegenfeldt, P. Silberzan, Christelle Prinz, S. Park and R. Huang. This research is supported by a U.S. National Science Foundation MRSEC grant (DMR 98-09483) and by the National Inst. Health (NIH HG01506).

---

[1] C. J. Murphy *et al.*, Science **262**, 1025 (1993); S. O. Kelley and J. K. Barton, Science **283**, 375 (1999).

[2] H.-W. Fink and C. Schonenberger, Nature **398**, 407 (1999).

[3] E. Braun *et al.*, Nature **391**, 775 (1998).

[4] D. Porath, *et al.*, Nature **403**, 635 (2000).

[5] P. J. de Pablo *et al.*, Phys. Rev. Lett. **85**, 4992 (2000).

[6] A. J. Storm *et al.*, Appl. Phys. Lett. **79**, 3881 (2001).

[7] A. Yu. Kasumov *et al.*, Science **291**, 280 (2001).

[8] C. Gómez-Navarro *et al.*, Proc. Natl. Acad. Sci. USA **99**, 8484 (2002).

[9] M. Bockrath *et al.*, Nano Lett. **2**, 187 (2002).

[10] K. W. Hipps, Science **294**, 536 (2001).

[11] X. D. Cui *et al.*, Science **294**, 571 (2001).

[12] C. A. Mirkin *et al.*, Nature **382**, 607 (1996).

[13] User Guide to DNA Modification, Glen Research, 1999. See the refs. therein.

[14] D. D. Eley and D. I. Spivey, Trans. Faraday Soc. **58**, 411 (1962).

[15] In the modified nucleotide 4-thiothymidine-5'-triphosphate (S^4-dTTP, Trilink Biotechnologies), a sulfur atom is covalently bound to the C4 site of the thymine molecule. Its close proximity to the hydrogen ion at the N3 site results in a resonant state that forms the desired thiol group.

[16] A. G. Lezius and K. H. Scheit, European J. Biochem. **3**, 85 (1967); T. V. S. Rao *et al.*, Bioorg. Med. Chem. Lett. **10**, 907 (2000).

[17] The incorporation reaction was 100 μg/ml λ-DNA, 0.1 mM dATP, 0.1 mM dGTP and 0.2 mM S^4-dTTP in 1× EcoPol buffer(10 mM Tris-HCl, 5 mM $MgCl_2$ and 7.5 mM dithiothreitol (DTT); pH7.5 @ 25°C; New England Biolabs), for a total volume of 100 μl. Five units of Klenow fragment (3'→5' exo$^-$) were added. The mixture was incubated at 37 °C for 30 min. To stop the reaction, 1μl of 0.5 M EDTA was added, and the mixture heated at 75°C for 20 min. To exchange the buffer, the product was dialyzed against 30 ml 0.1×TE at room temperature for 45 min across a 50 nm Millipore membrane.

[18] One 5' overhang of the λ-DNA ends with an A, which is Watson-Crick matched to S^4-T. The other overhang ends with G's, which are matched to C's. While sulfur-modified dCTP is available, the sulphur is remote from H atoms and the resonant thiol group can not form. To maximize the probability of modified T's at both ends, we excluded dCTP altogether from the reaction, so that S^4-T:G pairing could occur in place of C:G. The mutated Klenow fragment used here is incapable of detecting the mis-matches.

[19] The Klenow fragment is a large fragment of DNA polymerase I lacking the error-correcting 5'→3' exonuclease activity (this function damages the λ-DNA 'sticky' ends). Here, we employed a mutated form of the Klenow fragment (3'→5' exo$^-$, New England Biolabs) in which the proof-reading 3'→5' exonuclease activity is deleted. S^4-dTTP binds more weakly to A than unmodified dTTP [16], and hence the proof-reading activity could possibly remove incorporated S^4-dTTP.

[20] The reaction was carried out in 1× ligation buffer (50 mM Tris-HCl, 10 mM $MgCl_2$, 10 mM DTT, 1 mM ATP and 25 μg/ml BSA; pH 7.5@25 °C) at a λ-DNA concentration of 50 μg/ml. 400 units of T4 DNA ligase (New England Biolabs) was added to the reaction volume of 20 μl, and incubated at room temperature for 5 h.

[21] 1% agarose gel in 0.5×TBE buffer; E=6 V/cm; 14 °C; 16 hours; switch time ramped from 0.1 sec to 40 sec.

[22] To clean the Au surface, freshly prepared chips were soaked in fuming HNO_3 for 30 min, and further cleaned in a mixture of 18 MΩcm deionized water, ammonium hydroxide and hydrogen peroxide (5:1:1 by volume, 70 °C) for 20 min. The chips were thoroughly rinsed in deionized and distilled water (DD H_2O), and kept in Ar-flushed DD H_2O for no more than 30 min before loading DNA samples. The Au surface was never allowed to dry during the process.

[23] 1×TE buffer contains 10 mM Tris (tris(hydroxymethyl)-aminomethane) and 1 mM EDTA (ethylene diamine tetra acetic acid), pH 8.0 .

[24] See videos at http://suiling.princeton.edu/research/DNAconductance/DNAconduction.html.

[25] The strong fluorescence observed after the resistivity measurements strongly argues against denaturation of DNA into single strands when affixed to quartz in vacuum. TOTO1 displays strong fluorescence only when bound to double-strand DNA. Moreover, AFM images of B-DNA in vacuum have recently been obtained by Takayuki Uchihashi *et al.*, Langmuir **16**, 1349 (2000); *ibid* Jpn. J. Appl. Phys. **39**, L887 (2000).

[26] A. Rakitin *et al.*, Phys. Rev. Lett. **86**, 3670 (2001).

[27] L. Cai, H. Tabata, and T. Kawai, Appl. Phys. Lett. **77**, 3105 (2000).

[28] J. Gu *et al.*, Appl. Phys. Lett. **80**, 688 (2001).

[29] To digest the DNA, we used 10 units of DNase I (RNase-free, Roche Molecular Biochemicals) dissolved in 10 μl reaction buffer (40 mM Tris-HCl, 10 mM $MgSO_4$, and 1mM $CaCl_2$).

[30] P. Tran, B. Alavi, and G. Gruner, Phys. Rev. Lett. **85**, 1564 (2000).

[31] H. Watanabe *et al.*, Appl. Phys. Lett. **79**, 2462 (2001).

Contactless experiments on individual DNA molecules show no evidence for molecular wire behavior

C. Gómez-Navarro*†, F. Moreno-Herrero*, P. J. de Pablo, J. Colchero, J. Gómez-Herrero, and A. M. Baró

Laboratorio de Nuevas Microscopías, Departamento de Física de la Materia Condensada, Facultad de Ciencias, Universidad Autónoma de Madrid, 28049, Cantoblanco, Madrid, Spain

Edited by Robert H. Austin, Princeton University, Princeton, NJ, and approved April 26, 2002 (received for review November 15, 2001)

A fundamental requirement for a molecule to be considered a molecular wire (MW) is the ability to transport electrical charge with a reasonably low resistance. We have carried out two experiments that measure first, the charge transfer from an electrode to the molecule, and second, the dielectric response of the MW. The latter experiment requires no contacts to either end of the molecule. From our experiments we conclude that adsorbed individual DNA molecules have a resistivity similar to mica, glass, and silicon oxide substrates. Therefore adsorbed DNA is not a conductor, and it should not be considered as a viable candidate for MW applications. Parallel studies on other nanowires, including single-walled carbon nanotubes, showed conductivity as expected.

Electrical transport through molecular wires (MWs) has been the subject of intense interest the last few years (1–4). MWs are expected to present conductive properties considerably different from those of bulk conductors (5). In addition, conductive molecules could be used to interconnect different parts of a circuit in nanoscale devices, playing an important role in future electronics (6). Among the different molecule candidates for MWs, carbon nanotubes and DNA have been the subject of a number of studies in the last few years, which dealt with the transport properties of these two molecules (7, 8).

Carbon nanotubes (9) are derived from a curved graphene sheet and, depending on the rolling direction of this sheet, the current versus voltage, I/V characteristics evolve from linear (without gap) to a semiconductor type, with a clear gap near 0 V (7). Although the precise mechanism for electron transport in nanotubes remains unclear (3, 10–12), there is general agreement on the possibility of carbon nanotubes being MWs.

The current situation of the conducting properties of DNA is less clearly resolved. Depending on the study, DNA is a good conductor with linear I/V characteristics (13), a conductor with a gap that gets wider with temperature (14), a fairly good insulator (15–17), or even a superconductor with very low resistance at room temperature (18). In addition, it has even been proposed that DNA can be doped from a semiconducting molecule to a metallic conductor with linear I/Vs (19). In summary, published claims on DNA electrical conductivity span over 10 orders of magnitude!

The simplest circuit to measure the resistance of a given object is likely to require a battery, a current meter, and two contacts to the object. In the macroscopic world, the technology to perform electrical contacts is well established. In the nanoscopic world making reliable contacts is a nontrivial problem. In ref. 17 a circuit similar to the one described above was used in an attempt to measure the resistance of DNA molecules. In that experiment, the DNA molecule was partially covered by a macroscopic gold electrode while the second electrode was a metallic scanning force microscopy (SFM) tip. The large resistance between the two contacts measured in that work was attributed to the high resistance of the DNA molecule. Since that was a two-terminal measurement, it is possible to argue that the large resistance was caused by unreliable electrical contacts.

In the present work we perform a systematic study on the electrical properties of individual double-stranded DNA molecules. The basic idea of this study is to minimize the effects of the electrical contacts on the measurements, aiming at the intrinsic electronic properties of the DNA molecules. Accordingly, the experiments described below avoid mechanical contact of the SFM tip with the sample. The electrical properties of the molecules studied are inferred from the electrostatic force between tip and sample, which is a contactless measurement. We have performed three different experiments. In the first two experiments, one end of the DNA molecules is directly connected (*i*) to a gold electrode and (*ii*) to a single-walled carbon nanotube (SWNT) that itself is connected to a macroscopic gold electrode. In the third experiment, the DNA molecules are simply adsorbed on an insulating substrate with no contact to any conducting object. From the measured electrostatic forces induced between tip and sample in all three set-ups we conclude that the DNA molecules do not have any significant DC conductivity.

The physical principles involved in the experiments are related to the electrostatic forces between metallic and dielectric objects. These are determined by the geometry and the density of mobile and bound charges. Electrical transport properties are closely related to the density of mobile charges and the ability of these charges to move. The two first experiments are realized by applying a potential difference between a molecule and a SFM tip by using a battery (Fig. 1*i*). From an electrostatic point of view, any MW can be modeled as a resistance and a capacitance. In this situation, charge passes through the resistor, charging the capacitor. The amount of charge in the capacitor can be measured by attaching a force detector to the upper plate of the capacitor (Fig. 1*i*). On a nanoscopic scale an SFM can be used as a force detector (20–23). To measure this force, an SFM metallic tip is placed over the molecule. The tip is oscillated at its resonance frequency ω_0, and the amplitude of the oscillation is monitored and kept constant. The electrostatic force gradient between the tip and the molecule induces a resonance frequency shift as is seen in the experimental data shown in Fig. 1*ii*. If no frequency shift is observed over the molecule we conclude that no charge has passed through the molecule and therefore it is an insulator.

To understand the third experiment we should consider the case of an object placed in an external electric field. Charges will then be induced in proportion to the dielectric constant ε (in a metal ε can be considered to be very high) through polarization. The force produced near a polarized material, although smaller than in the case of a metal object, can also be measured with SFM (24). Bare molecules adsorbed on an insulating substrate will modify the electrostatic force between tip and substrate. In principle the electronic properties of the molecules can be determined from a precise measurement of this force. Since a quantitative determination of the electrostatic force is very

This paper was submitted directly (Track II) to the PNAS office.

Abbreviations: MW, molecular wire; SFM, scanning force microscopy; SWNT, single-walled carbon nanotube.

*C.G.-N. and F.M.-H. contributed equally to this work.

†To whom reprint requests should be addressed. E-mail: cristina.gomez@uam.es.

www.pnas.org/cgi/doi/10.1073/pnas.122610899

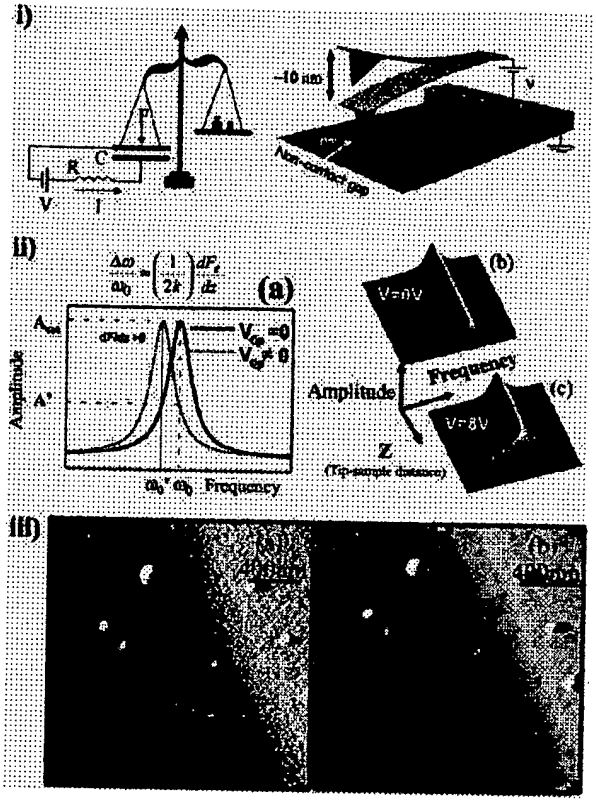

Fig. 1. The nonintrusive method used in this work is illustrated. (*i*) The MW, characterized by a resistance (R) and a capacitance (C), is connected to a metal electrode. A SFM metallic tip of force constant k is placed over the molecule. The tip is oscillated at its resonance frequency ω_0, and the amplitude of the oscillation is monitored and kept constant. When a voltage V is applied between the tip and the sample the molecule gets charged, and an attractive force appears between the tip and the sample. The RC factor of the MW determines the time required for the molecule to be charged. The experiment can be seen as a balance (force sensor), a battery, a resistor R, and a capacitance C. When the circuit is closed, electrical charges are accumulated at the plates, giving rise to an electrostatic force that is detected by the balance. The gradient of the electrostatic force introduces a shift of the resonance frequency to lower values. (*iia*) This frequency shift is shown. (*iib*) The oscillation amplitude A is measured as a function of the frequency ω and the tip-sample distance z $A(\omega,z)$, since no voltage is applied between the tip and metallic sample, no frequency shift caused by long-range interaction is observed. (*iic*) A bias voltage of 8 V is applied, producing a clear frequency shift. The total z displacement in these images is 200 nm. (*iiia*) SFM topography showing randomly dispersed SWNT on a silicon oxide substrate where some of the molecules appear partially covered by a gold electrode. (*iiib*) SFM topography showing the same area as in *iiia* but with a tip-sample bias voltage of +2 V. Notice that those SWNTs electrically connected to the metal electrode appear wider and higher because of the electrostatic interaction.

difficult for a complex system such as SFM, in the present work we have performed a comparative measurement of DNA molecules with two other materials of known electronic properties: SWNTs and isolating substrates such as mica, glass, and silicon oxide.

Samples were prepared in a two-step process. The first step is the adsorption of a random population of molecules on an insulating substrate.‡ The sample is then inspected by SFM to check the density of adsorbed molecules. The second step, which is not always required, is the evaporation of a metal electrode. Along the electrode edge a number of molecules are partially covered by metal. In the present work we will focus on two different kinds of samples: SWNTs on SiO_2 and SWNTs and DNA molecules coadsorbed on a variety of insulating substrates.

As a test, we measured the electrostatic response of a sample with SWNTs. Fig. 1*iiia* is an SFM topographic image showing the edge of a gold electrode and SWNTs randomly dispersed on the SiO_2 substrate.§ A number of SWNTs are in direct contact with the gold electrode. When a biased metal tip is driven to contact with one of those molecules, an electric current passing between the SFM tip and the gold electrode through the SWNT is detected (25). Fig. 1*iiib* is an SFM topographic image of the same area shown in Fig. 1*iiia* but a bias voltage of 2 V is applied to the SFM tip.¶ We note that during acquisition of both images (Fig. 1 *iiia* and *iiib*) the tip is not driven to contact with the nanotube. The connected nanotubes appear wider and higher in Fig. 1*iiib* than in Fig. 1*iiia*. This is caused by the electrostatic force present between the tip and the conducting SWNTs. As the voltage is reduced the apparent width and height of the connected SWNTs decrease.

When the SFM cantilever, driven at its free resonance frequency, feels the electrostatic interaction of the molecule, the resonance frequency of the system shifts to smaller values, the oscillation amplitude decreases (see Fig. 1*ii*), and the SFM feedback withdraws the tip to recover the set point amplitude. For a more detailed discussion of this effect see ref. 26. Therefore, the biased SWNTs appear higher and wider in the topographic images. An important feature seen in Fig. 1*iiib* is that not only the SWNTs directly connected to the gold electrode show this effect, but those nanotubes connected via a second or even a third nanotube also present this electrostatic contrast. Thus, the experiment shown in Fig. 1*iiib* is able to detect a network of SWNTs electrically connected to the gold electrode (26).

To compare the electrical properties of DNA and SWNTs, both molecules were coadsorbed on an isolating substrate.‡ Based on the above result, DNA molecules should also present electrostatic contrast if they are conducting. Fig. 2*a* shows an SFM topographic image of a mica substrate with a SWNT and a DNA molecule partially covered by the gold electrode. Fig. 2*b* is an image of the same area shown in Fig. 2*a* but with a bias voltage of +1.6 V applied between tip and electrode. Notice that while the SWNT appears higher and wider because of the presence of the electrostatic interaction, the DNA molecule remains unmodified. Therefore, no charges have passed from the gold electrode to the DNA, implying that DC conductivity in DNA is negligibly small. As a double-check experiment, the tip was driven into mechanical contact with the DNA. No current was detected above the noise level (1 pA) in good agreement with the results of ref. 17.

It could be argued that the connection to the DNA molecule by means of an evaporated macroscopic electrode could modify its properties. Therefore, in a further experiment, a more gentle electrical contact to the DNA was established through a SWNT. Fig. 2*c* shows a DNA molecule connected to a carbon nanotube

‡Sample preparation. Clean substrates were pretreated with 3-aminopropyltriethoxysilane (APTES) by immersing them in a 0.1% volume of APTES for 15 min. Then, they were rinsed with 2-propanol and ultrapure water and dried with nitrogen. Substrates prepared this way are positively charged. A mixture of λ DNA and SWNT was dropped over the substrates and allowed to bind for 1 h. Then, it was washed with water and dried. Concentrations of DNA and SWNT were adjusted by SFM inspection until a final concentration of about one λ DNA molecule and 5–10 SWNT per micron square was obtained.

§SFM imaging. The experiments were carried out by using a SFM working in noncontact dynamic mode. Olympus-type cantilevers with a resonance frequency of 80 kHz were consecutively covered with 20 nm of titanium and 20 nm of gold. Topography images were taken by using a dynamic force microscope with a free oscillating amplitude of 15 nm, and feedback was set at an amplitude slightly lower than this value (reduction of about 10%). The scan frequency was 1 Hz.

¶A similar effect was observed for negative voltages.

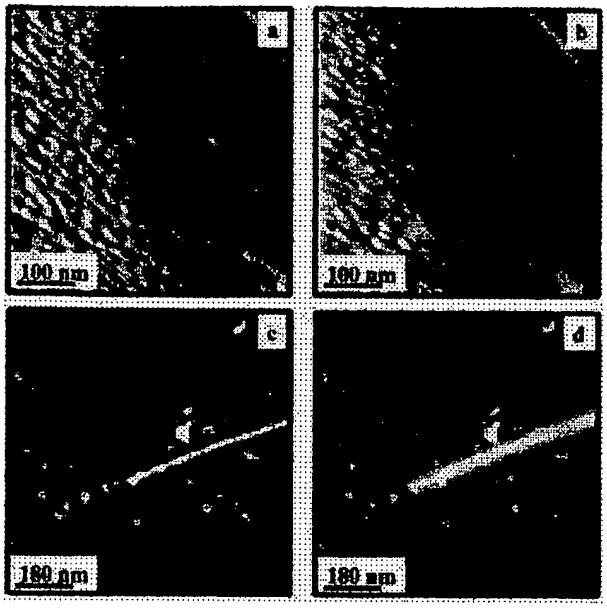

Fig. 2. (*a*) SFM topography showing a SWNT and a DNA molecule on a mica substrate. Both molecules are in clear contact with the gold electrode. (*b*) SFM topography showing the same area as in *a* but with a bias voltage of +1.6 V applied between the tip and the sample. While the effect of the bias voltage can be clearly seen on the gold electrode and the nanotube, the DNA molecule is not affected by the electrostatic interaction. (*c*) The SFM topographic image shows a DNA molecule on a glass substrate at zero bias voltage in contact with a SWNT. (*d*) Same as in *c* but with a voltage of +3 V between the tip and the sample. While the effect of the electrostatic interaction is clearly seen in the nanotubes, the contrast of DNA molecule does not change. To enhance the edges a high past filter has been performed on the images.

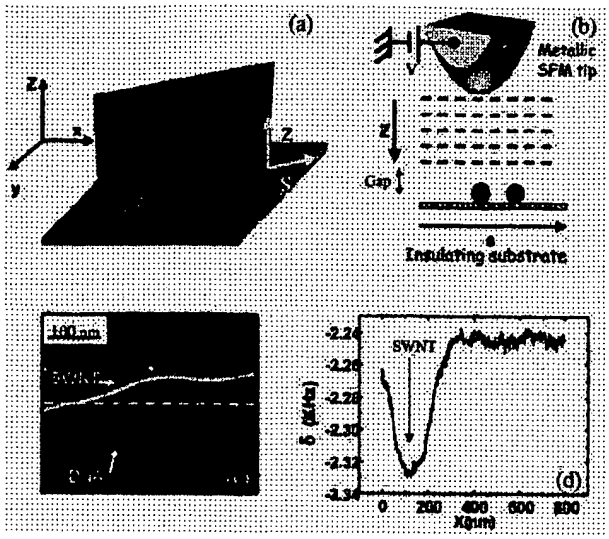

Fig. 3. (*a* and *b*) A scheme of the contactless experiment performed on two different molecules coadsorbed on an insulating substrate. Frequency-shift profiles are taken at different tip-sample distances. In the experiment, the SFM tip never establishes contact with the adsorbed molecules. (*c*) SFM topographic image showing a SWNT and a DNA molecule adsorbed on mica. (*d*) This graph shows a frequency-shift profile along the dashed line drawn in *c*. A clear frequency shift is observed above the SWNT, whereas no measurable change appears above the DNA molecule. This profile was taken with the tip placed at 10 nm above the surface. A phase-locked loop was used to keep the system at resonance. No feedback was applied on the oscillation amplitude.

in contact with a macroscopic gold electrode (not shown). Fig. 2*d* is a topographic image of the same area but with a tip-sample bias voltage of +3 V. As expected the SWNT is affected by the bias in the same way as in Fig. 1. On the contrary, the DNA molecule remains unmodified. The latter result can be contrasted with the experiments reported in Fig. 1*iiib* where several nanotubes, connected to the gold electrode via an intermediate SWNT, show electrostatic contrast.

Electrostatics deals with a system of charges in equilibrium. In a conductor electrostatic equilibrium is reached well below the typical time for SFM image acquisition (~100 s). Hence in the SWNT case, we are measuring a system in electrostatic equilibrium since the charges have passed through SWNT molecules until their electrostatic potential has become equal to the one of the electrode. If a molecule with poor, but nonzero conductivity is adsorbed on a perfect insulator the time required to reach the electrostatic equilibrium with the electrode can be, in principle, very large. In this case, SFM images taken at a fixed bias would show molecules that begin to present electrostatic contrast as the charge slowly passes through them. Eventually, electrostatic equilibrium will be reached and the molecule will present an electrostatic contrast in the SFM image as observed for SWNTs. Therefore, electrostatic interaction can be used to measure extremely small currents since the time to reach electrostatic equilibrium can be very long. We have never observed this charging effect on DNA, even when a bias was applied to the electrode overnight. The interpretation of this result is that the insulating substrate has a high, but finite, resistance. Charges pass along the surface of the insulator into the volume and into the ground or surrounding atmosphere. Since we see no electrostatic contrast between the DNA and the insulating substrate, we conclude that the DNA molecules must have a resistance comparable to that of the substrate. In the case of glass (one of the substrates used) a lower bound for its resistivity is 10^{12} Ω·cm.

We have confirmed the above reported results in many additional experiments testing different substrates (mica, glass, silicon oxide) and metal electrodes (gold, silver, chromium). All of these experiments confirmed the results described above: electrostatic contrast in the case of SWNT but not in the case of DNA molecules. If poly(C)–poly(G) is used instead of λ DNA again a negative result is obtained. Therefore, this experiment is in disagreement with the one reported by Cai *et al.* (27). To test the influence of high-resistance nanowires, electrostatic images of vanadium pentoxide fibers (10 nm width, 1.5 nm height) were adsorbed on SiO_2. V_2O_5 is a semiconductor MW with a high resistivity (0.5 Ω·cm, 500 times larger than the average values found in SWNTs) (28). When these molecules are used, a clear and marked contrast is obtained as the bias voltage is increased. This experiment suggests that the electrostatic method proposed in this work is a general tool, which can be applied to test nonzero conductivity of any MW.

We have further confirmed our results by carrying out a final experiment without any electrodes, avoiding any problem caused by electrical contacts. This experiment is shown in Fig. 3. Fig. 3*c* shows an SFM topographic image of a DNA molecule parallel to a SWNT (upper molecule). Both molecules are not connected to any electrode. After this topographic image, the tip is lifted 100 nm above the mica substrate while oscillating at the free-resonance frequency (Fig. 3*a*). A bias voltage of +6 V is then applied to the metal-covered tip. As the tip approaches the surface while scanning over the SWNT and the DNA molecule (Fig. 3*b*) a monotonic decrease of the resonance frequency $\delta\omega$ is observed because of the electrostatic force produced by the polarization of the insulating substrate (29). Fig. 3*d* shows a frequency-shift profile taken along the dashed line drawn in Fig.

3c, with the tip positioned at 10 nm above the sample. Whereas a remarkable decrement of the resonance frequency appears at the nanotube position, no signal, above our noise level, is detected when the tip is over the DNA molecule. Since the electrostatic force between tip and sample is basically produced by the effect of the polarization induced by the applied bias, the absence of a signal over the DNA molecule implies that the dielectric constant of the DNA and that of the substrate are similar. No significant contrast was detected over the DNA molecule at any bias voltage between ±10 V. However, the SWNT is a good conductor and hence its dielectric constant is very high. Thus, it presents a marked electrostatic signal with respect to the insulating substrate. If the experiment is repeated on a glass substrate a similar behavior is observed. This result is especially significant since it does not depend on any contact with the electrodes.

Our experiments agree with a number of previous scanning tunneling microscopy (STM) experiments on DNA. Imaging DNA adsorbed on a surface has been always difficult because of the poor conductivity of the molecule (30–32). Guckenberger *et al.* (15) have obtained STM images of DNA adsorbed on mica. Their experiments were interpreted as resulting from the presence of a water layer adsorbed on the substrate, which carried H^+ charges. Our experiments strongly disagree with the results of refs. 18 and 27 since our findings suggest a resistance similar to the resistance of the insulating substrates. DNA could still support AC conductivity as suggested in ref. 33, but according to our results DC conductivity in adsorbed DNA molecules must be ruled out. First, principle calculations performed in poly(C)–poly(G) DNA shows a band structure typical of a semiconductor (17), but in the λ DNA case the disorder introduced by the random base pair sequence entirely destroys the band structure. Electrical transport caused by polarons has been put forward as a second mechanism for DNA conductivity (34). Since polarons are associated with phonons, it is expected that adsorbed DNA molecules have a reduced degree of freedom, which significantly suppresses the phonon modes. Therefore, one would expect a decrease in the conductivity based on polaronic effects. Moreover, the structure of adsorbed DNA might also present distortions because of the molecule-substrate force that could modify its transport properties.

Our result is just another piece of evidence of an intriguing puzzle. To clarify the situation further, more theoretical and experimental work is required. In particular, precise calculations of the charge transfer rate caused by polarons for both free-standing and adsorbed DNA molecules would be particularly interesting. A recent theoretical work (35) shows that diffuse electrical transport at low rates only occurs in DNA in aqueous solution. This theoretical calculation together with our experimental results provide compelling evidence that shows that adsorbed DNA molecules do not exhibit MW behavior.

We thank S. Gómez-Moñivas, J. J. Sáenz, J. M. Soler, and R. Reifenberger for helpful discussions; M. T. Martinez, A. M. Benito, and W. K. Maser for kindly providing the solution with the SWNT; and M. Burghard for kindly providing the vanadium pentoxide fibers sample. We also acknowledge support from Ministerio de Educación y Cultura through Dirección General de Enseñanza Superior e Investigación Científica Projects Nos. BFM2001-0209 and MAT2001-0664. F.M.-H. is supported by a scholarship from Comunidad de Madrid.

1. Datta, S., Tian, W., Hong, S., Reifenberger, R., Henderson, J. I. & Kubiack, C. P. (1997) *Phys. Rev. Lett.* **79**, 2530–2533.
2. Kondo, Y. & Takayanagi, K. (1997) *Phys. Rev. Lett.* **79**, 3455–3458.
3. Frank, S., Poncharal, P., Wang, Z. L. & de Heer, W. A. (1998) *Science* **280**, 1744–1746.
4. Ohnishi, H., Kondo, Y. & Takayanagi, K. (1998) *Nature (London)* **395**, 780–783.
5. Datta, S. (1997) *Electronic Transport in Mesoscopic Systems* (Cambridge Univ. Press, Cambridge, U.K.).
6. Jortner, J. & Ratner, M. (1997) *Molecular Electronics* (Blackwell, Oxford).
7. Saito, R., Dresselhaus, M. S. & Dresselhaus, G. (1998) *Physical Properties of Carbon Nanotubes* (Imperial College Press, London).
8. Giese, B., Amaudrut, J., Kohler, A. K., Spormann, M. & Wessely, S. (2001) *Nature (London)* **412**, 318–320.
9. Iijima, S. (1991) *Nature (London)* **354**, 56–58.
10. Batchold, A., Strunk, C., Salvetat, J.-P., Bonard, J.-M., Forro, L., Nussbaumer, T. & Schonenberger, C. (1999) *Nature (London)* **397**, 673–675.
11. Tans, S. J., Devoret, M. H., Dai, H., Thess, A., Smalley, R. E., Geerligs, L. J. & Dekker, C. (1997) *Nature (London)* **386**, 474–477.
12. Kasumov, A. Y., Deblock, R., Kociak, M., Reulet, B., Bouchiat, H., Khodos, I. I., II, Gorbatov, Y. B., Volkov, V. T., Journet, C. & Burghard, M. (1999) *Science* **284**, 1508–1511.
13. Fink, H. W. & Schonenberger, C. (1999) *Nature (London)* **398**, 407–410.
14. Porath, D., Bezryadin, A., de Vries, S. & Dekker, C. (2000) *Nature (London)* **403**, 635–638.
15. Guckenberger, R., Heim, M., Cevc, G., Knapp, H. F., Wiegrabe, W. & Hillebrand, A. (1994) *Science* **266**, 1538–1540.
16. Braun, E., Eichen, Y., Sivan, U. & Ben-Yoseph, G. (1998) *Nature (London)* **391**, 775–778.
17. de Pablo, P. J., Moreno-Herrero, F., Colchero, J., Gómez-Herrero, J., Herrero, P., Baro, A. M., Ordejon, P., Soler, J. M. & Artacho, E. (2000) *Phys. Rev. Lett.* **85**, 4992–4995.
18. Kasumov, A. Y., Kociak, M., Gueron, S., Reulet, B., Volkov, V. T., Klinov, D. V. & Bouchiat, H. (2001) *Science* **291**, 280–282.
19. Rakitin, A., Aich, P., Papadopoulos, C., Kobzar, Y., Vedeneev, A. S., Lee, J. S. & Xu, J. M. (2001) *Phys. Rev. Lett.* **86**, 3670–3673.
20. Terris, B. D., Stern, J. E., Rugar, D. & Mamin, H. J. (1989) *Phys. Rev. Lett.* **63**, 2662–2672.
21. Schoenenberger, C. & Alvarado, S. F. (1990) *Phys. Rev. Lett.* **65**, 3162–3164.
22. Hao, H. W., Baro, A. M. & Saenz, J. J. (1991) *J. Vac. Sci. Technol. B* **9**, 1323–1329.
23. Hu, J., Xiao, X. D. & Salmeron, M. (1995) *Appl. Phys. Lett.* **67**, 476–478.
24. Hu, J., Xiao, X. D., Ogeltree, D. F. & Salmeron, M. (1995) *Science* **268**, 267–271.
25. de Pablo, P. J., Martinez, M. T., Colchero, J., Gómez-Herrero, J., Maser, W. K., Benito, A. M., Muñoz, E. & Baro, A. M. (2000) *Adv. Materials* **12**, 573–576.
26. de Pablo, P. J., Gómez-Navarro, C., Gil, A., Colchero, J., Martinez, M. T., Benito, A. M., Maser, W. K., Gómez-Herrero, J. & Baró, A. M. (2001) *Appl. Phys. Lett.* **79**, 2979–2981.
27. Cai, L., Tabata, H. & Kaway, T. (2000) *Appl. Phys. Lett.* **77**, 3105–3106.
28. Muster, J., Kim, G. T., Krstic, V., Park, J. G., Roth, S. & Burghard, M. (2000) *Adv. Materials* **12**, 420–424.
29. Gómez-Navarro, C., de Pablo, P. J., Moreno-Herrero, F., Horcas, I., Fernandez-Sanchez, R., Colchero, J., Gómez-Herrero, J. & Baro, A. M. (2002) *Nanotechnology* **13**, 314–317.
30. Salmeron, M., Beebe, T., Odriozola, J., Wilson, T., Ogletree, D. F. & Siekhaus, W. (1990) *J. Vac. Sci. Technol. A* **8**, 635–639.
31. Garcia, R., Yuqiu, J., Schabtach, E. & Bustamante, C. (1992) *Ultramicroscopy* **42–44**, 1250–1254.
32. Dunlap, D. D., Garcia, R., Schabtach, E. & Bustamante, C. (1993) *Proc. Natl. Acad. Sci. USA* **90**, 7652–7655.
33. Tran, P., Alavi, B. & Gruner, G. (2000) *Phys. Rev. Lett.* **85**, 1564–1567.
34. Conwell, E. M. & Rakhmanova, S. V. (2000) *Proc. Natl. Acad. Sci. USA* **97**, 4556–4560.
35. Barnett, R., Cleveland, C., Joy, A., Landman, U. & Schuster, G. (2001) *Science* **294**, 567–571.

Top Curr Chem (2004) 237:183–227
DOI 10.1007/b94477

Charge Transport in DNA-Based Devices

Danny Porath[1] · Gianaurelio Cuniberti[2] · Rosa Di Felice[3]

[1] Department of Physical Chemistry, Institute of Chemistry, The Hebrew University, 91904 Jerusalem, Israel
E-mail: porath@chem.ch.huji.ac.il
[2] Institute for Theoretical Physics, University of Regensburg, 93040 Regensburg, Germany
INFM Center on nanoStructures and bioSystems at Surfaces (S3),
[3] Università di Modena e Reggio Emilia, Via Campi 213/A, 41100 Modena, Italy
E-mail: rosa@unimore.it

Abstract Charge migration along DNA molecules has attracted scientific interest for over half a century. Reports on possible high rates of charge transfer between donor and acceptor through the DNA, obtained in the last decade from solution chemistry experiments on large numbers of molecules, triggered a series of direct electrical transport measurements through DNA single molecules, bundles, and networks. These measurements are reviewed and presented here. From these experiments we conclude that electrical transport is feasible in short DNA molecules, in bundles and networks, but blocked in long single molecules that are attached to surfaces. The experimental background is complemented by an account of the theoretical/computational schemes that are applied to study the electronic and transport properties of DNA-based nanowires. Examples of selected applications are given, to show the capabilities and limits of current theoretical approaches to accurately describe the wires, interpret the transport measurements, and predict suitable strategies to enhance the conductivity of DNA nanostructures.

Keywords Molecular electronics · Biomolecular nanowires · Conductance · Bandstructure · Direct electrical transport

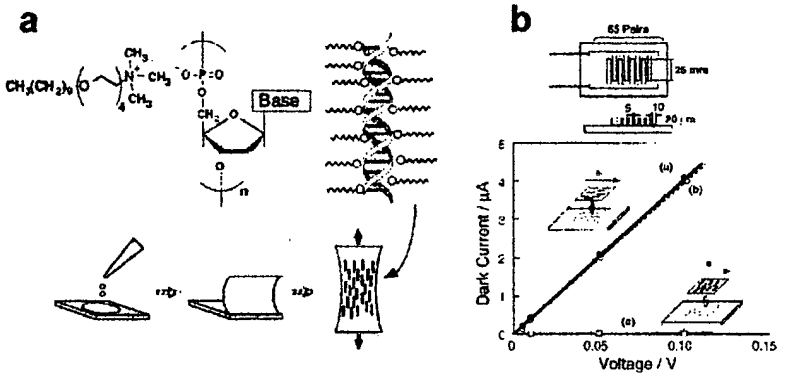

Fig. 12 a Schematic illustration of a flexible, aligned DNA film prepared from casting organic-soluble DNA–lipid complexes with subsequent uniaxial stretching. b Experimental geometries and measured dark currents for aligned DNA films (20×10 mm, thickness 30±5 μm) on comb-type electrodes at 25°C. In the dark-current plot, the three curves represent different experimental settings and environments: (a) DNA strands in the film placed perpendicular to the two electrodes (scheme in the *upper inset*) and measured in ambient; (b) the same film as in (a) measured in a vacuum at 0.1 mmHg; (c) DNA strands in the film placed parallel to the two electrodes, both in a vacuum and in ambient (from [49], with permission; Copyright 1998 by the American Chemical Society)

Measurements on a different type of DNA-based material were reported by Rinaldi et al. [68] (see Fig. 13). In this experiment they deposited a few layers of deoxyguanosine ribbons in the gap between two planar metal electrodes, ~100 nm apart. The current–voltage curves showed a gap followed by rise of the current beyond a threshold of a few volts. The curves depended strongly on the concentration of the deoxyguanosine in the solution.

2.3
Conclusions from the Experiments about DNA Conductivity

More and more evidence accumulating from the direct electrical transport measurements shows that it is possible to transport charge carriers along short single DNA molecules, in bundles of molecules, and in networks, although the conductivity is rather poor. This is consistent with the picture that emerges from the electron-transfer experiments. By this picture, that is becoming a consensus, the two most fundamental electron-transfer processes are coherent tunneling over a few base pairs and diffusive thermal hopping over a few nanometers. However, transport through long single DNA molecules (>40 nm) that are attached to the surface is apparently blocked. It may be due to the surface force field that induces many defects in the molecules and blocks the current or any additional reason.

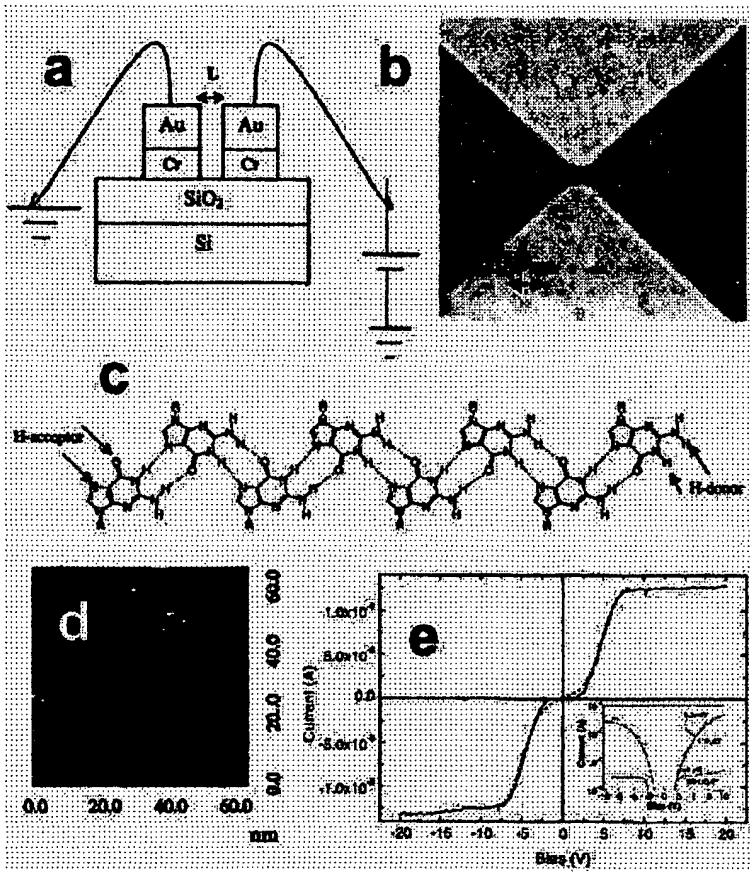

Fig. 13 a Schematic of the device used in the experiment. b SEM image of the gold nanoelectrodes, fabricated by electron-beam lithography and lift-off onto a SiO_2/Si substrate. c Schematics of the ribbon-like structure formed by the deoxyguanosine molecules connected through hydrogen bonds. R is a radical containing the sugar and alkyl chains. d AFM micrograph of the ordered deoxyguanosine film obtained after drying the solution in the gap. Regular arrangement of ribbons ranges over a distance of about 100 nm. The ribbon width of about 3 nm is consistent with that determined by X-ray measurements. e *I–V* characteristics of the device (from [68], with permission; Copyright 2001 by the American Institute of Physics)

Therefore, if one indeed wants to use DNA as an electrical molecular wire in nanodevices, or as a model system for studying electrical transport in a single one-dimensional molecular wire, then there are a few possible options. One option is to use doping by one of the methods that are described

in the literature [70–74] (e.g., addition of intercalators, metal ions, or O_2 etc.). Another way is to reduce the surface affinity of the DNA molecules and hence the effect of the surface force field (e.g., by a predesigned surface layer) on the attached DNA. Yet another way could be to use more exotic structures such as DNA quadruple helices instead of the double-stranded structure. Such constructions may offer an improved stiffness and electronic overlap that possibly enhance the conductivity of these molecules.

3 Theoretical Understanding of Charge Transport in DNA-based Nanowires

The theoretical approaches that have been applied so far to the study of charge mobility in DNA molecules can be divided into two broad classes.

(i) The kinetic determination of the charge-transfer rates between specific locations on the base sequence, after the Marcus–Hush–Jortner theory [76, 77], is the preferred route by the (bio)chemistry community. In these approaches, the electronic structure information is employed only at the level of individual bases or couples of stacked neighboring bases. The results obtained may be compared to the measured charge-transfer rates, and employed to devise models for the mobility mechanisms, addressing dynamical processes by which the charges might move along the helix, e.g., one-step superexchange, hopping, multiple hopping, polaron hopping [41, 46–48, 78–80].

(ii) The computation of the molecular electronic structure for model and real extended DNA-base aggregates, which affects the quantum conductance and hence the quantities directly measured in transport experiments, is instead linked to the investigations performed by the nanoscience community to explore the role and the efficiency of DNA in electronic devices. The results of such calculations may help devise models for charge mobility from a different point of view, e.g., to unravel the role of the electronic structure in determining the shape of the measured current–voltage characteristics.

The two approaches are not unrelated and a complementary analysis of both kinds of studies would finally shed light onto the detailed mechanisms for charge migration along DNA wires [51]. The kinetic theories are reviewed in other chapters of this book. Here, we focus on results obtained for the electronic structure of extended DNA base stacks, and describe their influence on the electrical conductivity of DNA-based nanostructures.

3.1 Methods to study Quantum Transport at the Molecular Scale

In principle, one would like to perform accurate computations of the relevant measurable quantities to assess the conductivity of the fabricated mo-

structure of the molecular device [84–87, 129] with the well-established Green function formalism, to compute the transport characteristics. In such a way, it would be possible to distinguish self-consistently in the calculations different mechanisms, and their relative importance in experimental settings.

4 Conclusions and Perspectives

Charge migration along DNA molecules has attracted a considerable scientific interest for over half a century. The results of solution chemistry experiments on large numbers of short DNA molecules indicated high charge-transfer rates between a donor and an acceptor located at distant molecular sites. This, together with the extraordinary molecular recognition properties of the double helix and the hope of realizing the bottom-up assembly of molecular electronic devices and circuits using DNA molecules, has triggered a series of direct electrical transport measurements through DNA. In this chapter we provided a comprehensive review of these measurements and of the intense theoretical effort, in parallel and following the experiments, to explain the results and predict the electronic properties of the molecules, using a variety of theoretical methods and computational techniques.

After the appearance of some initial controversial reports on the conductance of DNA devices, recent results seem to indicate that native DNA does not possess the electronic features desirable for a good molecular electronic building block, although it can still serve as a template for other conducting materials [12, 13, 132]. Particularly, it is found that short DNA molecules are capable of transporting charge carriers, and so are bundles and DNA-based networks. However, electrical transport through long single DNA molecules that are attached to surfaces is blocked, possibly due to this attachment to the surface.

In a molecular electronics perspective, however, the fascinating program of further using the "smart" self-assembly capabilities of DNA to realize complex electronic architectures at the molecular scale remains open for further investigation. To enhance the conductive properties of DNA-based devices there have already been interesting proposals for structural manipulation. These include intrinsic doping by metal ions incorporated into the double helix (such as M-DNA [71–74]), other ions [119–120] exotic structures like G4-DNA [93, 118, 133], along with the synthesis of other novel helical structures. The reach zoology of DNA derivatives with more promising electrical performance will definitely represent a great challenge in the agenda of researchers involved with the transport in DNA wires.

A last comment is due on the need for progress in the investigation tools. Further development in the study of potential DNA nanowires requires the advancement of synthesis procedures for the structural modifications, and an extensive effort in X-ray and NMR characterization. Concerning direct conductivity measurements, techniques for deposition of the molecules onto inorganic substrates and between electrodes must be optimized. Moreover,

the experimental settings and contacts must be controlled to a high degree of accuracy in order to attain an uncontroversial interpretation and high reproducibility of the data. On the theoretical side, a significant breakthrough might be the combination of mesoscopic theories for the study of quantum conductance and first-principle electronic structure calculations, suitable for applications to the complex molecules and device configurations of interest. Given this background, we believe that there is still plenty of room to shed light onto the appealing issue of charge mobility in DNA, for both the scientific interest in conduction through one-dimensional polymers and the nanotechnological applications. The high interdisciplinary content of such a research manifesto will necessarily imply a crossing of the traditional borders separating solid-state physics, chemistry, and biological physics.

Acknowledgements Funding by the EU through grant FET-IST-2001-38951 is acknowledged. DP is thankful to Cees Dekker and his group, with whom experiment [14] was done, to Joshua Jortner, Avraham Nitzan, Julio Gomez-Herrrero, Christian Schönenberger, and Hezy Cohen for fruitful discussions about the conductivity in DNA and critical reading of the manuscript. DP research is funded by: The First foundation, The Israel Science Foundation, The German-Israel Foundation, and Hebrew University Grants. GC acknowledges the collaboration with Luis Craco with whom part of the work reviewed was done. The critical reading of Miriam del Valle, Rafael Gutierrez, and Juyeon Yi is also gratefully acknowledged. GC research has been funded by the Volkswagen Foundation. RDF is extremely grateful to Arrigo Calzolari, Anna Garbesi, and Elisa Molinari for fruitful collaborations and discussions on topics related to this chapter, and for a critical reading of the manuscript. RDF research is funded by INFM through PRA-SINPROT, and through the Parallel Computing Committee for allocation of computing time at CINECA, and by MIUR through FIRB-NOMADE.

References

1. Luryi S, Xu J, Zaslavsky A (1999) (eds) Future trends in microelectronics: the road ahead. Wiley, New York
2. Joachim C, Gimzewski JK, Aviram A (2000) Nature 408:541
3. Aviram A, Ratner MA (1998) (eds) Molecular electronics science and technology. Annals of the New York Academy of Sciences, vol 852. The New York Academy of Sciences, New York
4. Aviram A, Ratner MA, Mujica V (2002) (eds) Molecular electronics II. Annals of the New York Academy of Sciences, vol 960. The New York Academy of Sciences, New York
5. Tour JM (2000) Acc Chem Res 33:791
6. Aviram A, Ratner MA (1974) Chem Phys Lett 29:277
7. Metzger RM (1999) Acc Chem Res 9:2027
8. Collier CP, Wong EW, Bolohradsky M, Raymo FM, Stoddart JF, Kuekes PJ, Williams RS, Heath JR (1999) Science 285:391
9. Reed MA, Zhou C, Muller CJ, Burgin TP, Tour JM (1997) Science 278:252
10. Collier CP, Mattersteig G, Wong EW, Luo Y, Beverly K, Sampario J, Raymo FM, Stoddart JF, Heath JR (2001) Science 289:1172
11. Chen J, Reed MA (2002) Chem Phys 281:127
12. Braun E, Eichen Y, Sivan U, Ben-Yoseph G (1998) Nature 391:775
13. Keren K, Krueger M, Gilad R, Ben-Yoseph G, Sivan U, Braun E (2002) Science 297:72
14. Porath D, Bezryadin A, de Vries S, Dekker C (2000) Nature 403:635
15. Rinaldi R, Biasco A, Maruccio G, Cingolani R, Alliata D, Andolfi L, Facci P, De Rienzo F, Di Felice R, Molinari E (2002) Adv Mater 14:1453

J Biotechnol. 2004 Aug 26;112(1-2):91-5.

Absence of intrinsic electric conductivity in single dsDNA molecules.

Kleine H, Wilke R, Pelargus Ch, Rott K, Puhler A, Reiss G, Ros R, Anselmetti D.

Experimental Biophysics, Faculty of Physics, Bielefeld University, Universitatsstrasse 25, D-33615 Bielefeld, Germany.

The intrinsic dc conductivity of long, individual lambda phage dsDNA molecules has been investigated by ultrasensitive low current-voltage-spectroscopy (IV) under ambient conditions and controlled low humidity inert gas atmosphere on microfabricated metal-insulator-metal gap structures. We found a strong dependence of the measured conductivity on the apparent humidity, which we attribute to capillary condensation of water to the immobilized DNA molecules, giving rise to additional ionic currents. Additional IV-spectroscopy experiments under controlled argon atmosphere always revealed a significant drop in electrical conductivity to 4 x 10(-15)AV(-1)microm(-1), indicating almost no considerable contribution of electrical long range charge transport.

Electrical Properties of Biopolymers and Membranes

Shiro Takashima

Department of Bioengineering
University of Pennsylvania

Adam Hilger, Bristol and Philadelphia

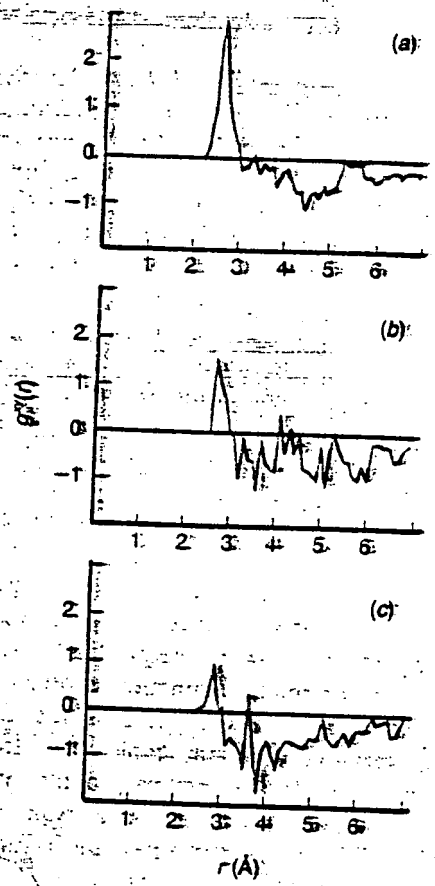

Figure 8.17 The dipole–dipole correlation function $g_\mu^{rr}(r)$ for wall water. (*a*) The distance from the wall is between 8 and 10 Å, (*b*) between 2.5 and 3.5 Å, and (*c*) between 0.5 and 1.5 Å. (From Marchesi 1983.) Reproduced by permission of Elsevier Science Publishers.

8.8 Bound Water in Biological Macromolecules

The structure and physical properties of bound water have been investigated for many years, yet we do not have a satisfactory model for the water of hydration due to various reasons. Bound water is a special form of bulk water perturbed by charges or hydrophobic interactions. Water molecules can have a variety of structures and physical states depending strongly on the circumstances. As discussed earlier, some biological water can be nearly identical to normal water. On the other hand, some portions of bound water may be like ice. Furthermore, as

discussed, water molecules in the vicinity of a charge have a structure which does not resemble either normal water or ice.

Structural water

First of all, some water molecules are found in biological polymers as an integral part of the structure. A number of x-ray crystallographic studies on proteins are able to detect these water molecules on electron density maps. The investigations by Lipscomb *et al* (1969) and by Dickerson and Geis (1969) on carboxypeptidase A are some of these examples. Figure 8.18 illustrates the spatial arrangement of water molecules in a triple helical collagen molecule (Ramachandran and Chandrasekharan 1968). As shown, a water molecule is hydrogen bonded to a carbonyl group as well as to an NH residue of one of the chains and also to a carbonyl group of another strand. The role of these water molecules is to bridge the helical chains and to stabilize the triple helical structure.

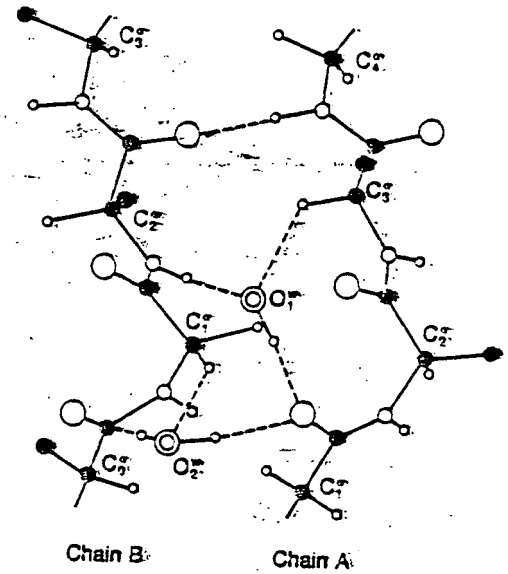

Figure 8.18 A side view of the chains A and B of collagen molecules. This diagram shows three different types of cross-linking secondary bonds. O_1^w and O_2^w represent oxygens of the water molecules. The full and open small circles are carbons and nitrogens. The large open circles represent carbonyl oxygens. (From Ramachandran and Chandrasekharan 1968.) Reproduced by permission of John Wiley & Sons, Inc. © 1968.

Thus, it can be inferred that removal of these water molecules would cause an instability of the helical structure. The presence of structural

water of this kind is presumed to be ubiquitous among biopolymers. A recent report by Kopka *et al* (1984) shows a chain of water molecules within a groove of six base pairs in double helical DNA (see figure 8.19). These water molecules are an integral part of the structure of biopolymers and have a very specific configuration which can be identified by x-ray analysis. Clearly, they are a part of the polymer and cannot be removed without disrupting the internal structure. Although they play an important role for the stability of biopolymers, their dielectric properties are unknown because of the difficulty of identifying them dielectrically. The number of these water molecules is relatively small compared with those which are bound to the surface of polymers. However, we can easily surmise that the orientational freedom of these water molecules is very restricted, with their dielectric constant being much smaller than that of normal water.

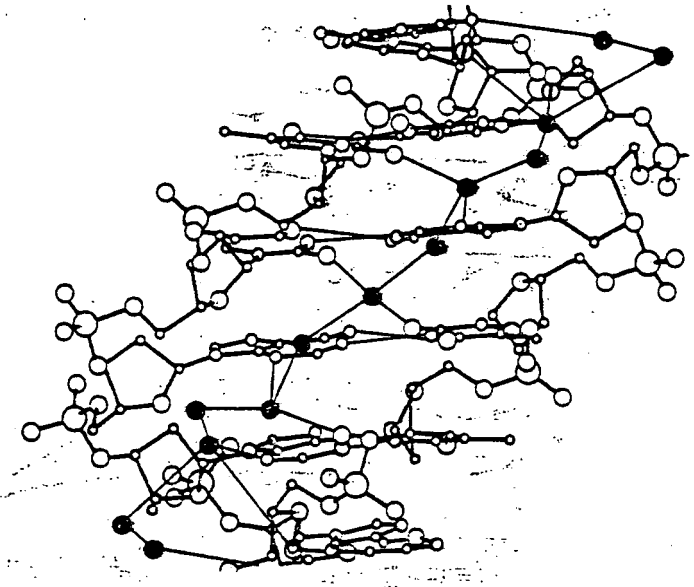

Figure 8.19 Water molecules found in the groove of the double helix of B-DNA. The sequence is CGCGAATTCG with the spine of hydration. Full spheres represent water oxygen. (From Kopka *et al* 1984.) Reproduced by copyright permission of the Biophysical Society.

Dielectric properties of water of sorption

The adsorption or desorption of water on the surface of protein crystals has been of considerable interest for many years. It is not certain

whether the adsorption of water is strictly a surface phenomenon or that adsorbed water penetrates, to some extent, into crystals and becomes bound to individual protein molecules. However, for the sake of simplicity, let us assume that the adsorption of water on protein crystals is strictly a surface phenomenon. When the crystalline powder of a protein is exposed to water vapour of known partial pressure p/p_0, uptake of water vapour on the surface of crystals will occur. This adsorption will continue until an equilibrium state is reached. A plot of the amount of adsorbed water at equilibrium against the partial pressure of water vapour is shown in figure 8.20. The amount of adsorbed water increases, as shown, as the partial pressure of water vapour increases, and the curve reaches a plateau. However, the curve rises again as the partial pressure of H_2O further increases. Intuitively, this curve indicates the formation of multilayers of adsorbed water. Some adsorption isotherms which have been observed with solid materials, however, do not indicate the formation of multilayers. For example, the adsorption of gas molecules on metal surfaces can be represented by curve A in the same figure. This curve is obviously different from curve B and indicates the formation of only one layer of adsorbed gas molecules.

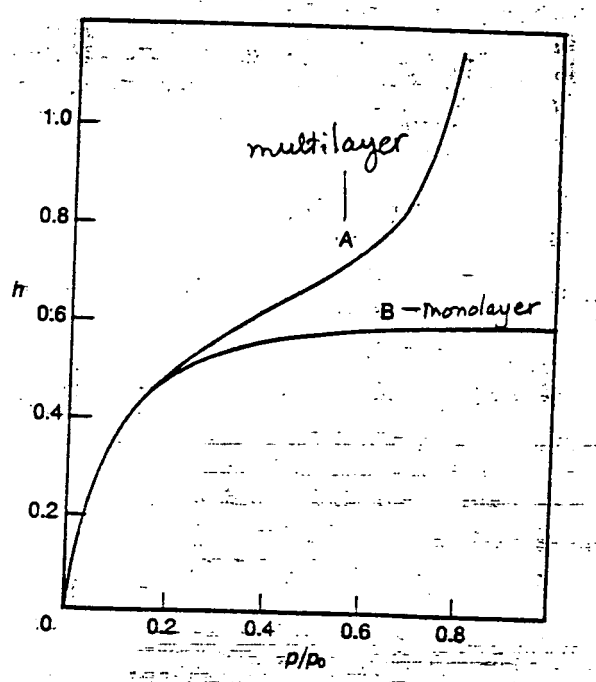

Figure 8.20 A schematic representation of monolayer (curve B) and multilayer (curve A) adsorptions of gaseous molecules on solid surfaces. h is the amount of adsorbed water in grams.

RADIO ENGINEERING HANDBOOK

KEITH HENNEY, Editor-in-Chief

Fellow, The Institute of Radio Engineers;
Co-author, "Principles of Radio," "Electron
Tubes in Industry"; Consulting Editor,
"Nucleonics"

Fifth Edition

McGRAW-HILL BOOK COMPANY, Inc.

NEW YORK TORONTO LONDON

1959

exactly 90-deg phase difference between the two quadrature dipoles, the radiation pattern is virtually circular in the plane of the dipoles. As a single element, considerable energy is radiated in the direction normal to the plane of the radiators, and for the specified excitation, the field in this direction is circularly polarized. The polarization can be changed by adjusting either the power divisions or the relative phasing or both. In this case, the radiation pattern in the plane of the turnstile is elliptically shaped. When two or more such radiators are stacked at $\lambda/2$ intervals and successively cophased, maximum radiation occurs in the plane of the radiators. When successive layers are antiphased, directivity normal to the planes of the turnstiles is obtained.[1]

A turnstile element has a certain advantage in providing a greater band width than that of the individual dipoles. This comes about from the method of feeding and phase-shifting whereby the feeder to each radiator is terminated and the two sections excited from a common generator by means of parallel lines from a junction point with the main feeder, one branch being $\lambda/4$ longer than the other.[2] This extra $\lambda/4$ section of line, in addition to providing the 90-deg phase lag, acts as an impedance-inverting section. Both radiators change impedance equally as the frequency is changed from mid-band, but the impedance inversion in one feeder causes a compensating effect at the main junction with the other feeder. This is a valuable property per se.

Figure 46*K* represents the *biconical antenna* whose principal special property is intrinsically greater band-width response than ordinary radiators have.[3]

Figure 46*L* presents again the folded dipole. As an impedance transformer and for its greater cross section providing broader band response than a simple straight dipole, it has special value in certain v-h-f and u-h-f applications.

Figure 46*M* is a variation in principle of Fig. 46*B*, where the central supporting member is a tube forming the outer conductor of a coaxial transmission line. The tube is slotted to a depth of $\lambda/4$, and the inner conductor of the transmission line attaches to one side of the $\lambda/2$ dipole welded to the tube. In general, this type of slotted-coaxial section is both a balance-to-unbalance transformer and an impedance transformer in the ratio of 4:1. That is, the impedance at the balanced terminals (the open end of the slotted section) is four times the impedance of the unbalanced line (assuming it is terminated in a matched load) in shunt with the reactance of the balanced stub formed by the slot in the coaxial line. If the slot is effectively $\lambda/4$ long, its impedance is infinite and the impedance transformation is 4:1. In practice, the characteristic impedance of the coaxial line is modified slightly by the presence of the slot. Unless the diameter of the coaxial line and the slot width are very much less than the wavelength, considerable radiation will occur from the slot.

Figure 46*O* is an example of a dipole, capable of many variations, where linear conductors are replaced by plane sheets of selected shapes for obtaining special characteristics.

In all these forms of electric dipoles, band width can be increased by increasing the radiator cross section when the application is associated with wide-band systems. Their radiation patterns are individually quite similar to any simple straight dipole, except for the turnstile element.

59. Magnetic Dipoles. Certain applications, such as navigational aids, require for their success the radiation of a field which is virtually pure horizontal polarization at any orientation from the antenna. Other less critical applications also use horizontal polarization, the purity of which is not essential. To obtain virtually pure horizontal polarization a vertical magnetic dipole can be used. There are several types in existence, and others appear from time to time. What is wanted in a magnetic dipole is a loop of fairly large electrical diameter to have a high radiation resistance, with a uniformly distributed current around it, all elements of which are in time phase. It has generally been necessary to approach this by configurations made up of bent electric dipoles having standing-wave current distributions. The various forms developed

[1] See reference 291.
[2] A bridge-type network for this purpose is given in reference 295.
[3] See references 16, 265, and 88.

exhibit ingenuity in making magnetic dipoles from electric dipoles, with varying degrees of compromise.

Some of the most practical forms are shown in Fig. 47. In this figure, *a* is a square loop made up of two electric dipoles, folded at their centers and near their ends.[1] When they are attached by means of insulators at the ends, the current at the corner is not zero, though it is much less in amplitude than at the other corners, where the two dipoles are center-fed in balanced antiphased relationship. It is fed by a balanced

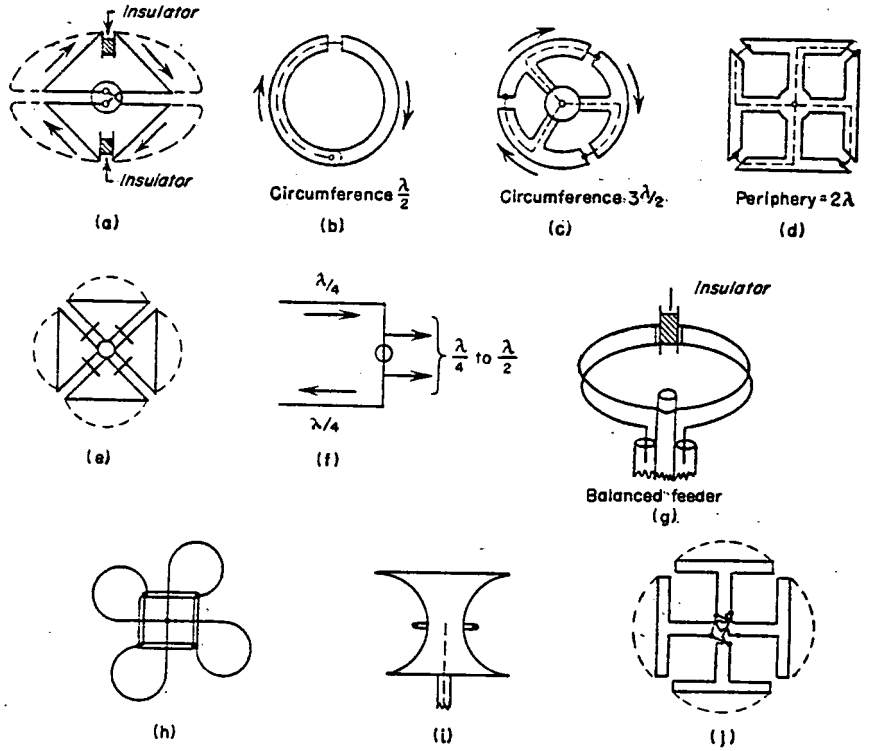

FIG. 47. Magnetic-dipole antennas of various forms.

feeder at the center. This has been used in aviation navigational aids. It is characterized by a nonuniform current distribution which produces an oval pattern, and by relatively low radiation resistance because of its small electrical diameter (approximately $3\lambda/16$ per side). The dipoles are made of wide bars of metal, and the feeder lines are ordinarily shielded up to the two corners where they are energized.

Figures 47*b*, *c*, and *d* are three versions of magnetic dipoles.[2] A circular or polygon loop, sectionalized and fed as shown from a coaxial feeder, permits cophasing the currents in the successive elements for relatively large electrical diameters and provides high values of radiation resistance to be realized. As the loop is increased in diameter, the periphery is sectioned into a larger number of segments, each $\lambda/2$ long, with its own radial feeder. One-half of each radiator acts as the coaxial line for the succeeding radiator.

Figure 47*e* is a square (or alternately a circular) loop radiator $\lambda/2$ per side. The ends are not closed and are connected by radial supporting stubs which are short-

[1] See reference 243.
[2] See reference 285.

Practical Antenna Handbook

2nd Edition

Joseph J. Carr

TAB Books
Division of McGraw-Hill, Inc.
New York San Francisco Washington, D.C. Auckland Bogotá
Caracas Lisbon London Madrid Mexico City Milan
Montreal New Delhi San Juan Singapore
Sydney Tokyo Toronto

The coils force the current antinodes toward the feedpoint, reversing the direction of the main lobe, and creating a gain of about +1 dB over a half-wavelength dipole.

The currents flowing in the antenna can be quite high, so when making the coils, be sure to use a size that is sufficient for the power and current levels anticipated. The 2- to 3-inch B&W/*Air-Dux* style coils are sufficient for most amateur radio use. Smaller coils are available on the market, but their use is limited to low-power situations.

1λ large loops

If size is not forcing you to a λ/2 loop, then a 1λ loop might be just the ticket. It produces a gain of about +2 dB over a dipole in the directions that are perpendicular to the plane of the loop. The azimuth patterns formed by these antennas are similar to the "figure-8" pattern of the dipole. Three versions are shown: the square loop (Fig. 14-3), the diamond loop (Fig. 14-4), and the delta loop (a.k.a. D-loop and triangle—Fig. 14-5). The square and diamond loops are built with λ/4 on each side, and the delta loop is λ/3 on each side. The overall length of wire needed to build these antennas is:

$$L_{\text{feet}} = \frac{1005}{F_{\text{MHz}}} \qquad [14.2]$$

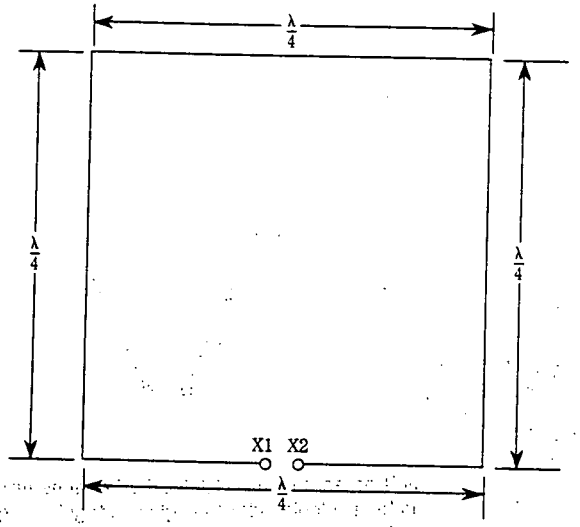

14-3 Quarter-wavelength square loop (single-element quad).

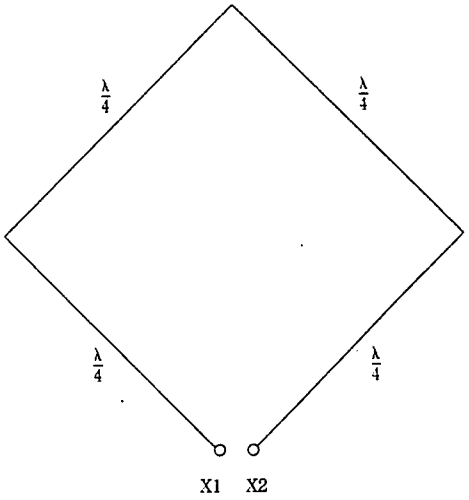

14-4 Bottom fed loop.

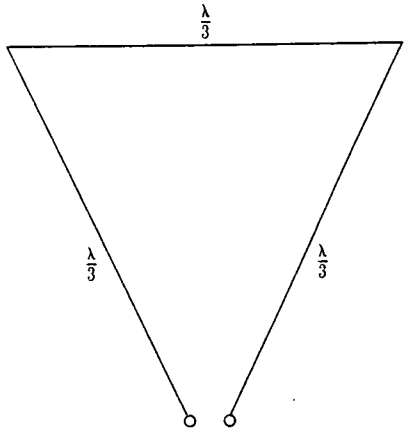

14-5 Delta loop antenna.

The polarization of the three loop antennas is horizontal, because of the location of the feedpoints. On the square loop, moving the feedpoint to the middle of either vertical side will provide vertical polarization. Similarly, on the diamond loop vertical